USING FINITE ELEMENT STRUCTURAL ANALYSIS OF RETROREFLECTIVE RAISED PAVEMENT MARKERS TO RECOMMEND TESTING PROCEDURES FOR SIMULATING THEIR FIELD PERFORMANCE

A Thesis

by

RAVI PRAKASH AGRAWAL

Submitted to the Office of Graduate Studies of
Texas A&M University
in partial fulfillment of the requirements for the degree of

MASTER OF SCIENCE

May 2006

Major Subject: Civil Engineering

USING FINITE ELEMENT STRUCTURAL ANALYSIS OF RETROREFLECTIVE RAISED PAVEMENT MARKERS TO RECOMMEND TESTING PROCEDURES FOR SIMULATING THEIR FIELD PERFORMANCE

A Thesis

by

RAVI PRAKASH AGRAWAL

Submitted to the Office of Graduate Studies of
Texas A&M University
in partial fulfillment of the requirements for the degree of

MASTER OF SCIENCE

Approved by:

Chair of Committee,	Gene Hawkins
Committee Members,	Paul Carlson
	Harry Hogan
	Yunlong Zhang
Head of Department,	David Rosowsky

May 2006

Major Subject: Civil Engineering

ABSTRACT

Using Finite Element Structural Analysis of Retroreflective Raised Pavement Markers (RRPMs) to Recommend Testing Procedures for Simulating Their Field Performance.

(May 2006)

Ravi Prakash Agrawal, B. Tech., Indian Institute of Technology, Delhi

Chair of Advisory Committee: Dr. Gene Hawkins

Retroreflective Raised Pavement Markers (RRPMs) supplement other pavement markings to provide guidance to road users. Previous research concerning durability of the RRPMs suggests that their performance has been degrading over the years. One of the main causes for underperformance of the RRPMs is the lack of appropriate laboratory testing standards that can test the adequacy of the RRPMs to perform in field conditions. There is a need to modify the existing standards or develop new testing procedures that can better simulate field conditions. This requires identifying critical locations and magnitudes of stresses inside the markers during the tire-marker impacts that happen on roads.

The goal of this research was to identify critical magnitudes and locations of the stresses in RRPMs during the tire-marker impacts by doing the finite element modeling and simulation of the impacts, and use the information to recommend laboratory testing procedures that could simulate real-world conditions. The researcher modeled and simulated the tire-marker impacts using the finite element tools Hypermesh and LS-

DYNA. He calibrated the material properties of the marker models to improve the tire-marker model.

Based on the tire-marker impact simulations, the researcher concluded that the critical compressive stresses during impacts are located at the edge contacts of retroreflective sides with the top surface. The critical stresses may also occur at lower and upper corners of the marker. The other areas, especially the lower half of the marker, had tensile stresses. Angle of impact was found to be a critical external variable that affected the stresses inside the markers and the marker-pavement interface forces.

The researcher then modeled and simulated a few laboratory-testing procedures that could simulate the field performance of the RRPMs. Based on these simulations, the researcher recommended that the ASTM compression test for evaluation of RRPMs be continued or a similar test be developed. He suggested development of one new test (named as offset compression test) that could better replicate the field conditions. He also recommended having a review of the ASTM flexural test.

ACKNOWLEDGEMENTS

I want to acknowledge the guidance from my thesis supervisor Dr. Gene Hawkins. He was instrumental in conceptualizing this thesis work and advised me on various issues relating to retroreflective raised pavement markers and their structural analysis. I want to thank Dr. Yunlong Zhang for guiding me and providing suggestions. I also want to thank other committee members Dr. Paul Carlson and Dr. Harry Hogan for guiding me. I want to especially thank Steven Schrock, my supervisor on the Texas Transportation Institute project no. 0-5089, who has kept me motivated for this research work while providing invaluable suggestions.

I would like to thank Dr. Akram Abu-Odeh, who helped me in the finite element analysis part of this research. He worked on building the finite element model of a truck tire, which was used for the modeling of tire-marker impacts. In addition, he helped me during the calibration and modeling process whenever I had problems with the finite element modeling tools. I would also like to thank Dr. Ray James and Dr. Harry Jones in providing the ideas for the calibration process. I especially want to thank Ryan Alberson, an undergraduate student, for assisting me in the process of modeling.

I also want to acknowledge that the analysis done in this research work is by no means an evaluation of different RRPM brands available in the market. I have used the marker prototypes only for modeling the tire-marker impacts. This research work also does not try to validate or invalidate any data on the RRPM material properties available from the manufacturers or online material databases.

TABLE OF CONTENTS

Page

Page

LIST OF FIGURES

FIGURE Page

FIGURE Page

FIGURE Page

FIGURE Page

FIGURE Page

FIGURE Page

LIST OF TABLES

TABLE Page

INTRODUCTION

Retroreflective raised pavement markers (RRPMs) provide delineation on highways. The *Manual on Uniform Traffic Control Devices* (MUTCD) defines an RRPM as "a device with a height of at least 10 mm (0.4 in) mounted on or in a road surface that is intended to be used as a positioning guide or to supplement or substitute for pavement markings or to mark the position of a fire hydrant (*1*)." They are especially useful in nighttime and in rainy conditions when applied pavement markings lose their effectiveness at providing guidance to drivers (*2*). In addition, the rumbling effect of RRPMs reminds drivers to remain in their lanes.

RRPMs come in a variety of configurations. They are available in different shapes. For example, they may be wedge, round and oval. They are also available in different colors. They can be classified as monodirectional or bidirectional depending on the purpose they serve. One can also classify them as snowplowable and non-snowplowable. The snowplowable markers are used in the areas where snow precipitation occurs.

This thesis follows the style and format of the *Transportation Research Record*.

BACKGROUND

Previous research concerning durability of the RRPMs suggests that their performance has been degrading over the years (*2*, *3*, *4*, *5)*. Arguably, major problems associated with RRPMs are structural damage while installed, poor adhesion to pavements, and loss of retroreflectivity over time. An effective RRPM system would have markers remain in the installed locations and have sufficient retroreflectivity over time. However, it has been found that markers lose most of their effectiveness on high traffic volume highways within short time of installation because of poor retention and durability (*2*, *3*, *4*, *5*). Various factors that can account for these failures are high traffic, severe loading (as from trucks), sand abrasion, and environmental factors like temperature, humidity, and ultra-violet radiation (*2*, *3*, *4*, *5*).

PROBLEM STATEMENT

One of the main causes for underperformance of RRPMs is the lack of appropriate laboratory testing standards, which could test the adequacy of the RRPMs to perform in field conditions. The existing testing standards are either inadequate for simulating real-world conditions in laboratories or do not test the RRPMs to their limits (*6)*. There is a need to modify the existing standards or develop new testing procedures that could better simulate field conditions. This requires identifying critical locations and magnitudes of stresses inside the markers during the tire-marker impacts that happen on roads.

While previous studies mainly tried to find out the factors affecting performance of RRPMs, little work had been carried out in finding the locations and magnitudes of

the stresses generated in markers during the tire-marker impacts. Moreover, measuring these stresses multiple times (and including various factors) in the field is not feasible. However, with the advent of finite element modeling (FEM) technology, it is possible to model and simulate the tire-marker impacts. It is a very popular method used these days for analyzing real applications in structures and mechanics.

A finite element computer modeling, simulation, and analysis of tire-markers impacts would give information on the locations and magnitudes of stresses during the impacts. A computer simulation gives the flexibility to analyze the tire-marker impacts with different factors such as varying tire loads and tire velocities, which would not be practical in the field. In addition, it is time and cost efficient. This research was designed to apply the finite element computational techniques for the analysis of tire-marker impacts in real-world conditions.

RESEARCH OBJECTIVES

The goal of this research was to identify critical magnitudes and locations of the stresses in RRPMs during tire-marker impacts by doing the FEM and simulation of the impacts; and use the information to recommend laboratory testing procedures that could simulate the real-world conditions. The research objectives are:

1. To model the tire-marker system using finite element tools and to calibrate the marker models,
2. To use the model to simulate tire impacts on markers and find the critical locations and magnitudes of stresses,

3. To analyze the effects of varying loads, velocities, and angles of impact on magnitudes and locations of the stresses in markers, and
4. To develop, model, and simulate laboratory testing procedures that could replicate the field performance of RRPMs and make recommendations based on the results.

RESEARCH BENEFITS

This research work compliments a Texas Transportation Institute (TTI) project sponsored by the Texas Department of Transportation (TxDOT) that is designed to improve the laboratory testing procedures for RRPMs so that the new tests could reflect the actual field conditions of markers. The results of this thesis will provide insights into critical locations and magnitudes of the stresses insider the markers, which would help the TTI project.

THESIS ORGANIZATION

The thesis is organized into five sections. The first section of the thesis provides the background to the thesis. It also lists the problem statement, research objectives, and benefits. The second section of the thesis is devoted to a review of state-of-the art and state-of-the-practice on RRPMs. The section also discusses fundamentals of finite element analysis (FEA) and some of the FEA tools employed in the research. The third section details the methodology adopted for this research work. This includes the description of study design, calibration of marker properties, and modeling and

simulation of the tire-marker impacts. The fourth section provides the results from the modeling and simulation of tire-marker impacts and a few laboratory testing procedures. The section also details analysis of the results. The final section lists the conclusions and recommendations for future work.

STATE-OF-THE-ART AND PRACTICE

RRPMs are used to supplement other pavement markings. California traffic authorities introduced the RRPMs in 1954 as convex buttons with glass beads on top. They were called as "botts-dots (*7*)." They were applied on concrete pavements using epoxy adhesive. Their initial application was to supplement traffic control devices in night and wet weather. Currently, wedge shaped RRPMs are used. This kind of rectangular RRPM was developed around 1955 to improve durability on asphalt pavement. The wedge shaped markers did not submerge in water. They also allowed one- and two-way delineation. Non-retroreflective ceramic buttons supplement these RRPMs (*7*). Figure 1 shows some of the RRPMs.

This section is a review of state-of-the-art and state-of-the-practice concerning RRPMs. First, it introduces pavement markings and retroreflectivity. Then, it describes RRPMs, their types, functions, and manufacturing processes. The next sub-section is on the research conducted on the durability of RRPMs. Then, the researcher describes some important results from the district surveys conducted as part of the associated ongoing research in the TTI. The researcher then briefly discusses the existing testing practices for RRPMs. The next sub-section is a brief overview of research conducted in the impacts of tires with small obstructions on pavements. The last sub-section describes the basics of FEA and introduces some of the FEA tools used in this research.

FIGURE 1 Typical retroreflective raised pavement markers.

PAVEMENT MARKINGS

Pavement markings are used as traffic control devices to provide 'information' and 'guidance' to road users (*1*). They are used either as stand-alone devices or to supplement other traffic control devices such as signs, signals and other markings. Markings have retroreflectivity to make them visible at night.

Retroreflectivity is the phenomenon of light reflecting back from a surface (retroreflector) once incident on it. A perfect retroreflector will reflect the entire light incident on it back to the source. That, however, does little to make it visible in night conditions. Fortunately, in real world conditions that does not happen and some of the light from the source is scattered in the environment, which makes the reflector and surroundings visible (*7*). Figure 2 graphically shows the phenomenon. Retroreflectivity is quite useful in providing guidance in wet weather as well, when standing water might obscure other pavement markings.

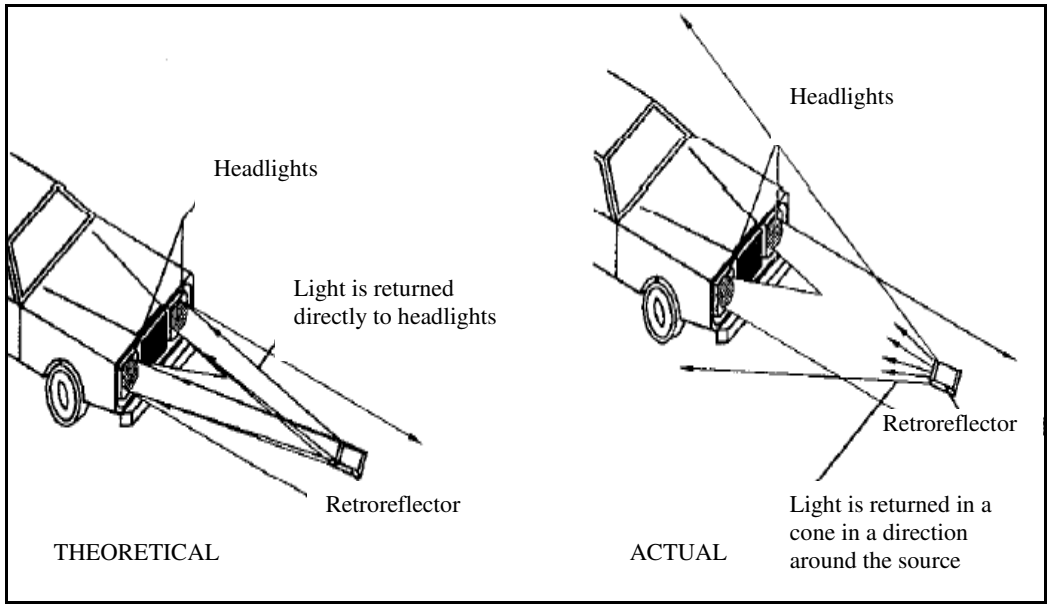

FIGURE 2 Difference between theoretical and actual retroreflection (*7*).

RETROREFLECTIVE RAISED PAVEMENT MARKERS

The *MUTCD* (*1*) defines a raised pavement marker (RPM) as "a device with a height of at least 10 mm (0.4 in) mounted on or in a road surface that is intended to be used as a positioning guide or to supplement or substitute for pavement markings or to mark the position of a fire hydrant." According to the MUTCD, "the color of raised pavement markers under both daylight and nighttime conditions shall conform to the color of the marking for which they serve as a positioning guide, or for which they supplement or substitute."

Functions

The inability of conventional pavement markings to provide enough retroreflectivity in wet weather and poor light caused the need for RRPMs. RRPMs have been very

effective in providing guidance to drivers in these conditions. As they are raised above the ground to some height, they can be effective even when a water layer covers other pavement markings. They are also effective at demanding locations like entry and exit ram/s, curves, bridge approaches, lane transitions, and construction zones, etc. where the roadway geometry hinders proper guidance for drivers.

RRPMs can provide directional information because of their color configuration. The white and yellow colors in RRPMs inform drivers of the right direction of travel while the red color represents wrong direction of travel. The blue RRPMs indicate the locations of fire hydrants. RRPMs also remind drivers to remain in their lanes. This happens when drivers stray over a laneline and strike the RRPMs with their vehicles' tires, which produces a rumbling sound and vibration in vehicles and reminds drivers to remain in their lanes (*8*).

The disadvantage of using RRPMs is the fact that they are expensive compared to pavement markings. The initial cost of installing RRPMs is very high, compared to applied markings (*7*). Their reduced durability, as seen in the last few years, reduces their cost effectiveness. Their use is typically limited to high volume roads.

The MUTCD details the guidelines for color, positioning, and spacing (Figure 3) between the markers. The figure shows how the RRPMs are positioned as substitutes or supplements to pavement stripes. In the figure, N is equal to 80 feet. The reader may refer to Traffic Control Devices Handbook (8), Roadway Practices Delineation Handbook (*7*), and Guidelines for the Use of Raised Pavement Markers (*9*) for more details on these aspects.

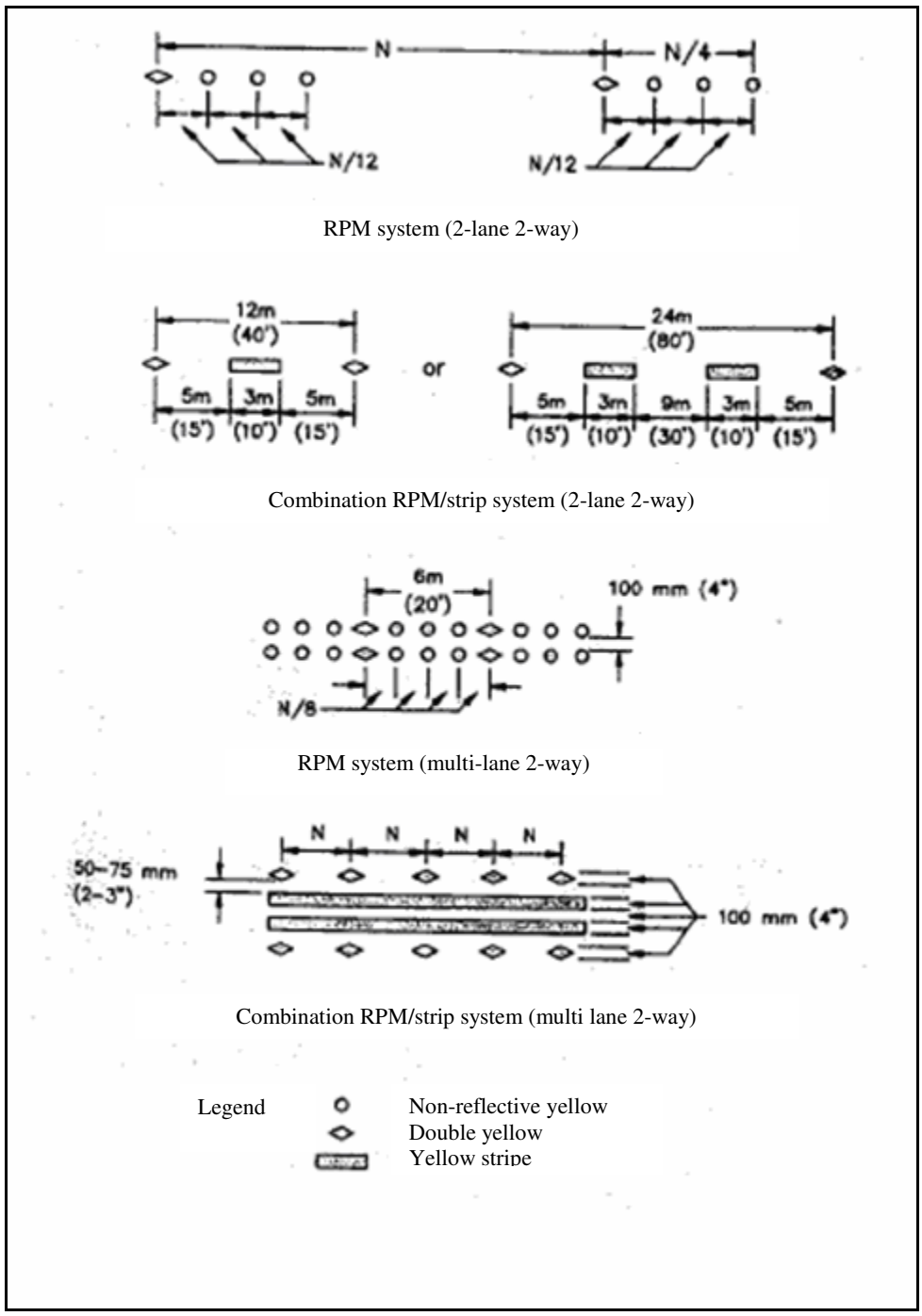

FIGURE 3 Typical arrangements of RRPMs on tangent sections (*8*).

Types

There can be many different kinds of RRPMs. One can classify them by:

1. Retroreflective capability- They can be both retroreflective and non-retroreflective. The non-retroreflective markers, known as just raised pavement markers (RPMs), are used to supplement retroreflective markings or RRPMs.
2. Shape, size, and material- RRPMs can be wedge shaped, round or oval. Figure 4 shows two markers of different shapes. RRPMs can also be made of different materials, as discussed in next sub-section.

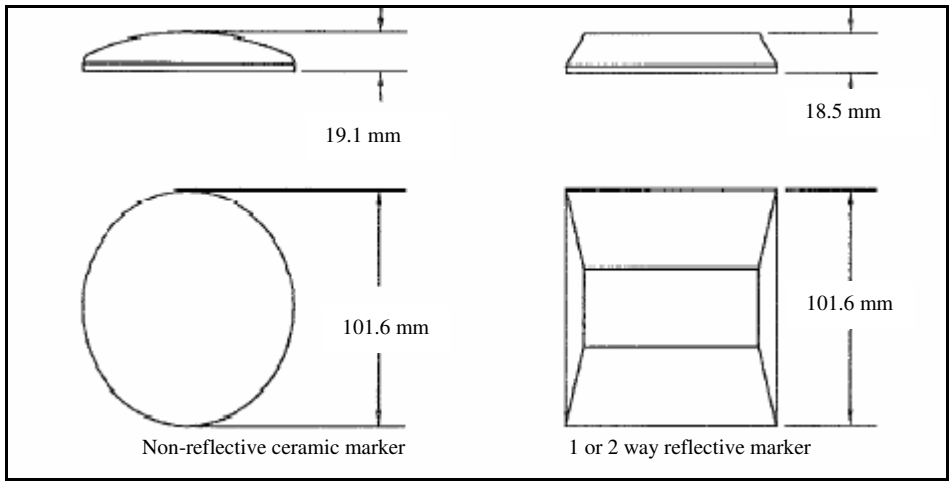

FIGURE 4 Typical RRPM configurations (*7*).

3. Directional configuration- The RRPMs can be monodirectional or bidirectional depending on the purpose they serve. Monodirectional RRPMs serve only one direction of traffic while bidirectional RRPMs serve both directions of traffic.

4. Color- RRPMs can come in many colors and their configurations. Generally, an RRPM can be white only, red only, 2-way white, white-red, 1-way yellow, 2-way yellow, or blue depending on the purpose it serves. For example, a white-red RRPM is a bidirectional RRPM with white and red retroreflective lenses on opposite sides. Yellow markers are used as centerline markers while blue markers are used to mark fire hydrants.
5. Lane position- RRPMs can be edgeline or centerline depending on their positions on highways.
6. Snowplowability- One can also classify RRPMs as snowplowable or non-snowplowable. The snowplowable markers are used in the areas where snow precipitation occurs, for instance, in the northern United States. Areas without snow precipitation use non-snowplowable RRPMs.

Manufacturing

The production design and manufacturing process for the RRPMs has evolved over the years. Traditionally RRPMs have had two components: an acrylic shell integrated with a lens and polyurethane resin as the filler. The interior of the shell in the area of the prism array is given a thin coating of aluminum as a mirrored surface. The filler then fills the shell. Some brands have a very thin glass surface bonded to the face of the prism array. More recently, companies have developed markers with no filler and a body made up of impact graded acrylonitrile butadiene styrene (ABS). The lens is again composed of methyl methacrylate with cube corner technology embedded. Figure 5 shows the

components of one marker. The RRPMs are applied on the pavements using epoxy (generally used for concrete pavements) or bitumen (generally used for asphalt pavements).

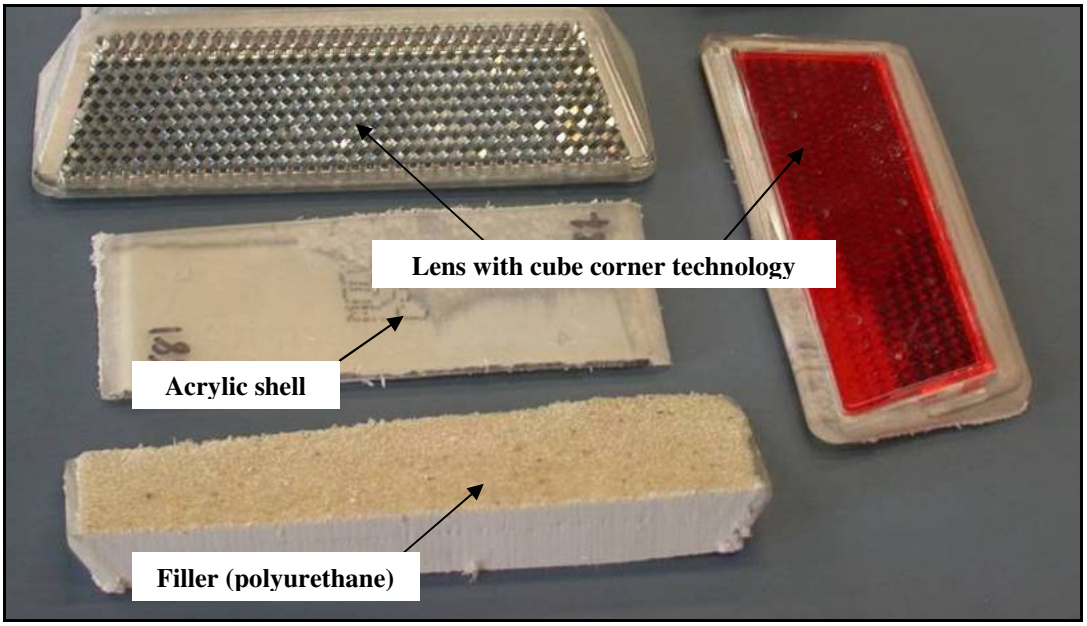

FIGURE 5 One synthesized RRPM.

RRPMs make use of retroreflective technology that includes the cube corner prism array. In this technology, three mirrored surfaces are arranged at 90-degree angles. They receive the rays of headlights on one of the three minors. It reflects the ray to the second, which reflects it to third. This results in the ray returning in exactly the opposite direction from which it entered. Approximately three hundred and sixty retroreflective corner cubes are contained in the face of an RRPM (*7*). Figure 6 illustrates the concept.

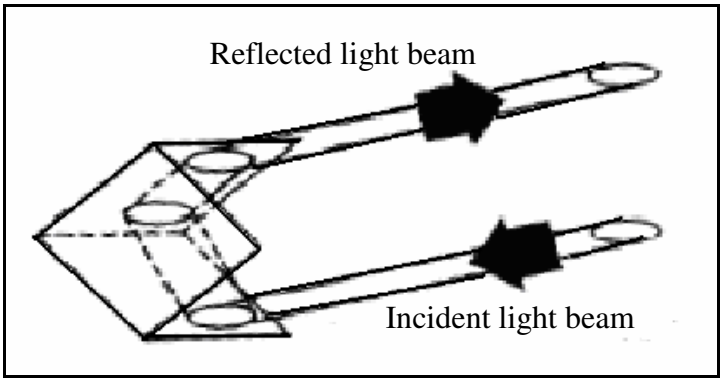

FIGURE 6 Cube-corner retroreflection principle (*8*).

PREVIOUS RESEARCH ON DURABILITY OF RRPM

Some state traffic agencies have sponsored research on the durability of RRPMs (*2*, *3*, *4*, *5*). Two major problems associated with the RRPMs have been poor retention on pavements and loss of retroreflectivity. Traffic agencies have expressed concerns that markers lose most of their effectiveness on high traffic volume highways in a short time of installation because of poor retention and durability.

Lower Durability

There is a little published research about the reasons behind the poor durability of the markers. The Louisiana Department of Transportation sponsored a study regarding the evaluation of raised pavement markers in which Rushing et al. developed a method of simulating field wear and tear of RRPMs (*10*). They developed a circular concrete test track on which they installed marker specimens. A tire with a certain load on its tire revolved over these markers. The researchers observed the deterioration of marker

specimens under these conditions. They recommended developing this test for better field simulation of performance of RRPMs (*10*).

Pigman et al. conducted another evaluation of RRPMs for the Kentucky Transportation Cabinet (then called as Kentucky Department of Transportation) (*11*). They found RRPMs to be very effective for roadway delineation. The study also resulted in the revision of specifications relating to RRPMs.

The Mississippi State Highway Department also sponsored a similar evaluation of RRPMs (*12*). They recommended some measures to reduce RRPM replacement cost, of which few are given here:

- Increase spacing between RRPMs,
- Test asphalt to determine factors that lead to early failure, and
- Make more low profile (lowered height) RRPMs.

TTI's McNees and Noel (*2*, *13*, *14*, *15*) conducted research for TxDOT (then called as the Texas State Department of Highway and Public Transportation). The researchers identified four problem areas with RRPMs: retention, resistance to wear and tear, high installation and maintenance costs, and early loss of retroreflectivity. They classified marker failures as (*15*):

- Failure in pavement,
- Adhesive-pavement failure,
- Adhesive failure,
- Adhesive-marker failure,
- Marker failure/wear, and

- Loss of retroreflectivity.

The major external factors causing the failures were:

- Traffic volume,
- Length of time on road,
- Location of markers e.g. centerline or laneline, and
- Truck traffic.

Other factors responsible for the failures were type of marker, bond size, temperature, humidity, marker height and slope, bond area, tire pressure, tire width, contact location across tread, and vehicle speed (*2*). Defective epoxies (applying watery or improperly cured epoxies), weak pavement materials (e.g. asphalt cement concrete), and deficient installation procedures may have contributed to the failures as well. The deficient installation procedures included (*2*):

- Application of RRPMs on surfaces with dirt particles,
- Using excessively darkened epoxies,
- Inadequately mixed epoxies,
- Improper ratio of resin to hardener or insufficient epoxy,
- Not covering the bonding surfaces completely or uniformly,
- Grinding the bond surface too deeply,
- Pushing markers too firmly or pounding markers,
- Putting markers over existing stripes, and
- Installing markers in hot/cold weather.

The primary mode of failure on asphalt concrete was shear or tension failure within the pavement material (asphalt) beneath marker and adhesive (*2*). Tearing forces came from impacts that tended to twist, slide, and/or rock the RRPM. The study observed that compression was predominant during tire-marker impacts. Pavement can bear compression, although pure compression can punch a marker into the pavement.

Any time a resultant downward force on a marker passes outside the center third of the bonded area between marker and pavement, the adhesive at the opposite edge of the marker will be subjected to simple tension (*2*). This manifests as the marker rolling about an axis in the bonded plane. Adhesive and pavement are least resistant to tension; so the tension causes a bond failure or a pavement failure (*2*). Loads, which are not directly vertical, may cause shear stresses. Horizontal stresses may be induced because of shape of marker or because of vehicle turning, accelerations, or decelerations. This may cause the curved surfaces cupped under marker to slide (analogous to sliding failures of sloping soil) (*2*).

The most damaging impact occurs when a tire side wall strikes a glancing blow on the near vertical side (non-reflective, parallel to traffic) of a marker, such as would be experienced during a turning-passing maneuver. Here the maximum force will tend to displace the marker laterally, twist it about its vertical axis and rotates it about its longitudinal (traffic direction) axis. The higher the marker, the greater these lateral and twisting forces will be. In addition, a greater slope of the marker wall with pavement will increase the severity of these forces. So a smoothly contoured low profile marker with a

large bond area to the pavement would be desired. A tall marker with near vertical sides and small bond area is not desired (*14*).

The loss of markers from pavements is primarily due to their inability to repeatedly absorb the total force imposed on them and transmit it to the pavement. Environmental and material related factors aid fracture in the pavement around the epoxy pad holding the markers to the surface. After some hits, the RRPM, along with some adhesive and asphalt, comes off the surface. Strengthening the pavement, redesigning the marker to reduce impact forces, and using an adhesive that better absorbs shock forces may increase retention of RRPMs (*14*).

Tielking and Noel (*3*) performed a study to increase the retention time of RRPMs on the asphalt concrete pavement surfaces. They observed the fatigue characteristics of asphalt pavements under the repetitive loads imparted by tires. The study hypothesized that a fatigue failure in the pavement surface limits a marker's retention time. They designed a fatigue test to simulate the repetitive loads that a marker imparts to the pavement, when hit by a car or truck tire. The test consisted of alternating loads that imparted a rocking motion to the marker installed on the asphalt surface. This generated both compressive and tensile stresses in asphalt under the plate (*3*). They found that the adhesive used to attach the marker influenced the fatigue strength of asphalt concrete. A softer adhesive such as bitumen would give new asphalt pavement (a more flexible pavement) longer fatigue life than a hard adhesive like epoxy. The advantages of bitumen decreased as pavement stiffness increased and as the input stress level increased. This meant that on high-traffic roads, bitumen would be less effective (*3*).

They also conducted a high-speed photography to evaluate the kinematics of tire-marker impacts. They found that a small high-pressure car tire did not bound over the marker but instead stayed in contact over entire top surface of the marker and remained in contact over the sloping exit surface. A truck tire was more likely to remain on top of a marker than a passenger car tire (*3*). They developed an instrumented hit marker as a part of this study to measure the number of hits a marker gets. This helped to relate the laboratory fatigue studies to retention time on a highway (*3*).

In the same study, they established that the most critical condition for pavement in terms of negative moment produced is the application of a vertical force on the edge of the non-reflectorized side. Assuming a marker completely rigid and perfectly attached to the surface of the pavement, the pavement force pattern would be like a uniform load of P/L (P being the tire load and L being the width of marker) and a triangular load of M on the marker top (*3*). Figure 7 and Figure 8 illustrate this concept.

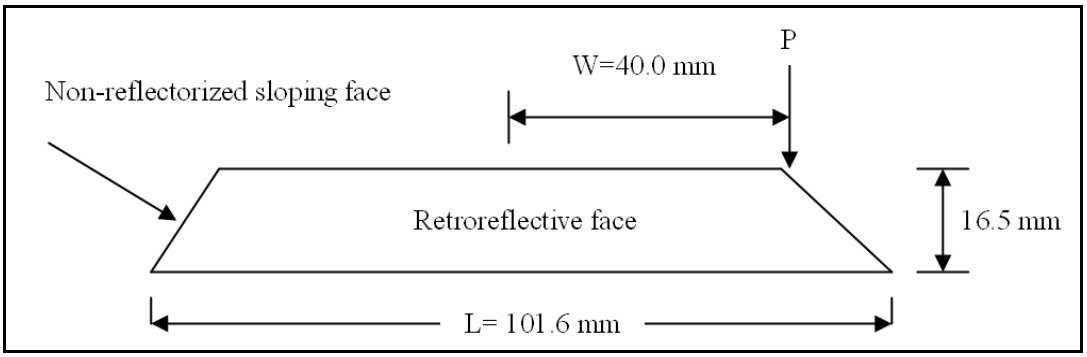

FIGURE 7 One critical force condition during a tire-marker impact (*3*).

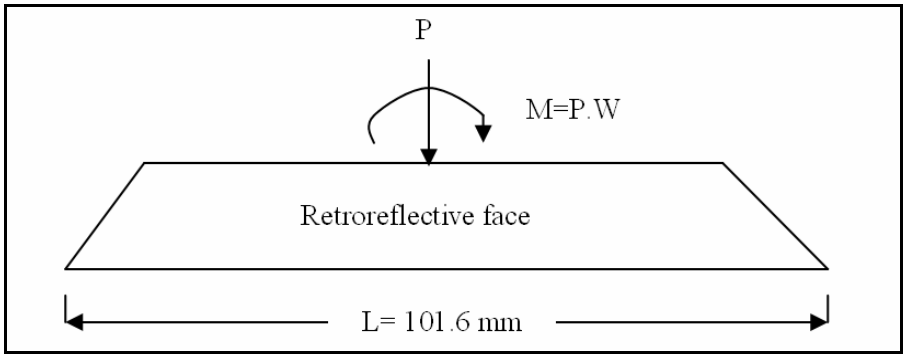

FIGURE 8 Force translation for the critical force condition (*3*).

Loss of Retroreflectivity

The primary causes for loss of retroreflectivity in RRPMs are abrasion of the retroreflective surfaces, dirt accumulation, extruded adhesives on the retroreflective surfaces, and their structural deterioration causing wear and breakage. Retroreflectivity loss may occur because of worn, missing, dirt covered or cracked lenses, or due to softening of filler in hot weather. The loss of retroreflectivity directly relates to the problem of retention and hence, high volume and high truck traffic are detrimental to retroreflectivity as well. Other factors are humidity (improper sealing can allow seepage of water into the marker causing reduction in retroreflectivity) and poor drainage (causing submergence of markers). During wet weather, the retroreflectivity may increase due to the clean up of dirt (*13*).

Pezoldt (*4*) conducted a study evaluating the retroreflectivity decay of RRPMs. He observed that physical damage to the retroreflective surface was the primary factor for decline in the retroreflectivity. He found that glass-faced markers faired better than the plastic ones. On the plastic-faced RRPMs subjected to abrasion, myriads of scratches

scatter light instead of transmitting it directly to reflective cube-corner prism array, hence causing loss in retroreflectivity. However, the glass-faced markers can get shattered with tire-marker impacts, thus causing loss in their retroreflectivities. The plastic face beneath the glass surface in the lens acts like an original all-plastic RRPM. Thus, a glass-faced marker with several chipped or broken areas may still perform better than a plastic-faced marker (*4*).

Ullman did a two-year evaluation of retroreflectivity of RRPMs in Texas and tried to correlate the field measurements and laboratory tests of retroreflectivities (*5, 16, 17*). The major findings were:

- Loss of retroreflectivity was largely dependent on the number of tire impacts, which is a function of traffic volume, especially truck traffic.
- Dirt accumulation was a major cause of loss of retroreflectivity, but it is prominent only in initial degradation in retroreflectivity. After a period, the marker lenses abrade due to a number of impacts.
- The glass-faced RRPMs performed better than the plastic ones.

DISTRICT SURVEYS

The TTI research project team conducted a survey of TxDOT district staff. The team chose a randomly selected sample of district staff. The team asked the engineers a few questions regarding the state of RRPMs in their respective districts, and to list the main causes that they thought would have caused the deterioration of RRPMs (Appendix A). From their responses, we found that:

1. The markers' performance varied with the traffic on highways. On high volume Interstate highways, many makers did not last for more than a year. In some of the districts, the markers did not last for more than 6 months. Most of the districts replaced or would have preferred to have replaced the markers every year on Interstates. On lower volume Farm-to-Market (FM) roads and state highways, the markers lasted for 3-5 years.
2. There was no consensus on the most frequent mode of marker failure. Lens failure, marker loss (off the pavement), and marker breakage were the major failures. A few times the pavement failed beneath the marker, removing the marker, adhesive, and some portion of the pavement.
3. The major factors accounting for marker failures were high traffic volume (urban area/intersections) and truck traffic. The type of pavement surface was a factor as well. All the districts had problem with the seal coat surface treatment, which uses a large rock. Environment was not a major concern, though some districts had problems with hot and rainy weather. The markers could be punched into the pavement in hot weather while rain could allow moisture to enter RRPMs through cracks causing retroreflectivity losses.
4. A few districts had a mass failure problem on a few projects where many markers failed just after installation. Poor installation practices were the primary cause of failure (e.g. using bitumen for concrete and epoxy for asphalt pavement surface).

5. Officials suggested improving the durability of lenses. Often the lens was damaged causing loss of retroreflectivity even though the marker body was intact with the pavement. They suggested an improvement in laboratory testing procedures for RRPMs. Some of them did not consider the American Society of Testing and Materials (ASTM) tests (*6*) to be adequate tests of the RRPMs. They thought that improved tests were needed which could simulate the vehicular forces on markers.

TESTING PRACTICES

In this subsection, the researcher discusses various laboratory and field tests on RRPMs done by different state and national agencies. They perform these tests on samples of markers before they can be installed on the roadways. The researcher focuses here on those tests that concern with structural performance of RRPMs.

The ASTM provides standard specifications for non-snowplowable RRPMs (*6*). Most state agencies follow the testing practices provided by ASTM. ASTM standard D 4280 (*6*) includes a longitudinal flexural test, a compression test, and a resistance to lens cracking test.

In the longitudinal flexural test or three-point bending test, the marker is placed on two steel bars each longer than the width of the marker base (*6*). The bars are kept at such a distance that they do not protrude beyond length of the marker. The traffic direction of the marker is perpendicular to the bars. A steel bar, wider than the marker and parallel to other bars, is placed on centered top of the marker. Elastomeric pads of

appropriate dimensions (minimum 3.175 mm or 1/8 inches thick) are provided between the bars and the marker. A load of 5.08 mm (0.2 inch) per minute is applied through top steel until the marker breaks. Figure 9 shows the experimental setup for this test.

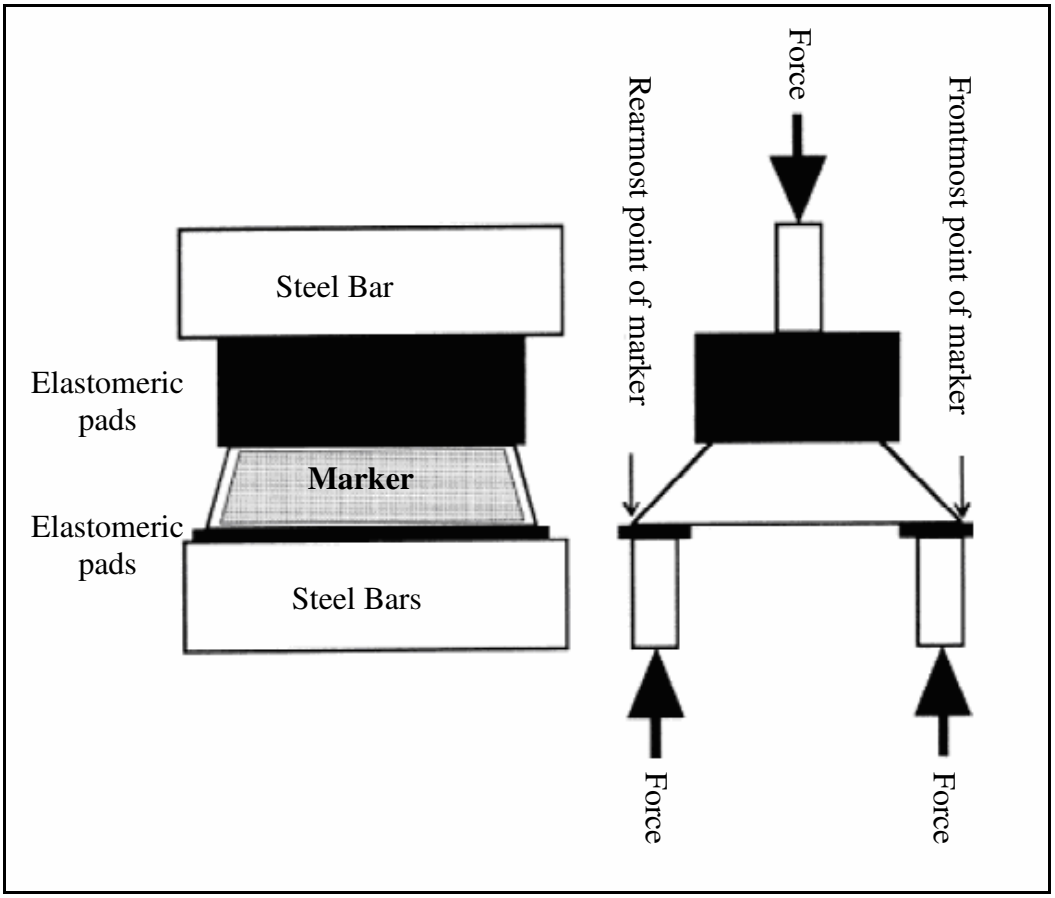

FIGURE 9 Longitudinal flexure test (*6*).

In the compression test (*6*), the marker is placed between two 12.70 mm (0.5 inches) thick steel plates larger than the marker. Elastomeric pads of appropriate dimensions are placed between the marker and the plates. Then, a load is applied at a rate of 2.54 mm (0.1 inches) per minute on the upper plate.

In the resistance to lens cracking test, a 0.19 kg (0.42-lb) dart fitted with a 6.35 mm (0.25-in) radius semi-spherical head is dropped from 457.20 mm (18 inches) height, perpendicularly onto the retroreflective surface of the marker (*6*). The marker is placed on a steel fixture designed to hold the retroreflective face horizontal (*6*).

Some states perform other tests in addition to these tests or perform some variations of ASTM tests. For instance, California (*18*) requires a water absorption test in which the marker is kept in water for 48 hours and then examined for any delamination or loss of retroreflection.

The American Association of State Highway and Transportation (AASHTO) officials voluntarily evaluate the laboratory and field performance of RRPMs (*19*). The plan, known as National Transportation Product Evaluation Program (NTPEP), evaluates the markers on a 0-5 scale with 0 for a marker that is absent to 5 for a marker present with structural integrity and retroreflectivity intact. Manufacturers may choose to have their products evaluated by this plan.

TIRE-OBSTRUCTIONS CONTACT FORCES

To understand the wear of RRPMs by tire impacts, it is important to study the effects of tire forces on small obstructions on roads. Many researchers have tried to understand tire-road interactions (*20, 21, 22, 23, 24, 25*), often using finite element methods. A few have tried to estimate dynamic forces produced when tires encounter large obstacles (*26*) or irregularities (*27*).

Bonse and Kuhn developed an apparatus for measuring the forces exerted at a point on the road surface by the tires of moving vehicles (*28*). They also investigated the influence of tire inflation pressures, speeds, accelerations, tire loads, height of the stud (a small obstacle, circular and 25.4 mm in diameter in this study) above road surface, etc. on these forces. They concluded that the inflation pressure and stud height influenced the vertical force (Figure 10). The figure shows that an increase in the height of stud increases the vertical force. In addition, the force increases away from the centre of the tread and then decreases at the edges.

In another study, Hansen et al. (*29*) found that an increase in the inflation pressure increase (at constant tire load) resulted in increase in the contact pressure in the tread's central region. Increased tire load (constant inflation pressure) resulted in lengthening of the contact patch (*29*).

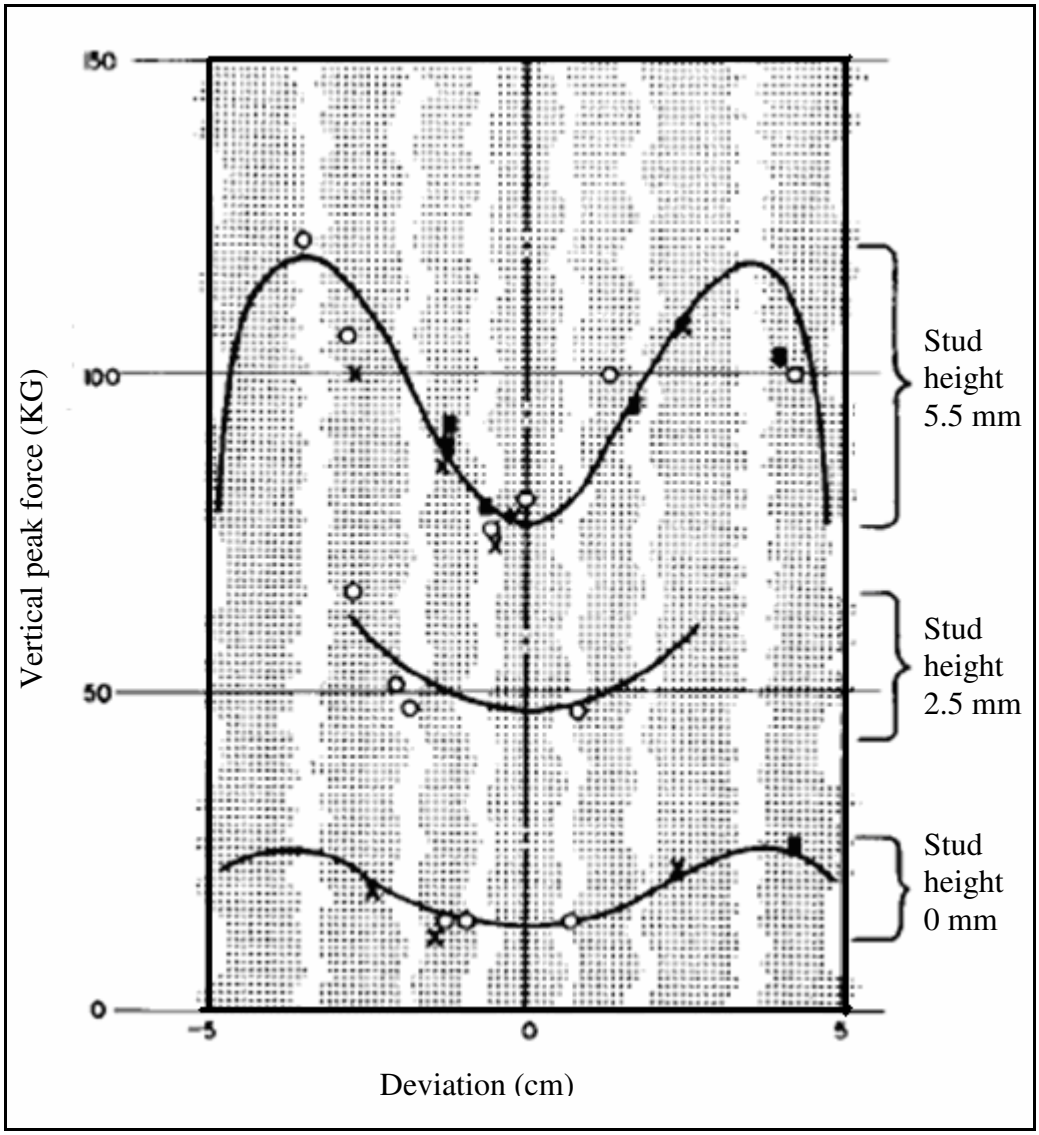

FIGURE 10 Influence of stud height on the transverse distribution of vertical force (*28*).

FINITE ELEMENT ANALYSIS-BASICS

The finite element analysis (FEA) has been in use for many centuries (*30)*. It involves replacing a complex system with a simpler but an approximately accurate representation. FEA was initially used for simple physical problems, but the advent of advanced

computer technology allows it to be applied to broad areas and problems. Martin has outlined the development of modern finite element method (*30*). Earlier, FEA was used in analyzing static and dynamic problems associated with aircrafts. In the1940s, when jet power aircrafts appeared, previous analytical techniques became obsolete in wake of improved speed and design (*30*). This led to broad application of FEA. Especially as the solution of complex problems required solving derivatives, which was tedious and difficult, approximate methods like FEA gained importance. In FEA, a differential equation is approximated by expressing derivatives in terms of the formulae obtained by the Taylor series expansion of a function (*30*). Boundary conditions, based on the solutions at discrete points, are imposed on the resulting algebraic equations (*30*).

To understand the basic concepts of FEA, let us consider the problem of estimating the circumference of a circle (*30*, *31*). One way this can be done is to break the circumference into easily measurable segments (Figure 11). It is similar to FEA, in which the domain is separated into separate sub-domains, the process being called discretization. Each sub-domain is called an element. Points, known as nodes, connect the elements. The collection of elements and nodes is called as finite element mesh. In this problem, the perimeter of the circle can be approximated as $P = (2R\sin(\theta/2))n$, where R is the radius of the circle and θ or $(2\pi/n)$ is the angle subtended at the center by the element. The error of the solution would be $\varepsilon = 2\pi R - P$ which will converge to zero as n approaches to infinity. Hence, the solution improves as the number of finite elements increases (*30*, *31*).

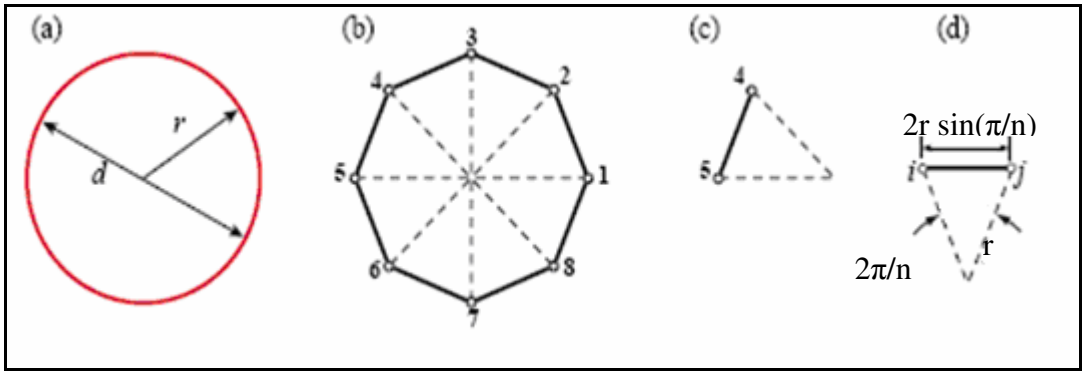

FIGURE 11 A simple example illustrating FEM (*31*).

FEA allows researchers to handle complex structures, even those with variable material or geometric properties. It can handle non-linear and time dependent properties. In short, FEA is a very powerful tool to solve boundary-value problems in complex domains (*30*). It has applications in civil engineering structures, aviation, heat conduction, geomechanics, hydraulics, nuclear engineering, biomedical engineering, and mechanical design (*32*, *33*, *34*).

This study uses FEM (modeling based on the FEA) for understanding tire-marker impacts. The dynamics of these impacts makes it difficult to measure the actual magnitudes and location of stresses generated in markers during impacts. FEM as a proven tool provides an opportunity to analyze these impacts in a cost and time efficient manner. The next section details the tools and methodology adopted in this research work.

METHODOLOGY

This research utilizes finite element tools to simulate tire-marker impacts in the real world and then analyze the results of those simulations to recommend ideal laboratory procedures for RRPM testing. Prior to start of this research work, the researcher had discussions with the experts at the Center of Excellence in Transportation Computational Mechanics of TTI about finding locations and magnitudes of stresses in RRPMs during the tire-marker impacts. It was found from the discussions that FEM of the tire-marker impacts would be a convenient and efficient solution for the problem. Hence, the researcher implemented the FEM of the tire-marker impacts.

Any finite element tool or code has three stages: pre-processing, processing and post-processing. The finite element tools used in this study are Hypermesh for pre-processing, LS-DYNA for processing and Hyperview for post-processing. Hypermesh (a finite element meshing tool) is a pre-processor for FEA applications (*35*). Meshing is the process of building a grid of finite elements bound by the model geometry. Hypermesh supports major finite element solvers like LS DYNA. The LS-DYNA is a general-purpose dynamic finite element program (*36*). It can simulate complex real world problems. It is widely used by the automotive industry to analyze vehicle design and by safety researchers for testing strengths of crash barriers. Its applications also lie in the aerospace industry, sheet metal forming etc. Post-processing was done on Hyperview. The Hyperview enables visual and interactive analysis of simulation results (*37*). The

researcher chose these tools as they were suitable for simulating dynamic forces on RRPMs as happened in real-world conditions.

This section first describes the modeling process, which included preliminary modeling and input parameters collection for the final model. Next, the section describes the calibration of the model to get accurate estimates of material properties. The researcher then describes the simulation of tire-marker impacts. The last subsection discusses the simulation of laboratory conditions, which the researcher developed and modeled in an attempt to replicate the stresses generated in markers during the tire-marker impacts.

MODELING

As a part of this task, the researcher first obtained a preliminary tire-RRPM model and gathered information required to initiate the modeling and simulation of tire-marker impacts. Dr Akram Abu-Odeh, an expert at the Center of Excellence in Transportation Computational Mechanics of TTI, made the preliminary model. Figure 12 shows the model.

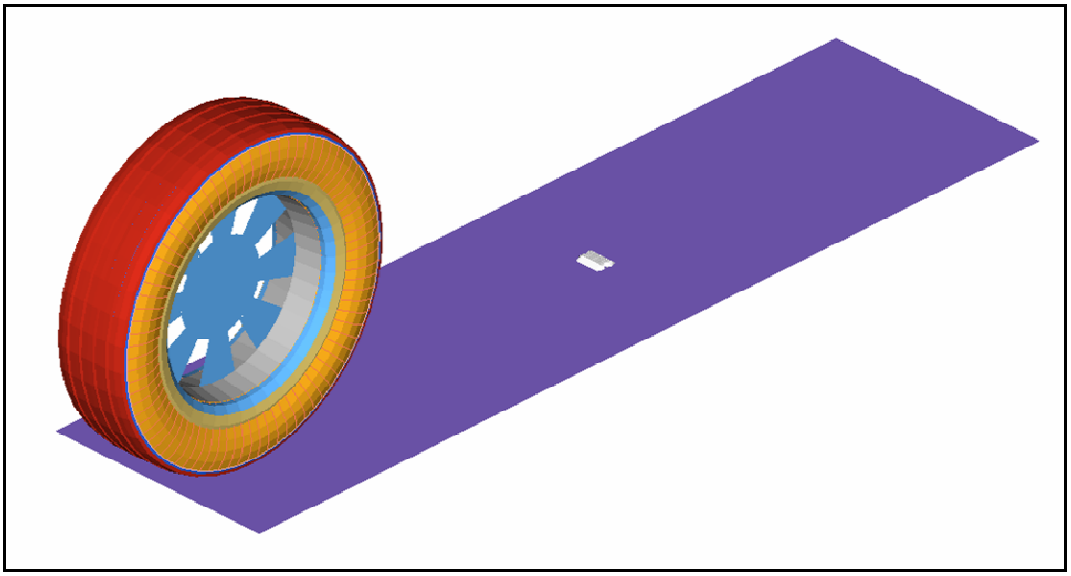

FIGURE 12 Preliminary finite element model of tire-marker impacts.

The model contains three major components: a tire (radius=525 mm), a marker, and the pavement. The tire contains various components like tire tread, rim, shell, steel sidewalls etc (More details on the tire components and properties would be available with the Dr Abu-Odeh). The marker in the preliminary model was a rigid object and did not have any constitutive material properties. Later versions of this model had finite element models of the RRPMs. The pavement was modeled as a rigid surface. Hence, it is emphasized that the analyses and results from this research work would be more applicable to the tire-marker impacts on the rigid (concrete) pavements than on the flexible (asphalt) pavements.

The following inputs were defined for the model.

- Components-tire, marker, and pavement;
- Geometry for components;
- Material and section properties;

- Loading conditions like tire weight; and
- Initial conditions like tire load, velocity, impact angle and impact location.

The researcher did FEM of the tire-marker impacts from this preliminary model. The FEM of the tire-RRPM impacts was necessary to identify the locations and magnitudes of stresses inside the RRPMs. The researcher used three RRPM brands for the study, which are described as RRPM Type A (Figure 13), Type B (Figure 14), and Type C (Figure 15).

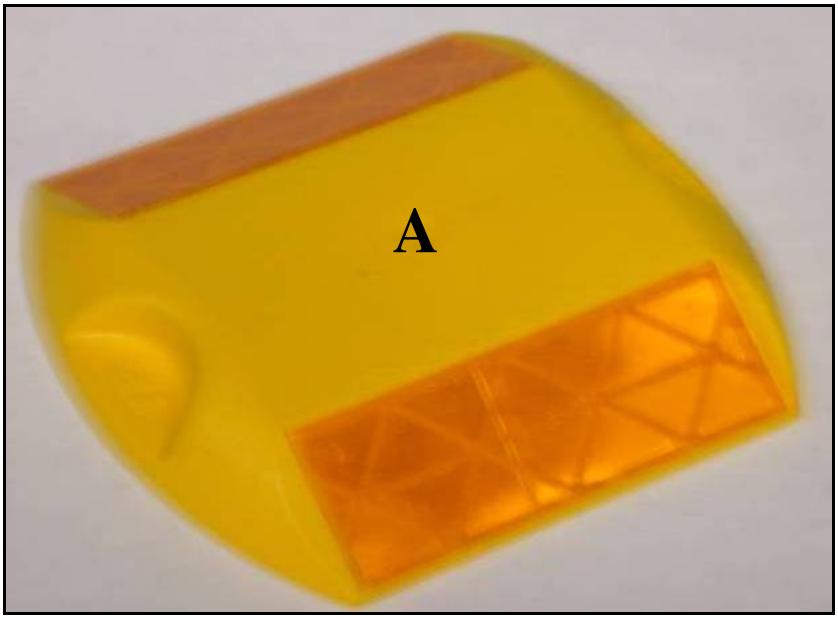

FIGURE 13 RRPM Type A.

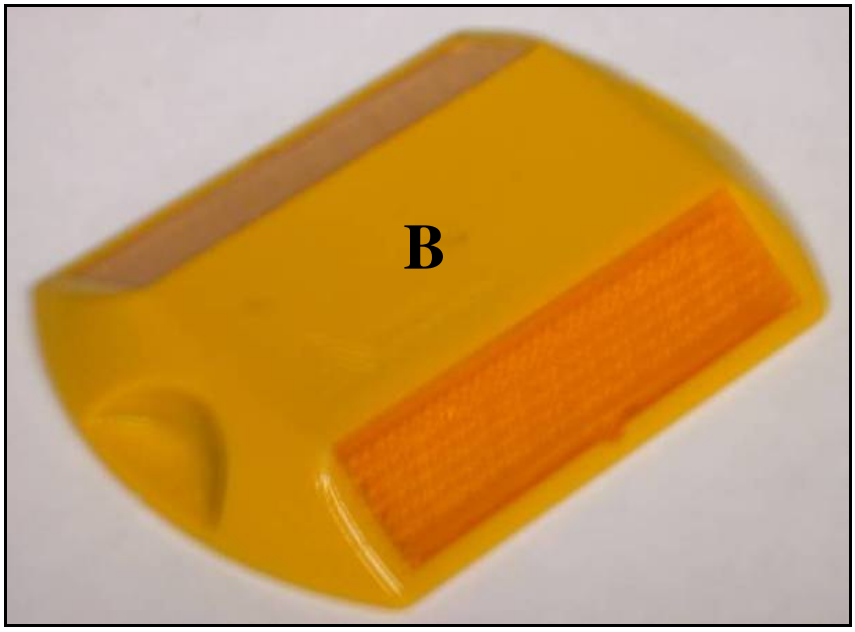

FIGURE 14 RRPM Type B.

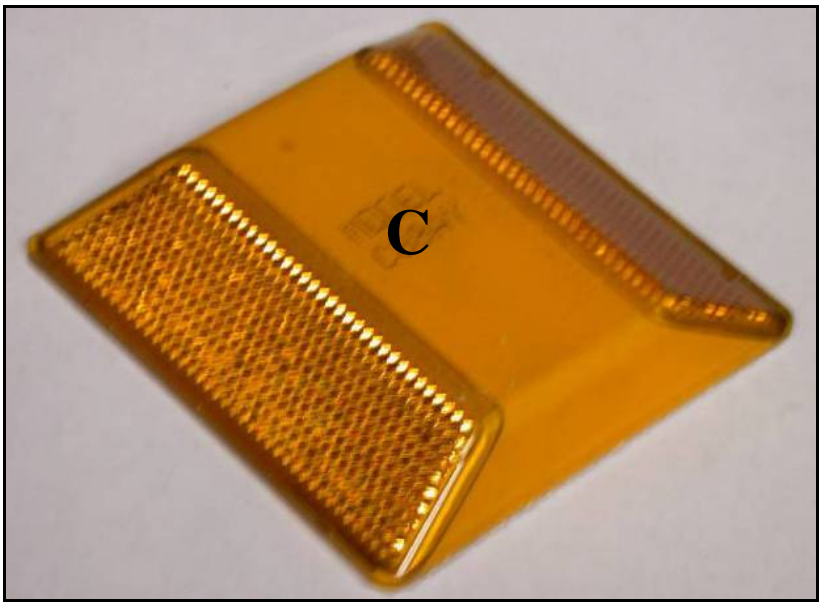

FIGURE 15 RRPM Type C.

The researcher meshed the three RRPM Types using Hypermesh. In Hypermesh, a finite element model consists of components called collectors. Every collector is

assigned attributes, depending on the kinds of materials (e.g.elastic, plastic etc.) or sections (e.g. solid, shell etc.) it has. These attributes are identified by inbuilt templates called as 'card images'. Table 1 lists the card images for the finite element models of the three RRPM Types. In the Table, MAT 24 refers to the material card image 'mat_piecewise_linear_plastciity'. This card image is used to define material properties for the elasto-plastic materials. The minimum properties required for this material kind are density, Poisson ratio, elastic modulus, and yield stress. In addition, the stress-strain curve can be defined for this material kind. MAT 96 refers to the material card image 'mat_brittle_damage'. This card image is used to identify materials that show brittle damage. The minimum properties required for this material kind are density, Poisson ratio, and elastic modulus. The 'Section_shell' and 'Section_solid' card images define the shell and solid finite element models respectively. After defining the card images described above, the researcher meshed the geometries of the RRPM Types by 2-D and 3-D finite elements as applicable. Figure 16, Figure 17, and Figure 18 show the finite element meshes for the three RRPM Types A, B, and C.

TABLE 1 Components and Card Images for the RRPM Types A, B, and C

RRPM Type	Component	Material card image	Section card image
Type A	Body+lens	Elasto-plastic material (MAT 24)	Section_shell
Type B	Body	Elasto-plastic material (MAT 24)	Section_shell
	Lens	Elasto-plastic material (MAT 24)	Section_shell
Type C	Body (Filler)	Brittle (MAT 96)	Section_solid
	Body (Shell)+lens	Elasto-plastic material (MAT 24)	Section_shell

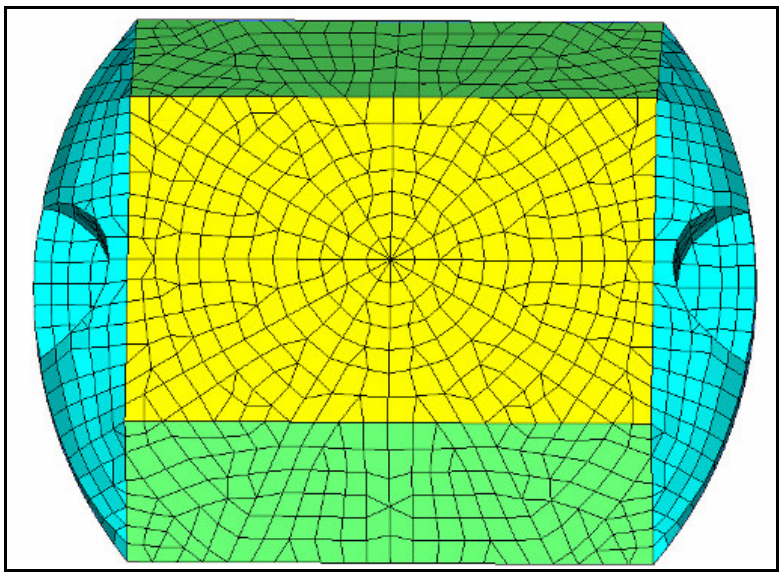

FIGURE 16 RRPM Type A mesh.

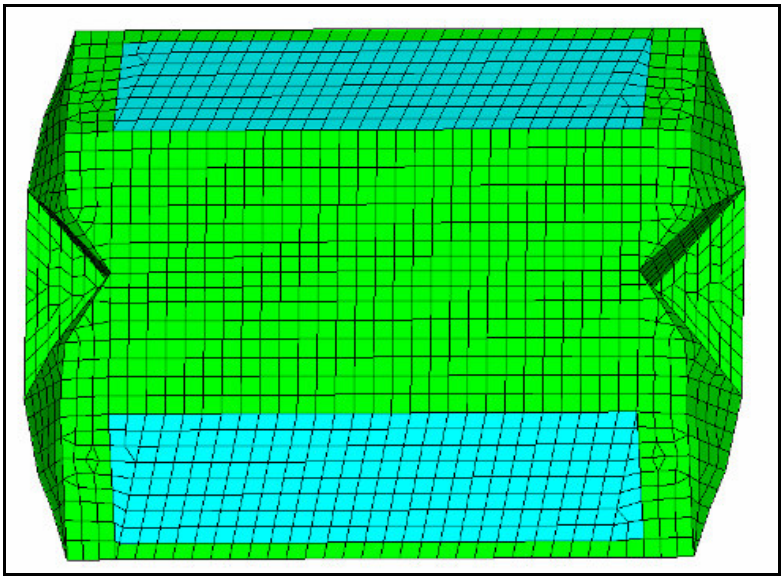

FIGURE 17 RRPM Type B mesh.

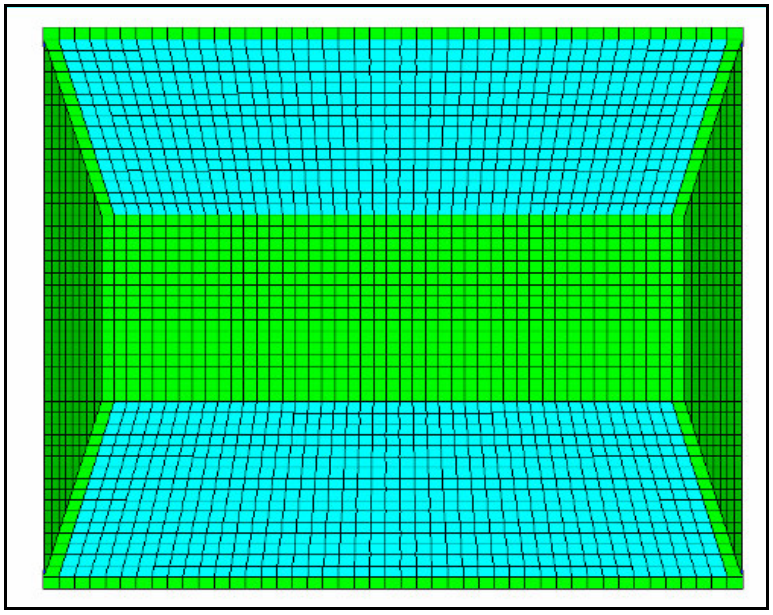

FIGURE 18 RRPM Type C mesh.

After meshing, the researcher needed constitutive chemical composition and material properties of different components of markers like tensile strength, compressive strength, modulus of elasticity, modulus of rigidity, etc., for accurate modeling of tire-marker impacts. Initially the researcher intended to perform laboratory tests on some markers to get their chemical composition and material properties. For this purpose, the researcher cut open some markers. Figure 19 shows how the markers were cut. The idea was to use the components of markers as specimens for getting constitutive material properties for the markers.

FIGURE 19 Marker body being cut.

However, from discussions with various experts, the researcher found that such laboratory testing is infeasible or impractical. The components were either too small or needed significant modifications to be converted into test specimens. Hence, the researcher took information from RRPM manufacturers and literary sources like online databases for the material properties.

Table 2, Table 3, and Table 4 provide the material properties used in the modeling process. In the tables, '[a]' refers to the material properties obtained from the manufacturers and '[b]' refers to the properties found from the online databases. Since this information was not based on any laboratory test performed by the researcher, it was considered useful for preliminary purposes only. Calibration was necessary to get accurate estimates of the material properties.

TABLE 2 Pre-calibration RRPM Type A Material Properties

Body and Lens (acrylic)[a]		
Density	1.35E-09	Metric tons/ mm^3
Young's modulus	5800	MPa
Poisson ratio	0.35	-
Yield strength	80	MPa

TABLE 3 Pre-calibration RRPM Type B Material Properties

Body (acrylic)[b]		
Density	1.04E-09	Metric tons/ mm^3
Young's modulus	2100	MPa
Poisson ratio	0.35	-
Yield strength	44	MPa
Lens (acrylic)[a]		
Density	1.19E-09	Metric tons/ mm^3
Young's modulus	3103	MPa
Poisson ratio	0.11	-
Yield strength	70	MPa

TABLE 4 Pre-calibration RRPM Type C Material Properties

Body (resin filler)[b]		
Density	1.10E-09	Metric tons/ mm^3
Young's modulus	2500	MPa
Poisson ratio	0.35	-
Shell and Lens (acrylic)[a]		
Density	1.19E-09	Metric tons/ mm^3
Young's modulus	3103	MPa
Poisson ratio	0.11	-
Yield strength	70	MPa

CALIBRATION

Model calibration was necessary to get accurate estimates of constitutive material properties of markers. This step gained more significance for the research as accurate data about the material properties was not available.

The researcher had several plans to calibrate the model. For instance, a load cell could give an estimate of the magnitude of contact forces on markers during the impacts from tires. It is a small cylindrical device, which can measure the global forces in x, y and z directions applied on it. A marker would be placed on it and then a tire would be made to run over it. It would then give magnitudes of the global forces on the marker that can be compared with the simulation results. However, the researcher rejected the idea as a load cell only gave the magnitudes of the global forces on the markers and not stresses or strains inside them.

A better way to calibrate the model would be to get the estimates for stresses and strains inside the RRPMs during the tire-marker impacts and then compare them with simulation results. Strain gauges could be used to measure these strains. From discussions with experts, the researcher found that estimation of strains using strain gauges in real tire-marker impacts was quite impractical. The impact of a tire over a marker could break the sensitive strain gauges. In addition, there were many external factors in the field that could not be controlled and thus would have affected the calibration process.

The researcher decided to calibrate the model using a laboratory set-up. It was a more practical and controlled way of calibrating the model. This way the researcher

could focus on calibrating intrinsic properties of markers while controlling external variables. In addition, the researcher could control damage to the strain gauges in laboratory conditions far better than in real-world environment.

The researcher designed a laboratory experimental setup for the calibration. The set-up was same as the ASTM D 4280 longitudinal flexural test for testing the markers (described on page 25) (*6*). Figure 20 and Figure 21 show the experimental setup.

FIGURE 20 Calibration test set-up.

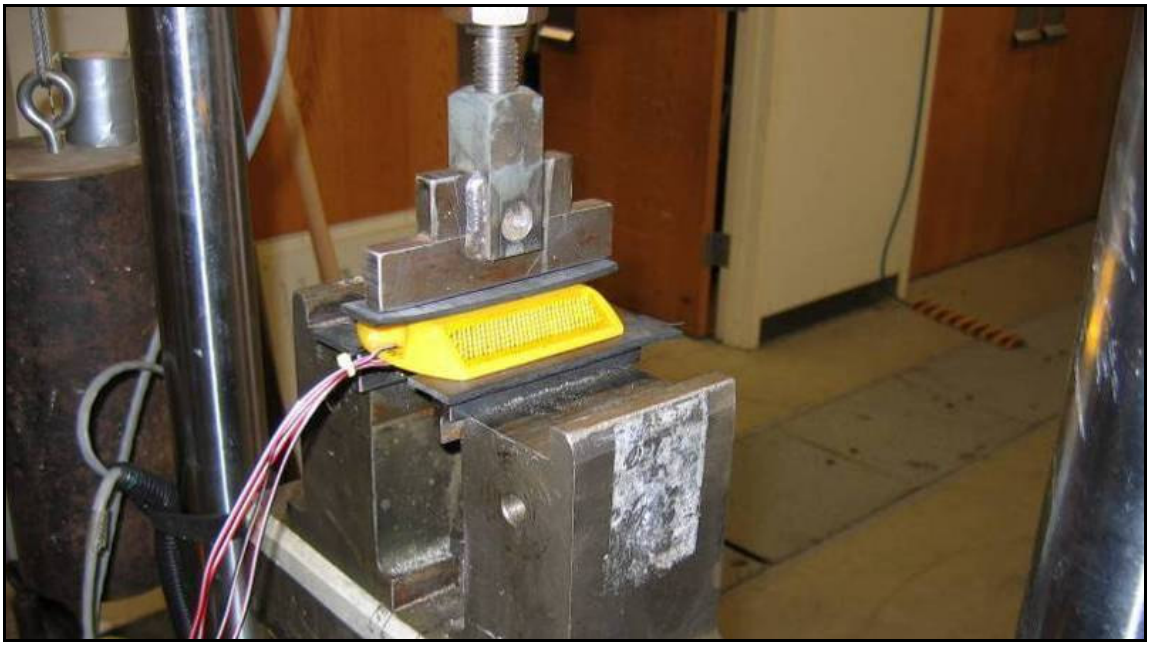

FIGURE 21 Calibration test set-up (close view).

The researcher put six strain gauges on each marker during the experiment. The strain gauges measured the strains in a pre-determined direction at the installed location on the marker. Figure 22, Figure 23, Figure 24, and Figure 25 show the arrangement of strain gauges on the markers.

The experiment results provided time plots of the magnitudes of displacement of the top steel bar and strains from the strain gauges.

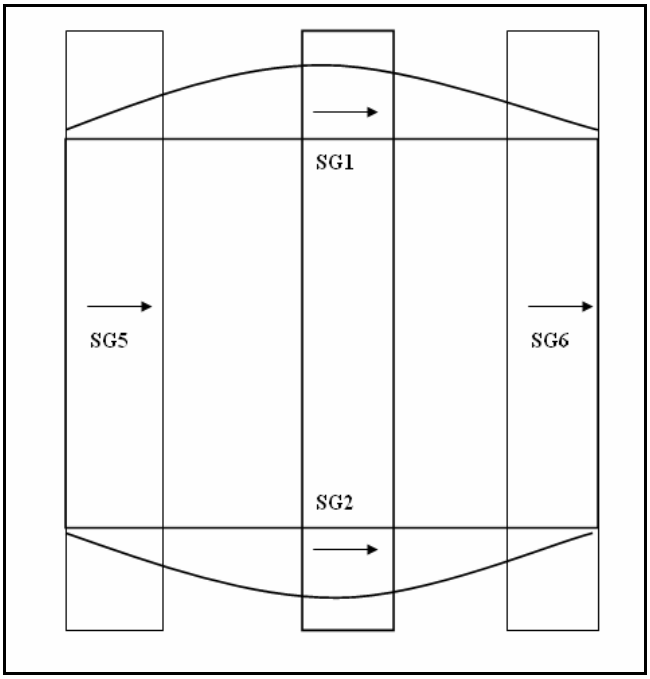

FIGURE 22 Strain gauged marker (top view).

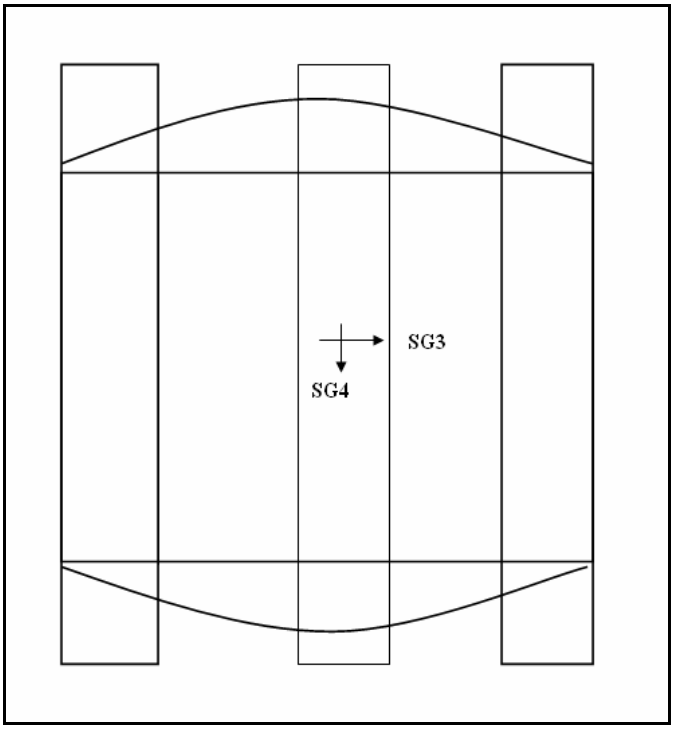

FIGURE 23 Strain gauged marker (bottom view).

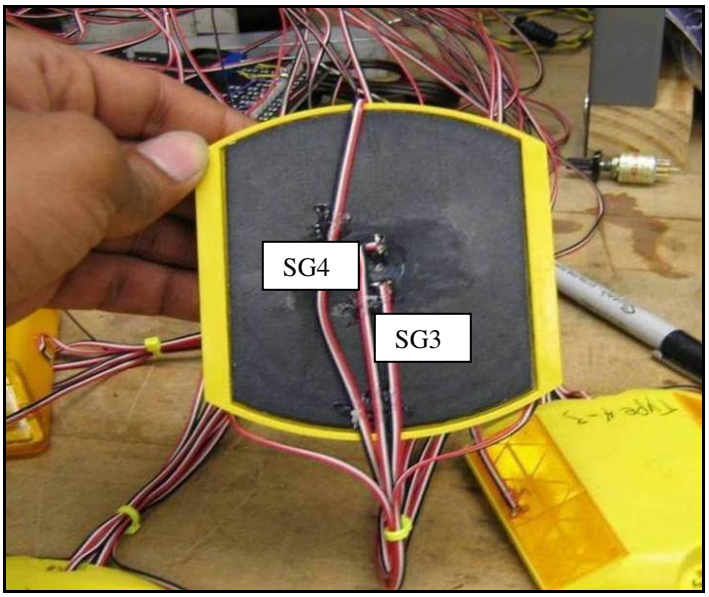

FIGURE 24 Arrangement for strain gauges 3 and 4.

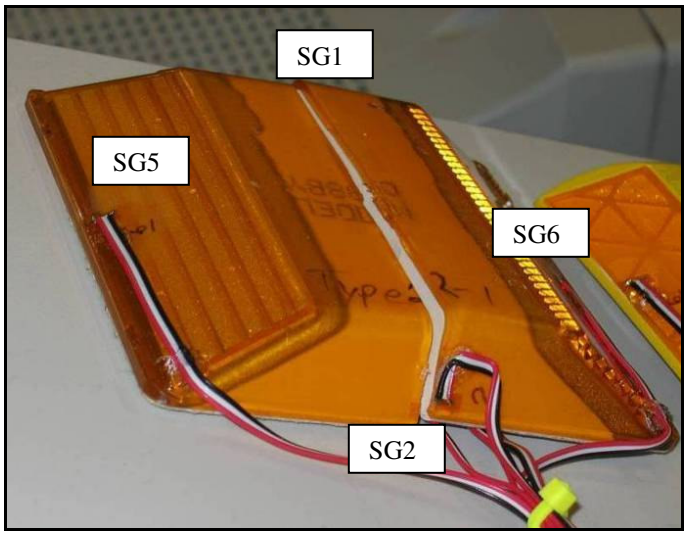

FIGURE 25 Arrangement for strain gauges 1, 2, 5, and 6.

The researcher then made a finite element model of the laboratory setup (with the same boundary conditions as in the experimental setup). The researcher did this so that he could compare the results from the simulation and experiment and adjust the material properties until the models were calibrated. The modeling was done on Hypermesh and the simulation was run on LS-DYNA. The modeling process for the RRPM Types has been described earlier (page 36). The finite element model for the calibration test had steel bars and elastomeric pads in addition to the RRPM models. The card image for the steel bars was MAT 20 (suitable for rigid materials) while the card image for the elastomeric pads was MAT 24 (suitable for elasto-plastic materials).

Once the meshing was completed, the next and final step was to assign boundary conditions and define the nature of contacts, if any. A boundary condition was applied at the top steel bar to displace it at a rate of 5.08 mm (0.2 inches per minute) in the downward z-direction (vertical direction). The card image for the boundary condition was 'boundary_prescribed_motion_rigid'. This card image is applicable for a node or a set of nodes belonging to a rigid body. Since, the top steel bar in the calibration was modeled as rigid, this card image applied well to it. The bottom steel bars were constrained in the z-direction (vertical direction). The researcher defined a surface contact between the steel bars (load and mount bars) and the marker models. The card image for the contact was 'automatic_single_surface', which is used for surface contacts with no orientation. The static and dynamic coefficients of friction between the steel bars and the marker surfaces were kept as 0.15.

Figure 26 shows the finite element model for calibration test for the RRPM Type A. and the Hypermesh interface.

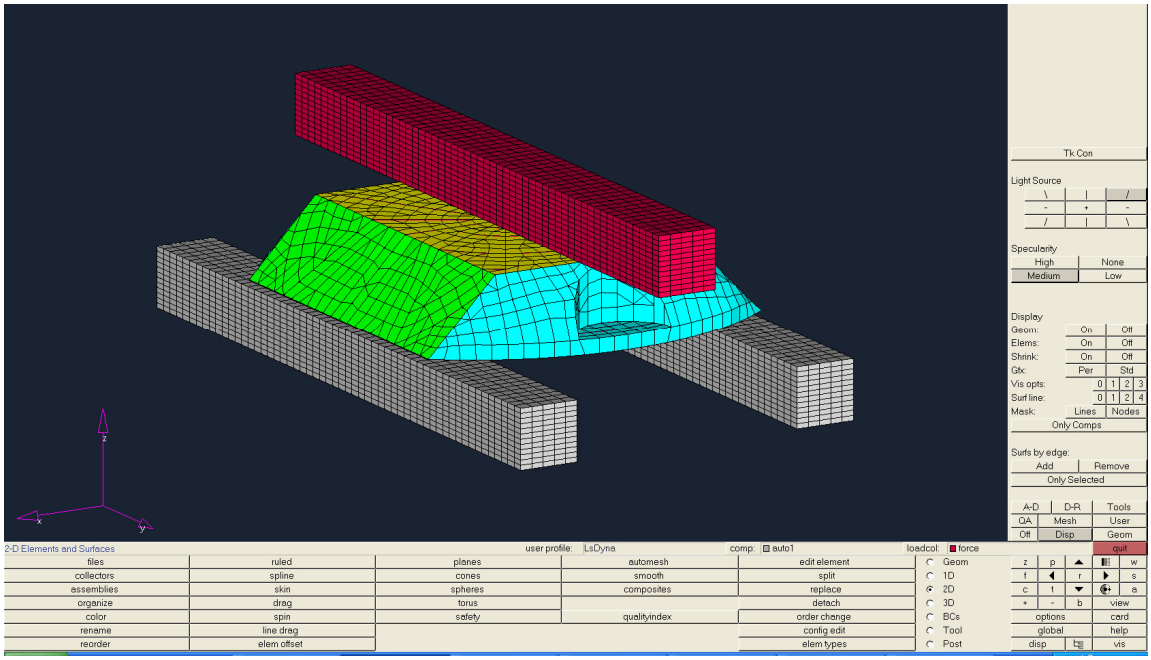

FIGURE 26 Calibration test model for the RRPM Type A in the Hypermesh interface (The top bar represents loading bar and the bottom bars represent mount bars).

The computer simulation provided stresses and strains inside the markers as the load was applied. The researcher compared these results from the simulations to those from the experiments: (a) displacement of top surface of the marker and (b) strains at the locations marked by strain gauges 1-6. The major criterion for calibration was that experimental and simulation displacements of top surfaces of the markers should be within 10 percent. The other results (i.e. strains) were primarily to reinforce the calibration.

The only control variables during the calibration process were intrinsic material properties of the markers. The researcher kept properties of the steel beam and elastomeric pads constant during the calibration process. Table 5 provides their properties as used in the experiment.

TABLE 5 Steel Beam and Elastomeric Pad Properties

Steel beam		
Density	7.85E-09	Metric tons/ mm^3
Young's Modulus	205000	MPa
Poisson ratio	0.29	-
Elastomeric pad		
Density	1.35E-09	Metric tons/ mm^3
Young's Modulus	1000	MPa
Poisson ratio	0.47	-
Yield Strength	50	MPa

The researcher varied intrinsic material properties of the markers (the ones listed in the Table 2, Table 3, and Table 4 on page 40) so that results of the computer simulation were in a reasonable range of results of the laboratory test. Appendix B (page

124) provides comparisons of results from the simulations and experiments. The solid curves in all the plots show the experimental results while the dotted curves show the simulation results.

The researcher did not do any quantitative analysis for comparing the theoretical and experimental strains as the comparisons between the two strains were for reinforcing the major calibration criterion only (as mentioned on last page). A visual inspection of the comparisons was performed instead. Good agreement between the strain magnitudes was achieved if the two curves for the strains were close to each other. There was an average agreement between the two strains if the two curves were at some reasonable distance from each other. A poor agreement was classified when curves were too far from each other.

The results show that:

- For RRPM Type A, there was a difference of less than 10 percent between displacements of top surfaces of the marker when simulation results were compared with experimental results (Appendix B, Figure 64). There was average agreement between the results for strain gauges 3 and 4 (Appendix B, Figure 66), and good agreement for strain gauges 5 and 6 (Appendix B, Figure 67). The results did not compare well for strain gauges 1 and 2 (Appendix B, Figure 65).
- For RRPM Type B, again there was a difference of less than 10 percent between displacements of top surfaces of the marker when simulation results were compared with experimental results (Appendix B, Figure

68). There was good agreement between the results for strain gauges 3 and 4 (Appendix B, Figure 70), and 5 and 6 (Appendix B, Figure 71). The results did not compare well for strain gauges 1 and 2 (Appendix B, Figure 69).

- For RRPM Type C, the results are similar to the RRPM Type A. There was a difference of less than 10 percent between displacements of top surfaces of the marker when simulation results were compared with experimental results (Appendix B, Figure 72). There was an average agreement between the results for strain gauges 3 and 4 (Appendix B, Figure 74), and a good agreement for strain gauges 5 and 6 (Appendix B, Figure 75). The results did not compare well for strain gauges 1 and 2 (Appendix B, Figure 73).

The researcher considered the models calibrated based on the observations as listed above. However, the calibration was not a perfect process, as evident from the results. There were a few constraints during the calibration that limited the accuracy of the results:

- It is possible that there was some experimental error, which would have caused the strains in strain gauges 1 and 2 to be far off from the simulation strains at the corresponding locations.
- All material properties were based on input from the manufacturers and online material databases. Getting accurate estimates of material properties is very necessary for getting the models right and the inability

of the researcher to obtain these properties limited the accuracy of the calibration part.

- The researcher used only online sources (and no input from manufacturers) for getting properties for the filler resin in RRPM Type C. Hence, results for RRPM Type C should be viewed with more caution.
- The finite element solvers themselves have their limitations, which can reduce the model accuracy. For example, simulating quasistatic loading conditions in LS-DYNA, as in the calibration test simulation, would take a long time. Hence, some compromise with respect to accuracy had to be made in getting the results in reasonable times. In addition to that, every model approximates reality, hence leading to differences with actual conditions.

Table 6, Table 7, and Table 8 provide the post-calibration material properties for the RRPM Types A, B, and C respectively. The values in the parentheses are the pre-calibration material properties.

TABLE 6 Post-calibration RRPM Type A Material Properties

Body and Lens		
Density	1.30E-09 (1.35E-09)	Metric tons/ mm^3
Young's modulus	3500 (5800)	MPa
Poisson ratio	0.35 (0.35)	-
Yield strength	60 (80)	MPa

TABLE 7 Post-calibration RRPM Type B Material Properties

Body		
Density	1.10E-09 (1.04E-09)	Metric tons/ mm^3
Young's modulus	1200 (2100)	MPa
Poisson ratio	0.36 (0.35)	-
Yield strength	50 (44)	MPa
Lens		
Density	1.20E-09 (1.19E-09)	Metric tons/ mm^3
Young's modulus	3500 (3103)	MPa
Poisson ratio	0.35 (0.11)	-
Yield strength	80 (70)	MPa

TABLE 8 Post-calibration RRPM Type C Material Properties

Body		
Density	1.10E-09 (1.10E-09)	Metric tons/mm^3
Young's modulus	4500 (2500)	MPa
Poisson ratio	0.30 (0.35)	-
Lens		
Density	1.19E-09 (1.19E-09)	Metric tons/ mm^3
Young's modulus	3500 (3103)	MPa
Poisson ratio	0.35 (0.11)	-
Yield strength	80 (70)	MPa

TIRE-MARKER IMPACT SIMULATION AND ANALYSIS

Once the calibration was completed, the markers with refined material properties were integrated with the preliminary tire-marker model. The next step was to simulate tire-marker impacts with the calibrated models. The researcher obtained stresses and strains inside markers from simulation of the impacts. The researcher performed simulations with different RRPM Types and external factors like tire loads, tire velocities, and angles of impacts.

First, the researcher simulated the impacts for a reference set of external conditions (called as base case) for the three RRPM Types. Then the researcher performed simulations with varying external conditions (each with two factors). Table 9 gives values for these variables. One more important input was the tire inflation pressure, which was kept as 0.7 MPa (100 PSI), The simulation provided the magnitudes and locations of critical stresses inside a marker when a vehicle tire runs over it. The researcher documented and analyzed the stress profiles under different conditions (tire loads, tire velocities, and impact angles). Next section describes the results of the tire-marker impact simulations.

TABLE 9 Variables in Simulation

Variable	Load		Velocity		Angle of impact
units	Newton (N)	Pounds force (lbf)	Meters per second (m/s)	Miles per hour (mph)	degrees (^{o}s)
Base case	22,241	5000	26.8	60	0
Factor 1	13,345	3000	17.9	40	10
Factor 2	31,138	7000	35.8	80	20

LABORATORY TEST SIMULATION AND ANALYSIS

The analysis of the tire-maker impacts was not sufficient for finding a laboratory test that would produce the same kinds of stresses in the markers as during real tire-marker impacts. To accomplish that, the researcher required simulating different laboratory loading conditions over markers. The simulation that produces stress profiles in markers similar to that produced during the tire-marker impact simulation would give insight into the laboratory test required for RRPMs.

The next step in the analysis was to simulate a few loading conditions on the markers. This was similar to modeling and simulating the ASTM longitudinal flexural test as was done for the calibration. However, no actual laboratory test was required for this part of the research. The researcher analyzed the principal and von Mises stress profiles inside the markers from simulating these loading conditions and compared them with those produced during the tire-marker impact simulations. The analysis provided an insight in the appropriate testing conditions needed for RRPMs.

RESULTS AND ANALYSIS

The researcher simulated field conditions, i.e. tire-marker impacts on LS-DYNA, after the calibration was completed. The effect of the variation in external factors during simulation was also evaluated. The researcher then simulated a few laboratory conditions, which could produce similar stress profiles in markers as during the tire-marker impacts.

This section provides results and analysis of these simulations. The section is divided into two sub-sections. The first sub-section provides results of the tire-marker impact simulations for the three RRPM Types; A, B, and C. The sub-section also details results of the simulations with variation in the external conditions. The researcher has listed the various factors in Table 9 (Page 53). The other sub-section details results of the laboratory field simulations.

TIRE-MARKER MODEL

The critical part of this research was to analyze stresses produced in the markers during their impacts by the tires. In this sub-section, the researcher details the von Mises stress profiles found from the tire-marker impact simulations. For every RRPM Type, the researcher has shown the stress contours in top view and isometric grid view. This helps to understand the surface and vertical profiles of the stresses.

Stress tensor is a six-vector quantity (a symmetric 3*3 matrix). Von Mises stress reduces it to a scalar number. It is found by combining 2-D or 3-D stresses, whichever applicable. It is given by;

$$\sigma_v = \sqrt{\frac{(\sigma_1 - \sigma_2)^2 + (\sigma_2 - \sigma_3)^2 + (\sigma_3 - \sigma_1)^2}{2}},$$

where σ_1, σ_2, and σ_3 are the principal stresses (*38*). Von Mises stress is compared with tensile strength of uniaxially loaded material and acts as a yield criterion for ductile materials. The researcher used the von Mises stresses, as most of the finite elements models for this research are elastic-plastic in which a ductile failure is possible. In addition, it is easy to compare these stresses across all RRPM Types and different external factors.

The researcher set up the simulations in such a way that the tire passes over the marker in three frames. The first frame simulates the ascendancy of the tire over the retroreflective face of the marker. The second frame simulates the instantaneous stay of the tire on top of the marker. The third frame simulates the movement of the tire over the other retroreflective lens of the marker as the tire leaves it. Hence, every figure for a tire-marker simulation result has three frames of the simulation. The retroreflective lens of the marker approached by the tire is at the top of every frame.

RRPM Type A Stress Analysis

Figure 27 shows von Mises stress contours in the RRPM Type A from the tire-marker impact simulation. The simulation was done considering the base magnitudes of external

variables i.e. tire load of 22,241 N, tire velocity of 26.8 m/s, and angle of impact being 0 degrees from the traffic direction of marker.

A few observations are made:

- The critical (maximum) stresses exist on the top edge of the retroreflective sides of marker, both during ascent and descent of tire. The maximum stresses are in the range of 54-60 MPa.
- There are large stresses at corners of the top surface of the marker where it meets the retroreflective surfaces.
- Stresses are not high in the middle components of the marker.
- The stress profiles extend vertically as seen in Figure 28. The figure shows stresses in the marker in an isometric view.

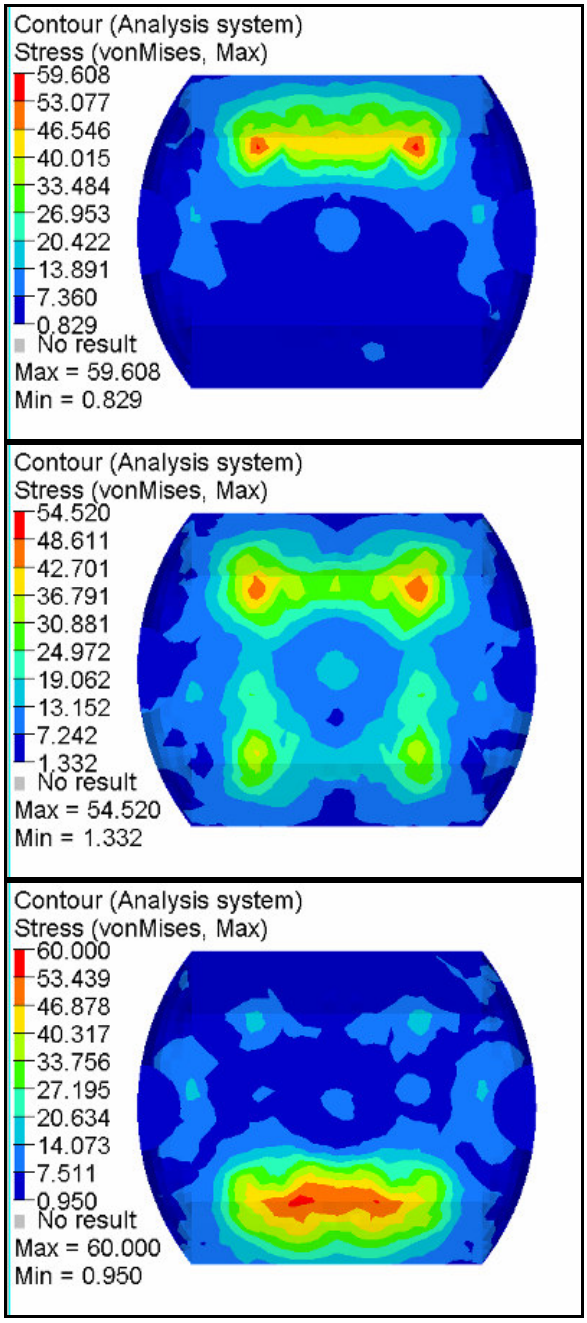

FIGURE 27 RRPM Type A von Mises stress profiles (in MPa) as a tire runs over the marker (in three frames).

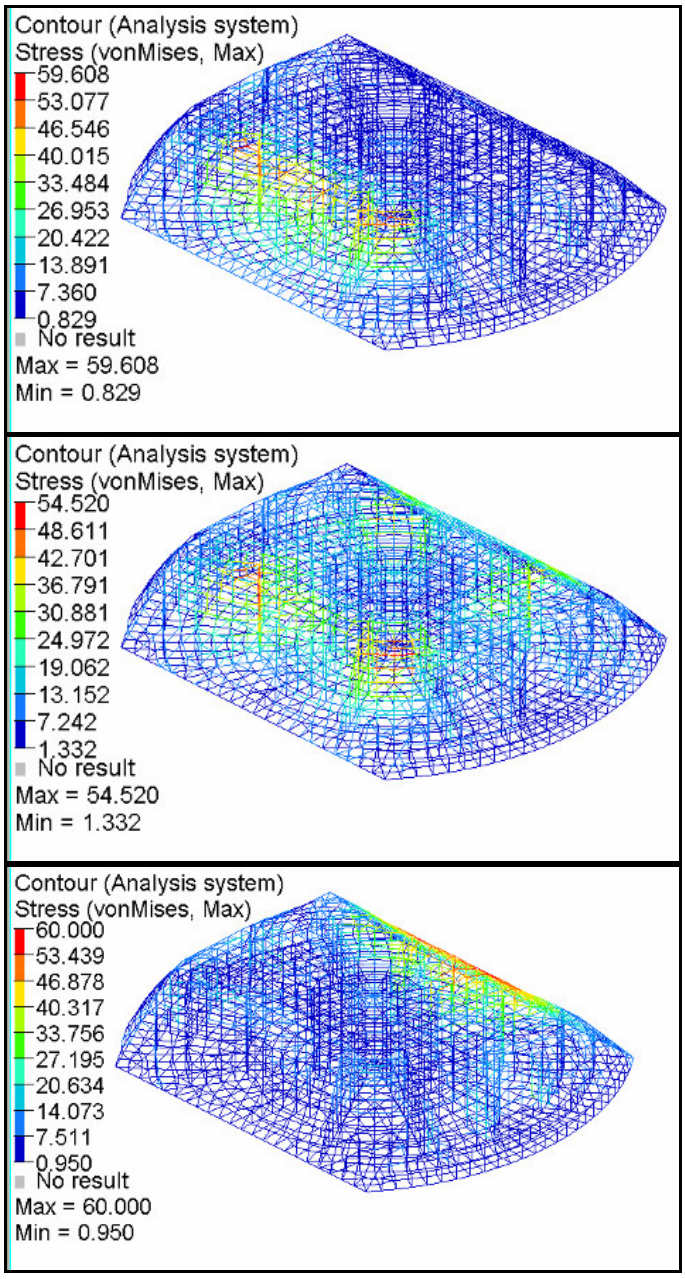

FIGURE 28 RRPM Type A von Mises stress profiles (in MPa) as a tire runs over the marker (isometric view).

The simulation results with different external factors for RRPM Type A are shown in Appendix C. The researcher compared the maximum stresses in the markers (as shown in the stress contours) in the three stages of simulation. Following observations are made:

- Although no conclusion can be drawn, it appears that higher tire load gives higher stresses (Figure 29). In addition, there is greater difference in maximum stresses between 13,345 and 22,241 N than between 22,241 and 31,138 N.

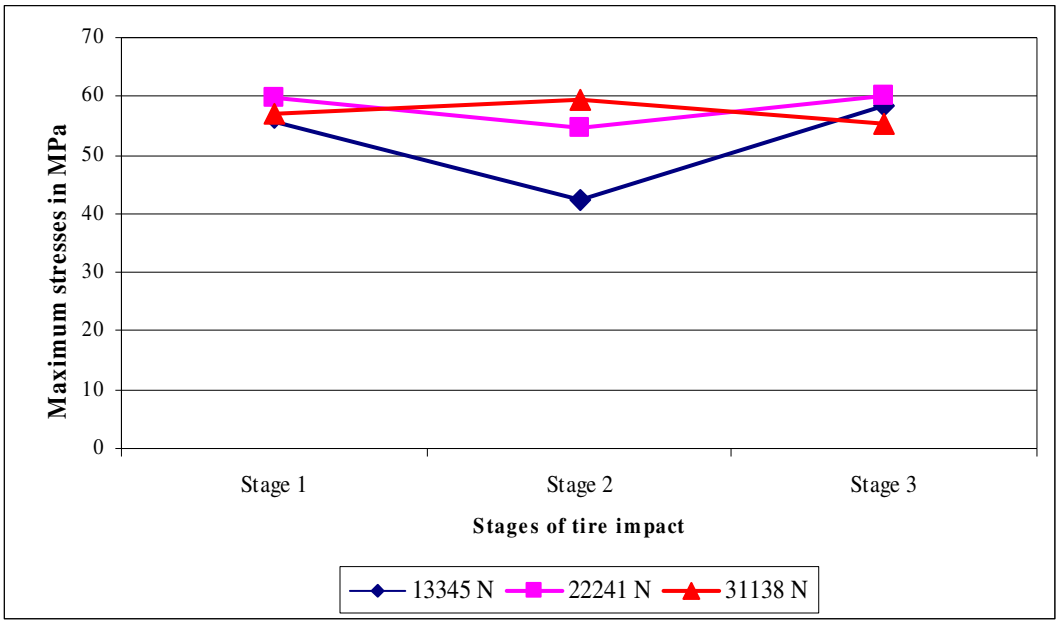

FIGURE 29 Comparison of maximum stresses in the RRPM Type A with different tire loads.

- No correlation is seen between the tire velocity and maximum stress (Figure 30). Greater stresses lie at 26.8 m/s than at 17.9 m/s but the same is not true for 35.8 m/s over 26.8 m/s.

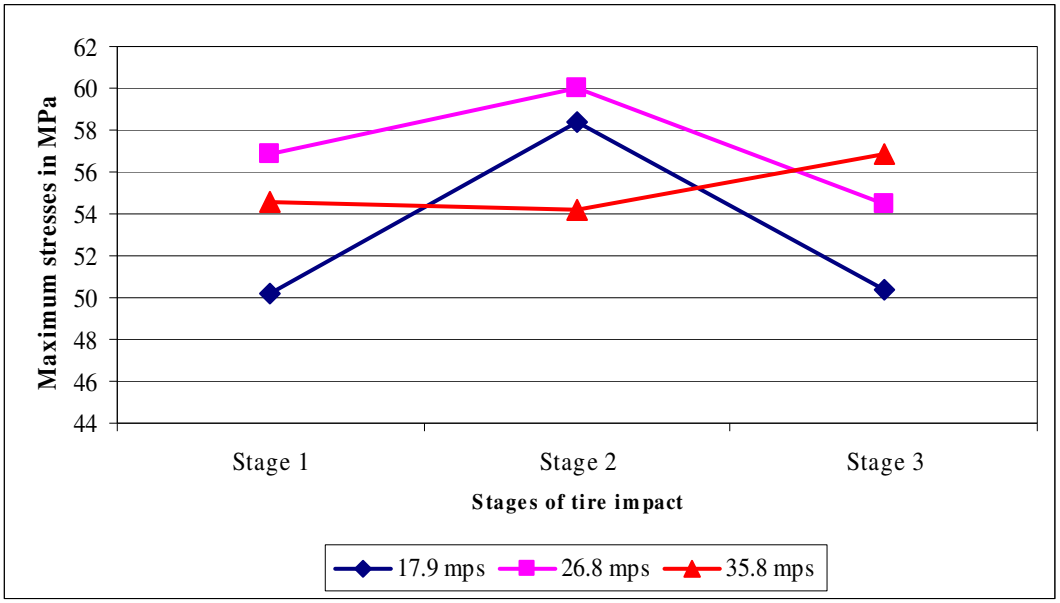

FIGURE 30 Comparison of maximum stresses in the RRPM Type A with different tire speeds.

- Clearly, the stresses are higher at greater angles of impact (Figure 31). The maximum stresses in the marker are greater at 20 degrees than at 0 and 10 degrees. There is not much difference in the maximum stresses for 0 and 10 degrees. The locations of the stresses vary as well with variation in the angles, with more stresses at the corners of the marker at higher angles (Appendix C, Figure 80 and Figure 81).

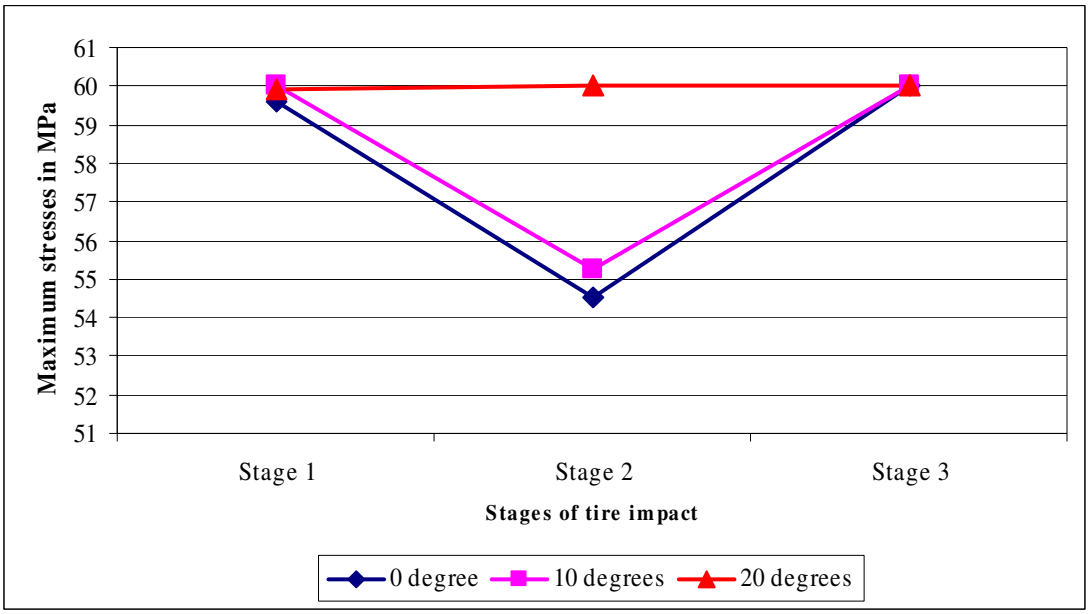

FIGURE 31 Comparison of maximum stresses in the RRPM Type A with different angles of impact.

RRPM Type B Stress Analysis

Figure 32 shows von Mises stress contours in the RRPM Type B from the tire-marker impact simulation (with base values for the variables). A few observations are made:

- The critical (maximum) stresses exist on the top edge of the retroreflective sides of marker, both during ascent and descent of the tire. The maximum stresses are in the range of 26-32 MPa.
- There are high stresses at the corners of the retroreflective surfaces (shown in frame 2) as in the case of RRPM Type A.
- Stresses are not high in the middle components of the marker.
- The stress profiles extend vertically as seen in Figure 33.

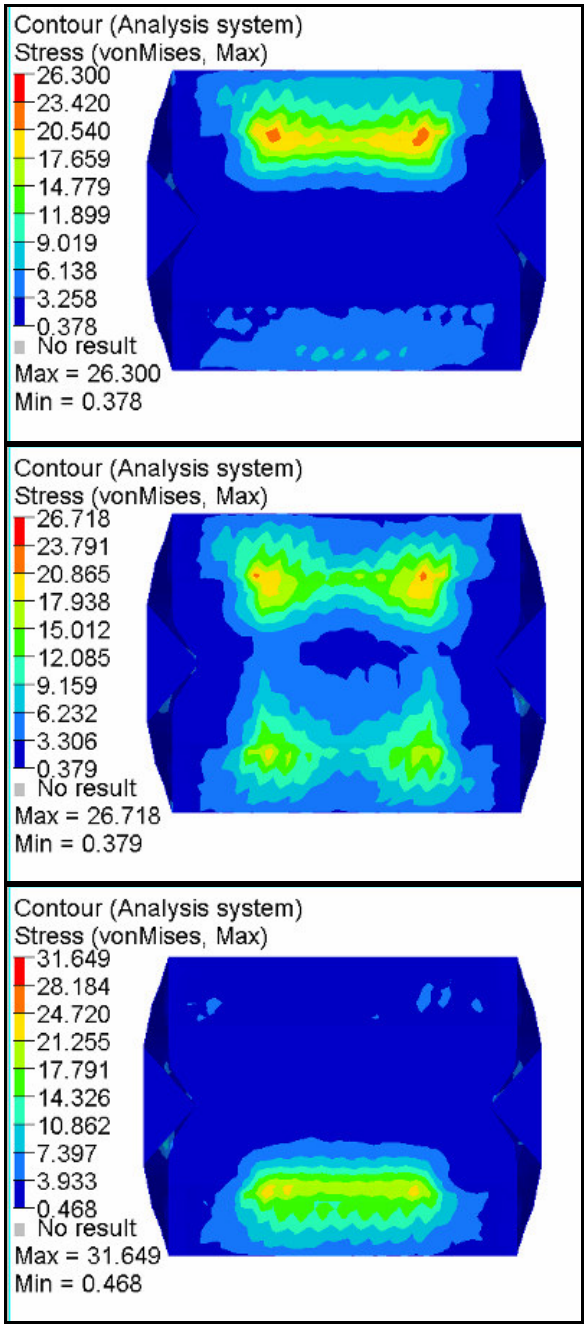

FIGURE 32 RRPM Type B von Mises stress profiles (in MPa) as a tire runs over the marker (in three frames).

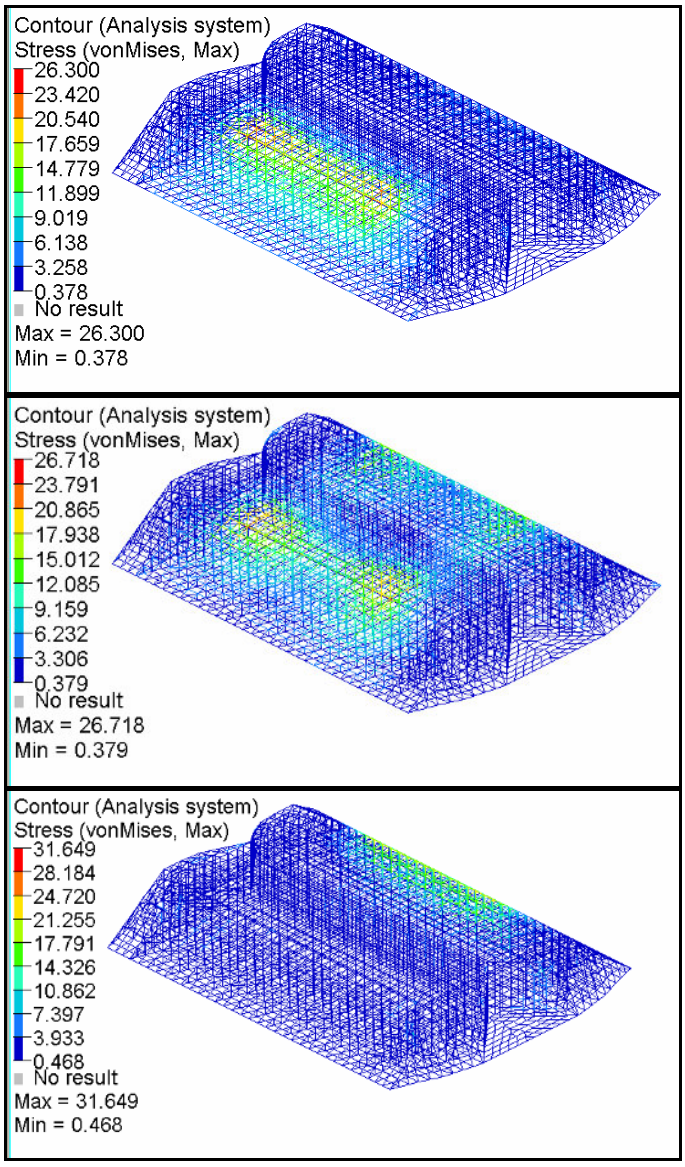

FIGURE 33 RRPM Type B von Mises stress profiles (in MPa) as a tire runs over the marker (isometric view).

The simulation results with different external factors for the RRPM Type B are shown in Appendix D. The researcher compared the maximum stresses in the markers in the three stages of simulation. Following observations are made:

- No conclusions can be drawn about the effect of tire loads on the maximum stresses (Figure 34).

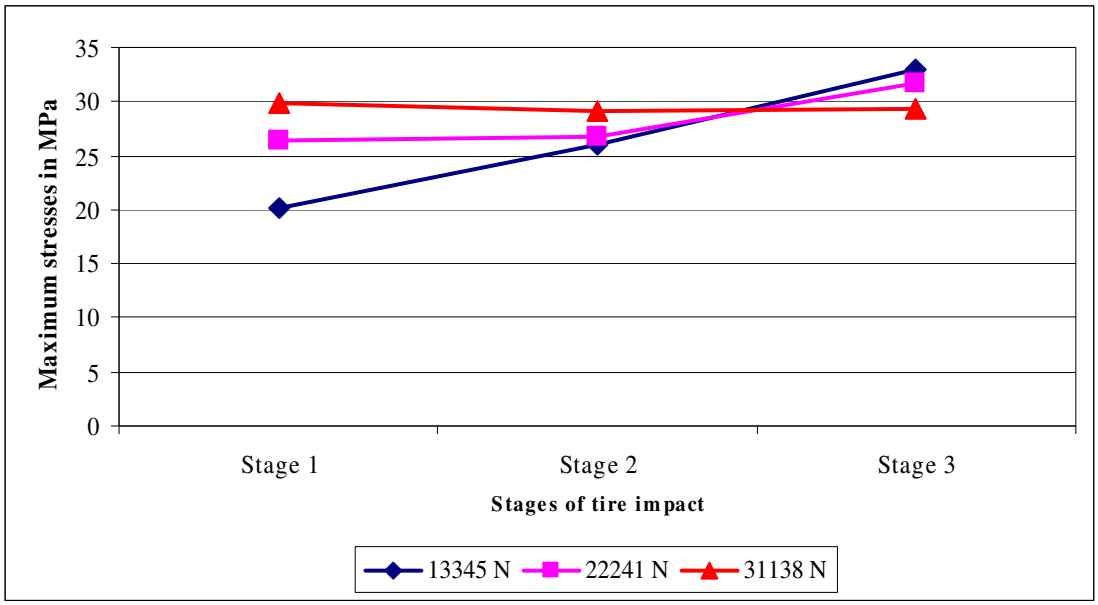

FIGURE 34 Comparison of maximum stresses in the RRPM Type B with different tire loads.

- There is no systematic effect of tire velocity on the maximum stress (Figure 35). The maximum stresses are at 17.9 m/s.

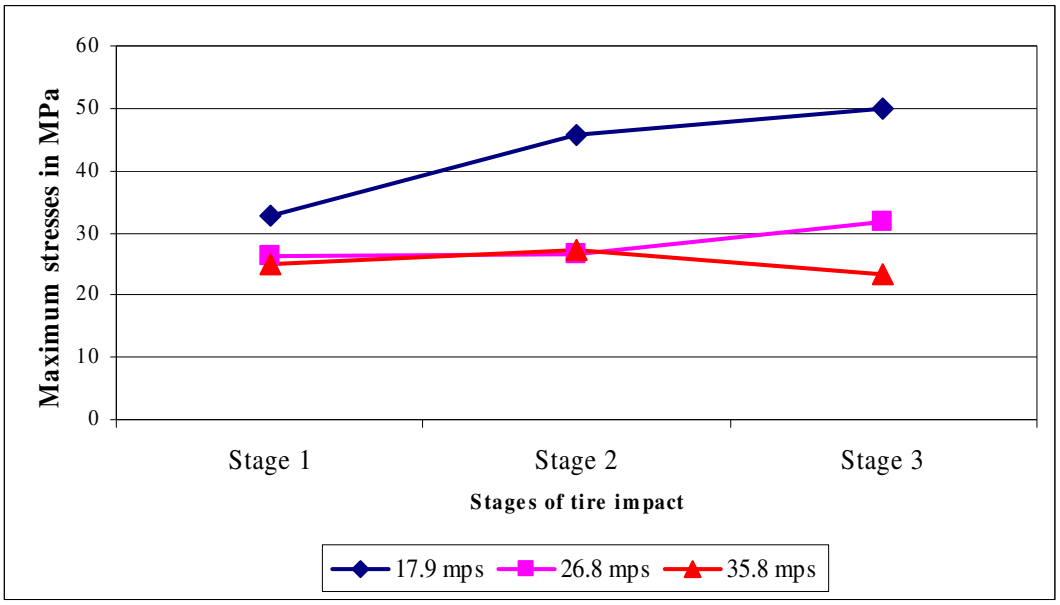

FIGURE 35 Comparison of maximum stresses in the RRPM Type B with different tire velocities.

- Clearly, the stresses are higher at greater angles of impact (Figure 36). The maximum stresses in the marker are at 20 degrees angle of impact. There is not much difference in the maximum stresses for 10 and 20 degrees. There are greater stresses at the corners of the marker with greater angles of impact (Appendix D, Figure 86 and Figure 87).

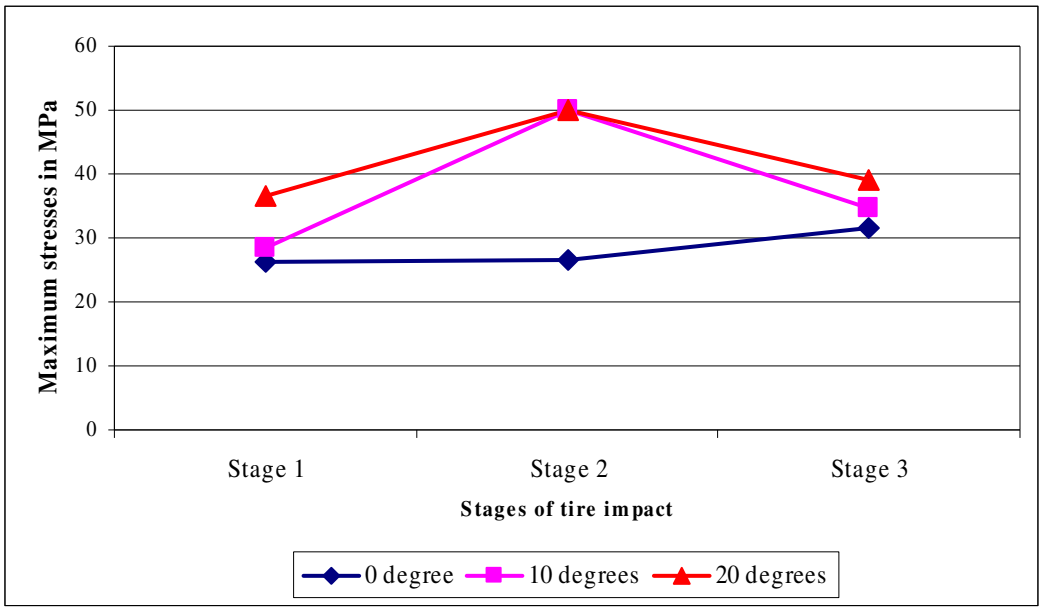

FIGURE 36 Comparison of maximum stresses in the RRPM Type B with different angles of impact.

RRPM Type C Stress Analysis

Figure 37 shows von Mises stress contours in the RRPM Type C from the tire-marker impact simulation (with base values for the variables). A few observations are made:

- The critical (maximum) stresses happen on the top edge of the retroreflective sides of the marker, both during ascent and descent of the tire. The stresses are as large as 30 MPa in magnitude.
- Stresses are also high on the side edges of the approached retroreflective surface.
- Stresses are not high in the middle components of the marker.
- The stresses profiles extend vertically as seen in the Figure 38.

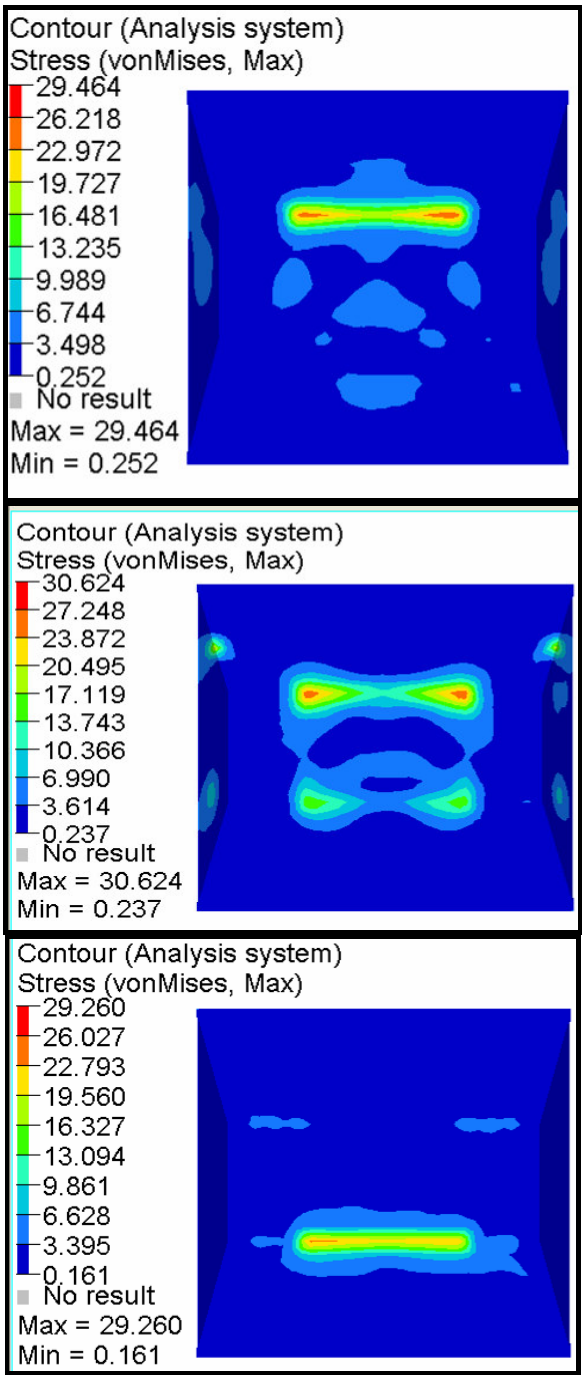

FIGURE 37 RRPM Type C von Mises stress profiles (in MPa) as a tire runs over the marker (in three frames).

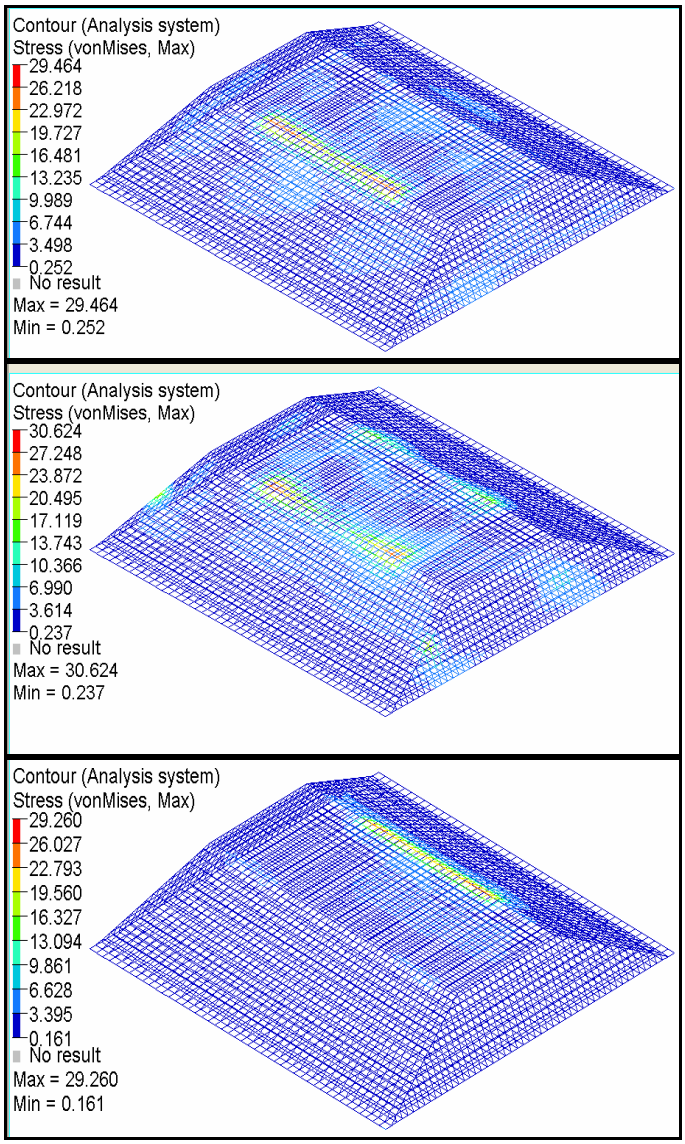

FIGURE 38 RRPM Type C von Mises stress profiles (in MPa) as a tire runs over the marker (isometric view).

The simulation results with different external factors for the RRPM Type C are shown in Appendix E. The researcher compared the maximum stresses in markers in the three stages of the simulation. The following observations are made:

- Although not evident, higher tire loads may give higher stresses (Figure 39).

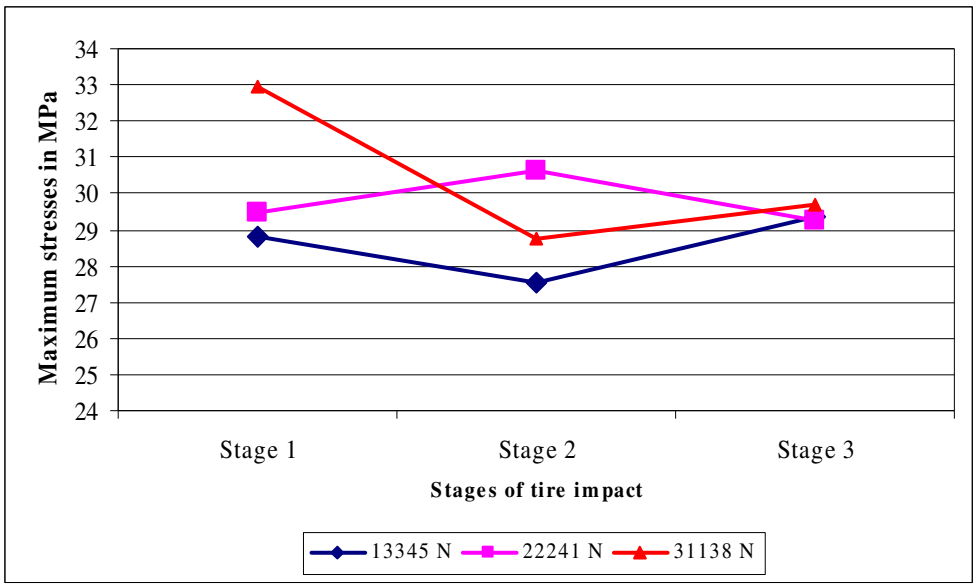

FIGURE 39 Comparison of maximum stresses in the RRPM Type C with different tire loads.

- There is no systematic effect of tire velocity on the maximum stress (Figure 40).

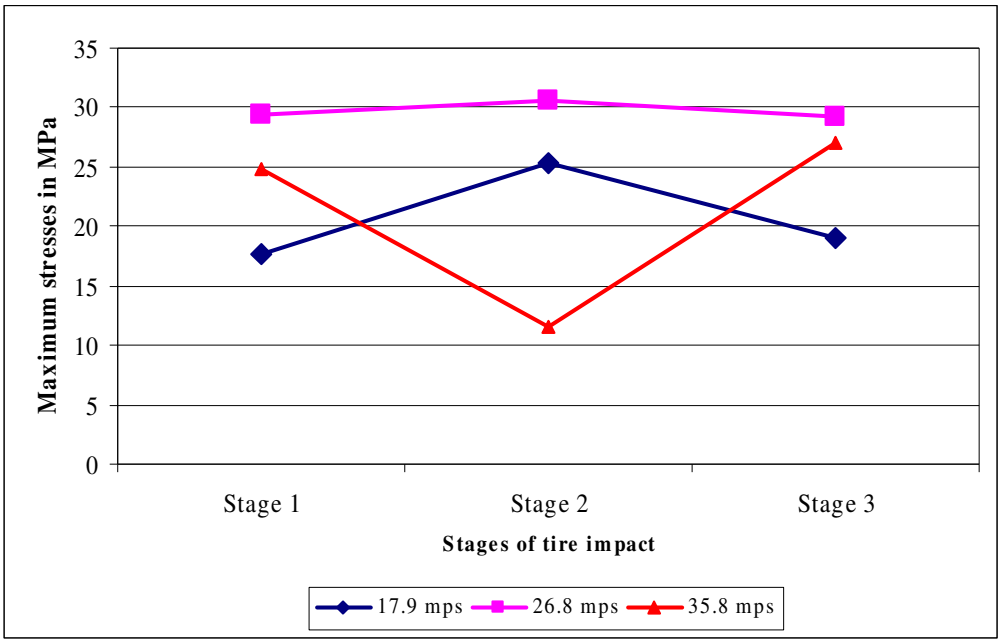

FIGURE 40 Comparison of maximum stresses in the RRPM Type C with different tire velocities.

- The stresses are higher at greater angles of impact (Figure 41). The maximum stresses in the marker are greater at 20 degrees and 10 degrees than at 0 degrees. Stresses are higher at the corners of the marker at greater angles of impact (Appendix E, Figure 92 and Figure 93).

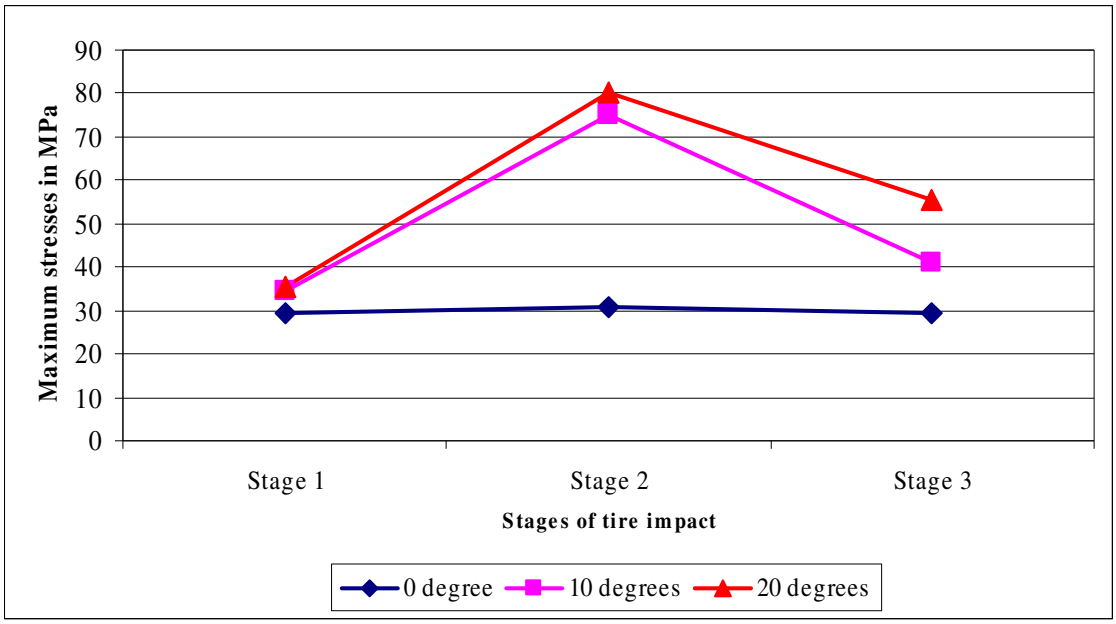

FIGURE 41 Comparison of maximum stresses in the RRPM Type C with different angles of impact.

It is important to note that the tire-marker impacts are modeled with rigid pavements. Thus, the von Mises stresses shown in the preceding results would be more appropriate for the rigid pavements than the flexible pavements. Further research is necessary to simulate the tire-marker impacts on the flexible pavements.

RRPM-Ground Interface Forces

The simulation also provided an insight into the interface forces between the RRPM and ground surface during tire-marker impacts. Although not integral to objectives of this research work, the analysis may prove to be useful and hence, is mentioned here. Appendix F provides plots of interface forces versus time for the three RRPM Types.

The figures provided in the appendix show variations in interface forces as external variables like tire load, tire velocity, and angle of impact are varied.

The interface forces between a marker and the pavement surface is about 11,000-15,000 N based on the simulation results. There is an effect of variation in angles of impact and tire velocities on the interface forces. Higher angle of impact leads to higher interface forces. Higher tire velocities may lead to higher interface forces (shown to be true for RRPM Type A and B). No effect of varying tire load was seen on the interface forces.

LABORATORY TESTING SIMULATION

The main objective of this research work was to recommend laboratory testing procedures that would simulate the real tire marker impacts. The simulation of tire-marker impacts helped in getting estimates of stresses that RRPMs encounter in field during the impacts. The researcher sought to simulate a few loading conditions that could produce the similar stresses. This sub-section first discusses the distribution of principal stresses as found from the tire-marker impact simulations. The sub-section then details the results of a few laboratory test simulations that the researcher carried out for simulating the tire-marker impacts.

Figure 42, Figure 43, and Figure 44 show the stress tensor plots of the three markers. Each figure has three frames that stand for the three stages of a tire-marker impact simulation respectively. Every frame shows distribution of the principal stresses σ_1, σ_2, and σ_3 across the marker. The top frame corresponds to the ascent of the tire over

the marker, the middle frame corresponds to the stage when the tire sits over the top of the marker, and bottom frame refers to the stage when the tire leaves the marker.

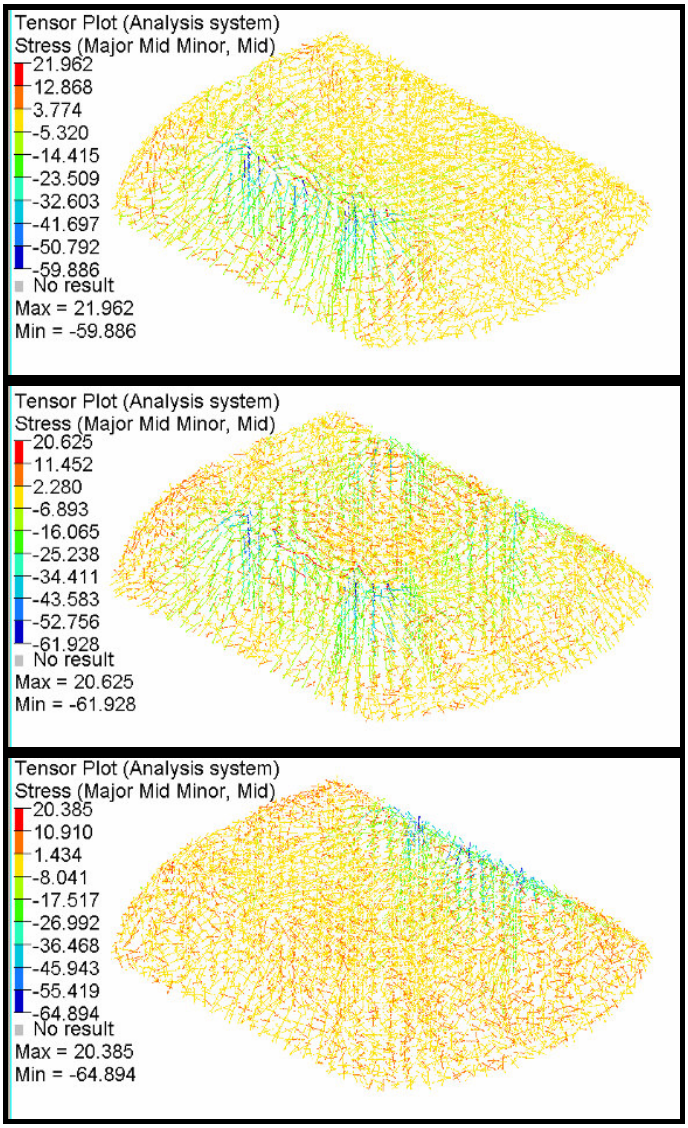

FIGURE 42 RRPM Type A stress tensor plots (in MPa) from the three stages of the tire-marker impact simulation.

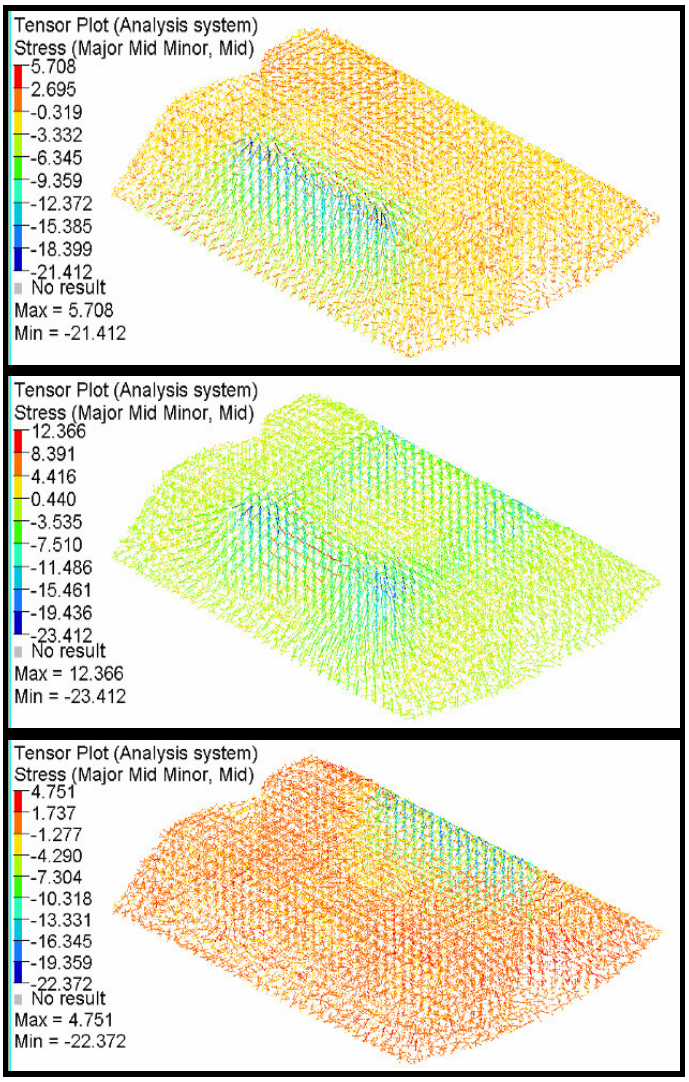

FIGURE 43 RRPM Type B stress tensor plots (in MPa) from the three stages of the tire-marker impact simulation.

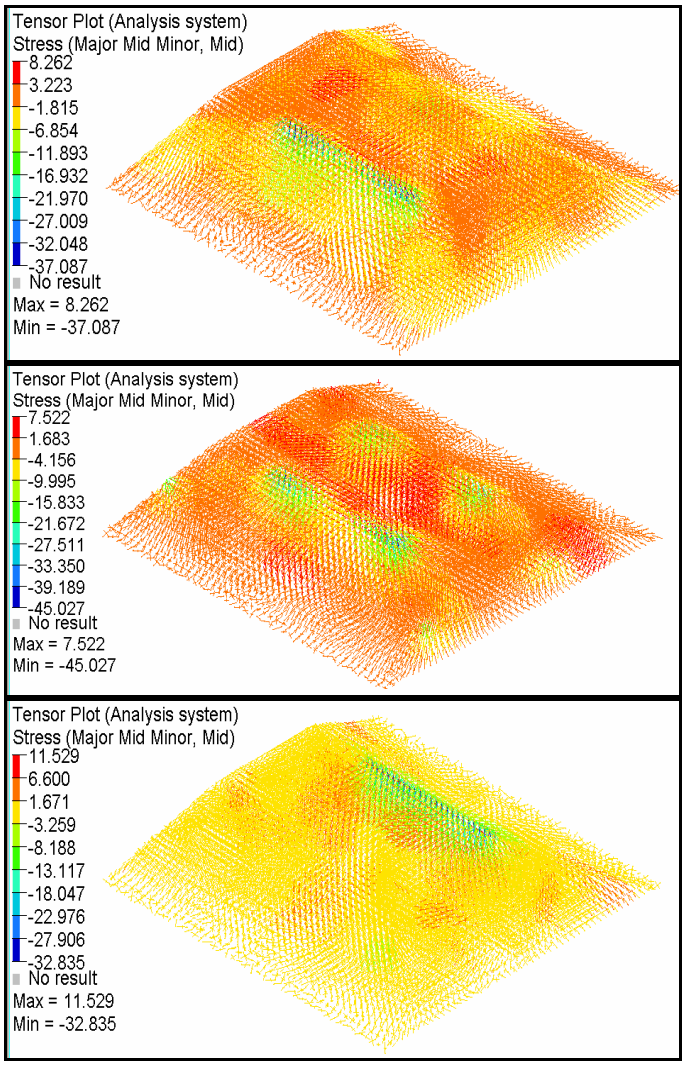

FIGURE 44 RRPM Type C stress tensor plots (in MPa) from the three stages of the tire-marker impact simulation.

For all the RRPM Types, the researcher made a few observations:

- When the tire ascends over the marker, it causes major compression (as indicated by negative stress values) on the upper half of the corresponding retroreflective side of the marker and on edge contacts of the top surface with the retroreflective side. The maximum compressive stresses were 59.886 MPa for the RRPM Type A, 21.412 MPa for the RRPM Type B, and 37.087 MPa for the RRPM Type C.
- The same thing happens during the descent phase, as the tire leaves the marker. The compressive stresses lie on upper half of the other retroreflective edge. The maximum compressive stresses were 64.894 MPa for the RRPM Type A, 23.372 MPa for the RRPM Type B, and 32.835 MPa for the RRPM Type C.
- During the stage when the tire sits over the marker, compressive stresses are concentrated at the top edges of both the retroreflective surfaces. The maximum compressive stresses were 61.928 MPa for the RRPM Type A, 23.412 MPa for the RRPM Type B, and 45.027 MPa for the RRPM Type C.
- The other areas of the marker have major tensile stresses (as indicated by positive values), especially the ones in the lower half of the marker. The maximum tensile stresses in the RRPM Type A were 21.962 MPa, 20.652 MPa, and 20.385 MPa for the three stages respectively. The maximum tensile stresses in the RRPM Type B were 5.708 MPa, 12.366 MPa, and

4.751 MPa for the three stages respectively. The maximum tensile stresses in the RRPM Type C were 8.262 MPa, 7.522 MPa, and 11.529 MPa for the three stages respectively. Clearly, the compressive stresses were larger in magnitude compared to the tensile stresses.

Based on the plots shown above, the researcher identified and designed a few laboratory testing procedures that could produce stresses in the markers similar to that produced by the tire impacts. The researcher then modeled and simulated these procedures using the finite element tools (Hypermesh for modeling and LS-DYNA for simulation). In all the laboratory simulations, post-calibrated material properties for the RRPM Types were used. The properties for the steel loading bars or the plates were kept same as those used in the calibration. The researcher did not include the elastomeric pads in the model as in calibration to keep the modeling simple. The researcher assumed that this would not make large difference to the simulation results. This was based on the results from the calibration process where the researcher had run simulations with and without the elastomeric pads. He did not find significant differences in the kinds of stress distributions in the two scenarios.

The researcher considered a laboratory test to be a good test if it simulated any one of the three stages of the tire-marker impact well. Thus, a laboratory test simulation should produce similar kinds of stresses in the markers as produced during any of the three stages of the tire-marker impact. Additionally, it should produce similar magnitudes of the stresses. The following paragraphs describe these laboratory loading conditions and results from their simulations.

The researcher analyzed the results in two ways for every laboratory test simulation. A good test should compare well for both the cases. The two ways of comparing are described as follows:

1. The researcher obtained stress tensor plots for all the RRPM Types for every laboratory test simulation and compared them qualitatively (locations and magnitudes of the tensile and compressive stresses) with the three stages of the tire-marker impact simulation.
2. He compared the von Mises stresses at some finite element locations of the markers from the tire-marker impacts and the laboratory tests simulations. The researcher chose the locations that could have critical stresses based on the results from the tire-marker impact simulations. The locations of these finite elements for the RRPM Type A are given in Figure 45. The locations of the finite elements were similar for other RRPM Types. The laboratory test simulation and the tire-marker impact simulation would compare well if the percentage differences in von Mises stresses between the laboratory test simulation and the tire-marker impact simulation were smaller for all the chosen elements 1-6. Additionally, a low variation in the percentage differences among the elements would be ideal, as it would mean that the laboratory test produced similar stress profiles to the tire-marker impact simulation.

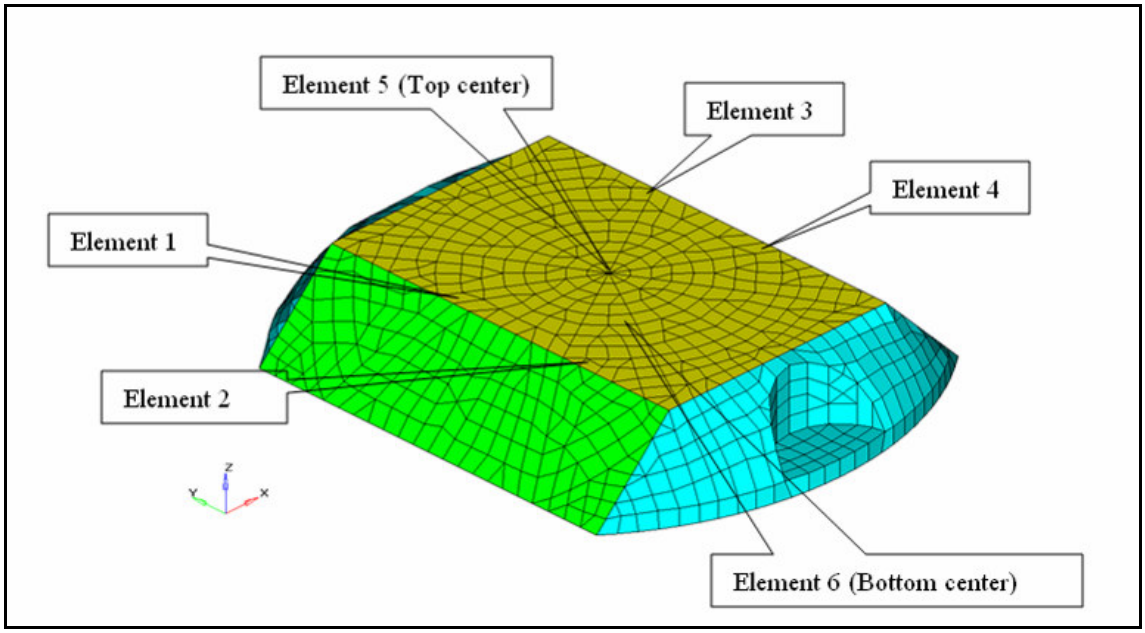

FIGURE 45 Locations of the finite elements 1-6 chosen for comparison between tire-marker impacts and laboratory tests simulations (for RRPM Type A).

ASTM Compression Test

The researcher modeled the ASTM compression test (*6*) described in ASTM standard D4280. The rate of loading was kept at 2.54 mm (0.1 inches) per minute as in the ASTM standard. The researcher did not include elastomeric pads between the steel plates and the marker. Figure 46 shows finite element model of the test.

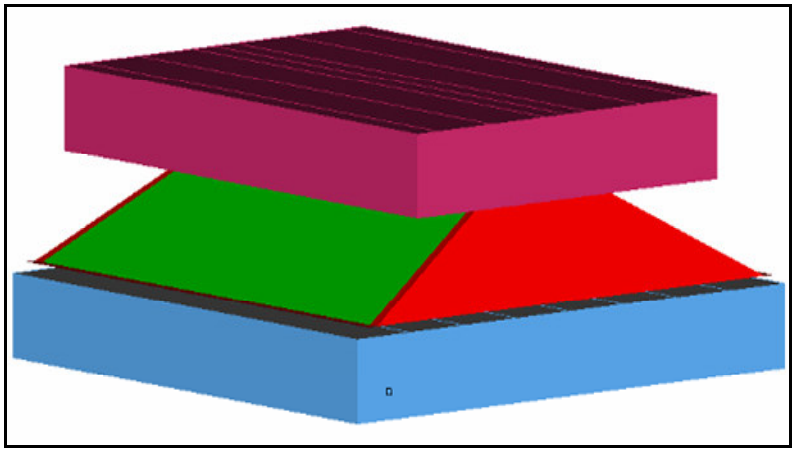

FIGURE 46 Finite element model of the ASTM compression test.

Figure 47 shows the stress tensor plots for the RRPM Types A, B, and C. The stress distributions from this simulation were similar to those found during the second stage of the tire-marker impact simulation. There were major compressive stresses on the edge contacts of the top surface with the retroreflective sides as during the second stage. The maximum compressive stresses were -68.366, -16.377, and -33.452 MPa for the RRPM Types A, B, and C respectively as opposed to the maximum tensile stresses 28.066, 7.644, and 41.092 MPa respectively.

Figure 48 (on page 84) shows percentage differences between maximum von Mises stresses (in the finite elements 1-6) from the ASTM compression test and the three stages of the base tire-marker impact simulation. It should be noted that the percentage differences have been truncated to ±100 percent in the Figure 48. The researcher did this for all the figures representing such analyses (including Appendix H). This was done to eliminate very high percentage differences and make it easier to analyze the variations among elements. Also note that a positive difference meant the laboratory test produced higher stresses than the tire-marker impact.

As seen from the figure, the von Mises stresses were comparable between the laboratory simulation and the stage 2 of the tire-marker impact for the elements 1-4. The percentage differences were in ranges of -45 to -53 percent for the RRPM Type A, -54 to-76 percent for the RRPM Type B, and 60 to 70 percent for the RRPM Type C. For the elements 5 and 6 of all the RRPM Types, the percentage differences were more (Refer Appendix G). For other stages, the percentage differences were very high and varied much.

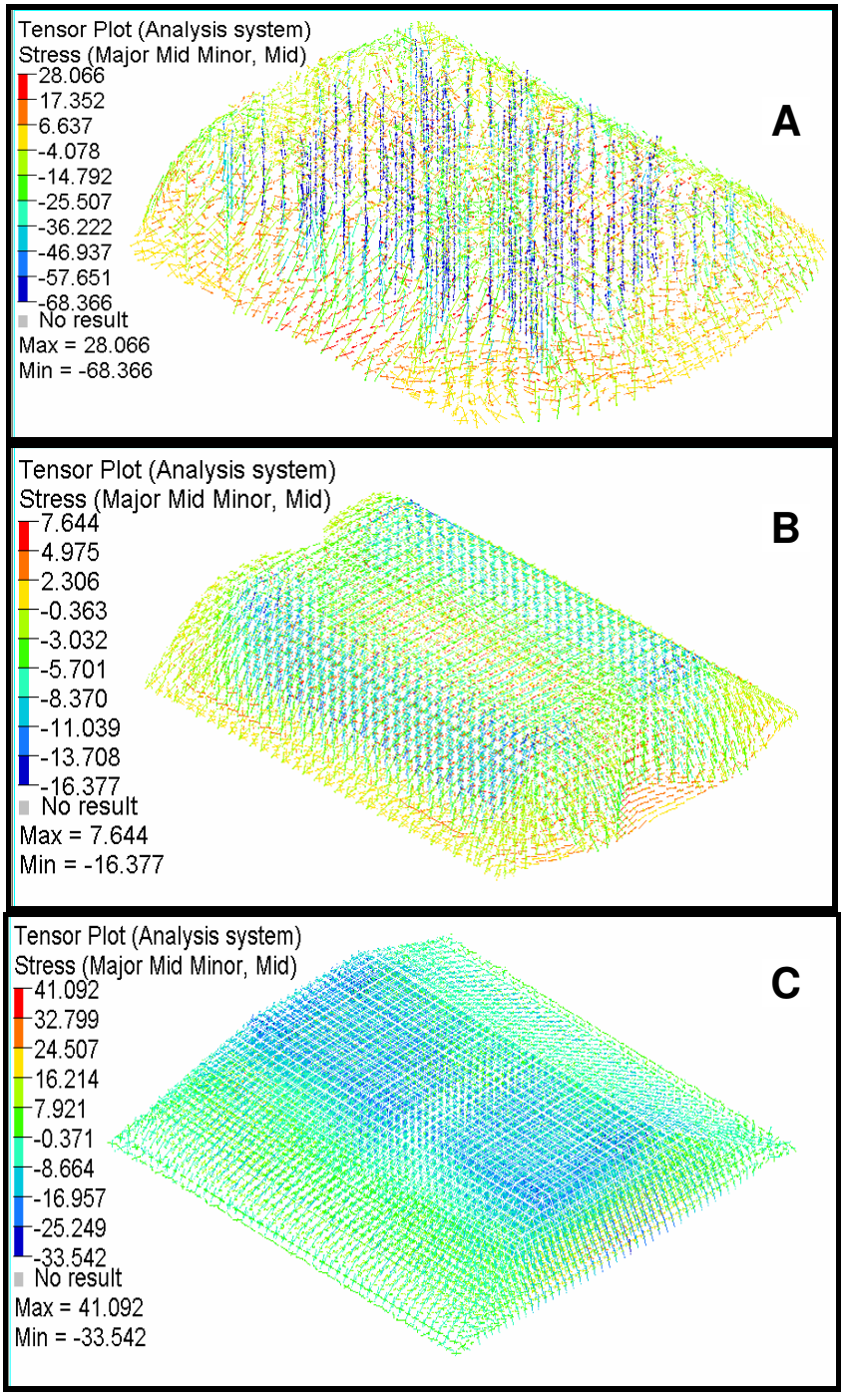

FIGURE 47 Stress tensor plots (in MPa) for RRPM Types A, B, and C (ASTM compression test).

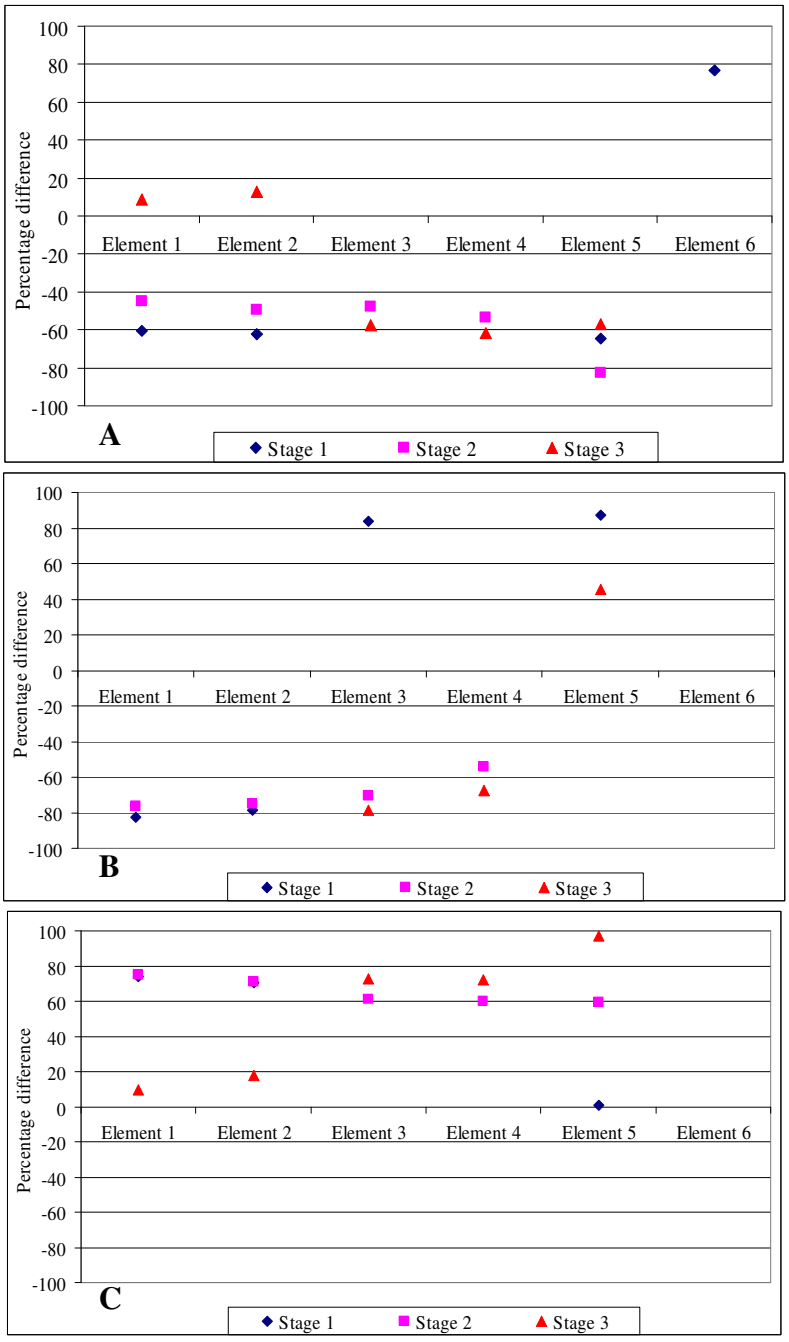

FIGURE 48 Percentage differences between maximum von Mises stresses from the three stages of the base tire-marker impact simulation and the ASTM compression test simulation in the finite elements 1-6 (RRPM Types A, B, and C).

ASTM Flexural Test

The researcher modeled the ASTM flexural test (*6*) described in ASTM standard D4280. The rate of loading was kept at 5.08 mm (0.2 inches) per minute as in the ASTM standard. However, there were no elastomeric pads. The same experiment had been used for the calibration part of the research. Figure 26 (page 47) shows finite element model of the test.

Figure 49 shows the stress tensor plots for the RRPM Types A, B, and C. The simulation caused compression at the areas around the marker where the loading bar was placed. It caused major tension at the bottom of marker. The maximum compressive and tensile stresses are comparable, which did not happen during any stage of the tire-marker impact simulation. The maximum compressive stresses were -68.992, -55.087, and 62.657 MPa for the RRPM Types A, B, and C respectively. The corresponding figures for maximum tensile stresses were 69.101, 51.257, and 76.066 MPa respectively.

Figure 50 (on page 87) shows percentage differences between maximum von Mises stresses (in the finite elements 1-6) from the ASTM flexural test and the three stages of the base tire-marker impact simulation. The von Mises stresses were comparable between the laboratory simulation and the stage 2, especially for elements 1-4 (Refer Appendix G). For other stages, the percentage differences were higher and varied much among the elements.

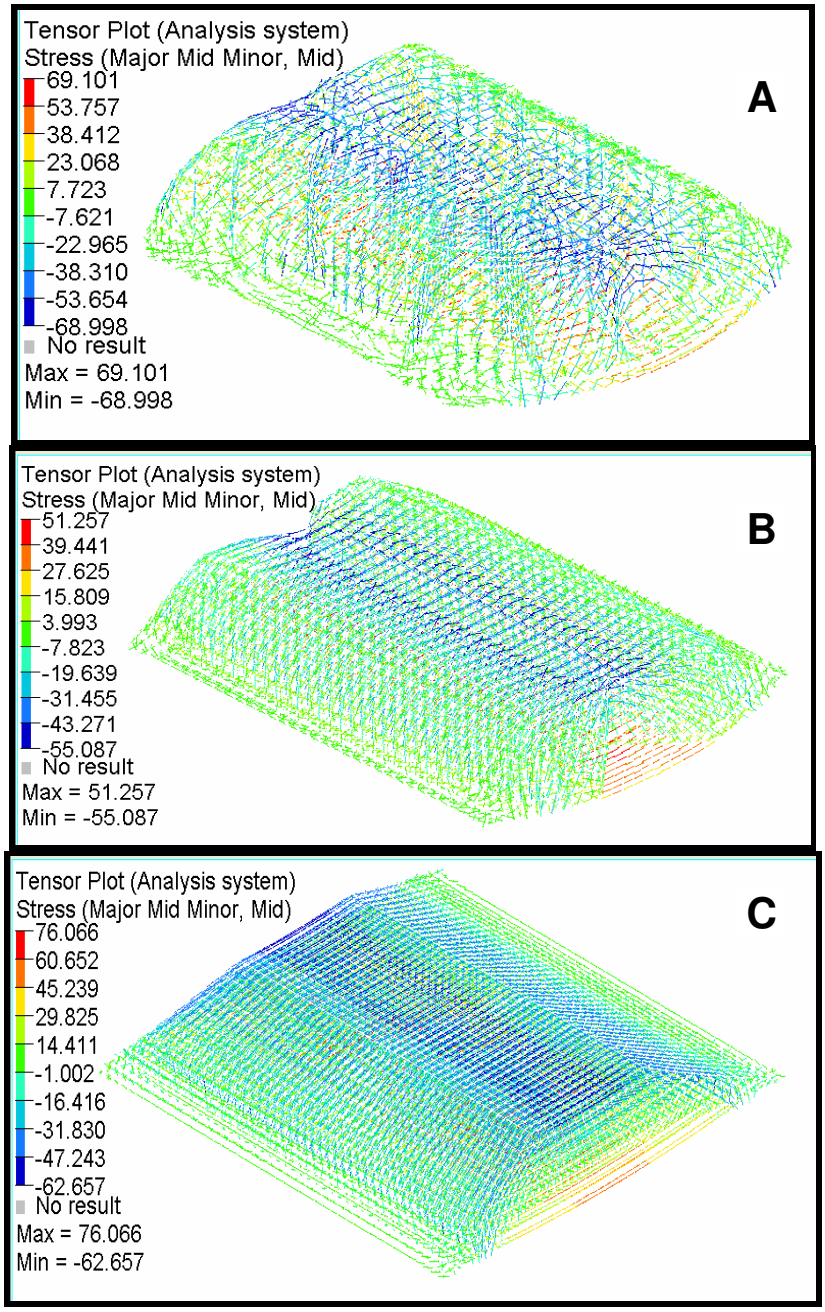

FIGURE 49 Stress tensor plots (in MPa) for RRPM Types A, B, and C (ASTM flexural test).

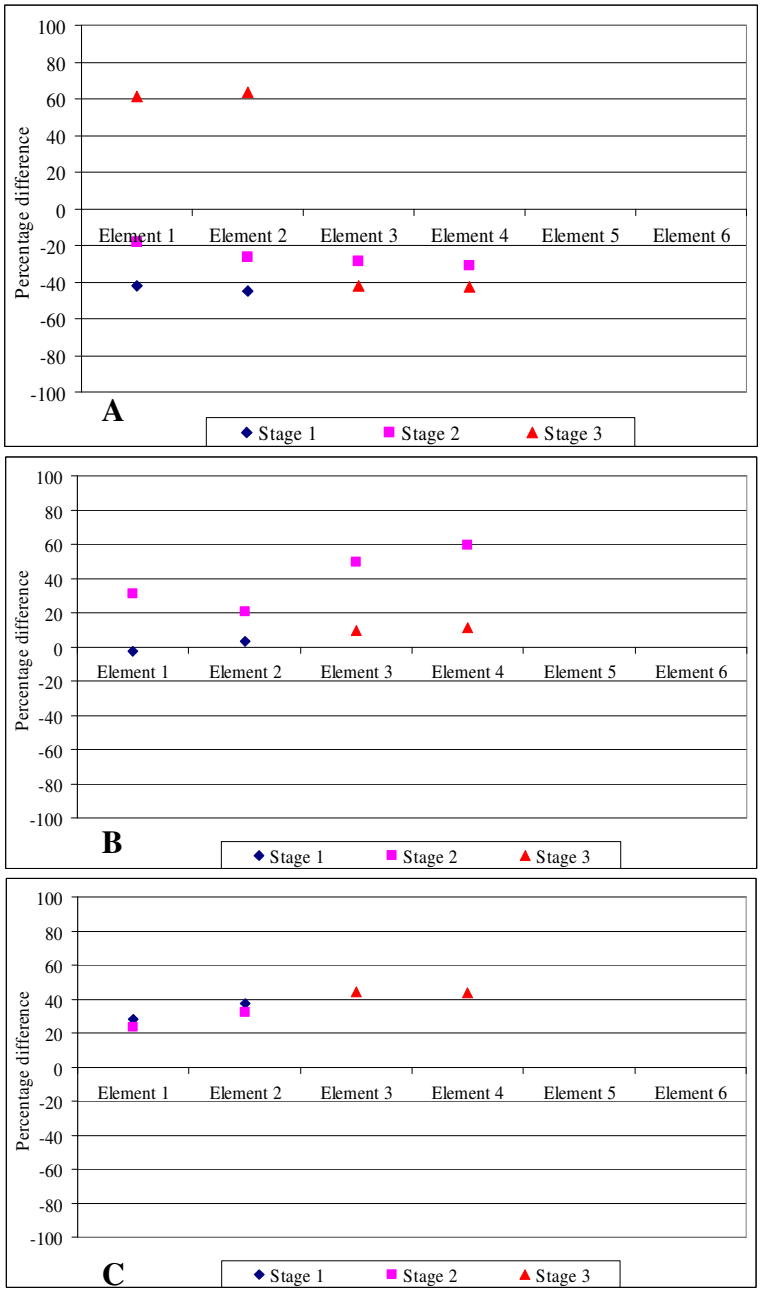

FIGURE 50 Percentage differences between maximum von Mises stresses from the three stages of the base tire-marker impact simulation and the ASTM flexural test simulation in the finite elements 1-6 (RRPM Types A, B, and C).

Cylindrical Compression Test

The researcher designed, modeled, and simulated a variation of the ASTM compression test. Instead of having two steel plates at the top and bottom of the marker, this test model had two hollow cylinders. The cylinder at the top had an outer diameter of 38.1 mm (1.5 inches) and a thickness of 3.175 mm (0.125 inches). The cylinder at the bottom had an outer diameter of 63.5 mm (2.5 inches) and a thickness of 3.175 mm (0.125 inches). The top and bottom cylinders had such dimensions that the top one could fit into the bottom one. The loading rate was kept at 2.54 mm (0.1 inches) as in the ASTM compression test. Figure 51 shows the finite element model of this test.

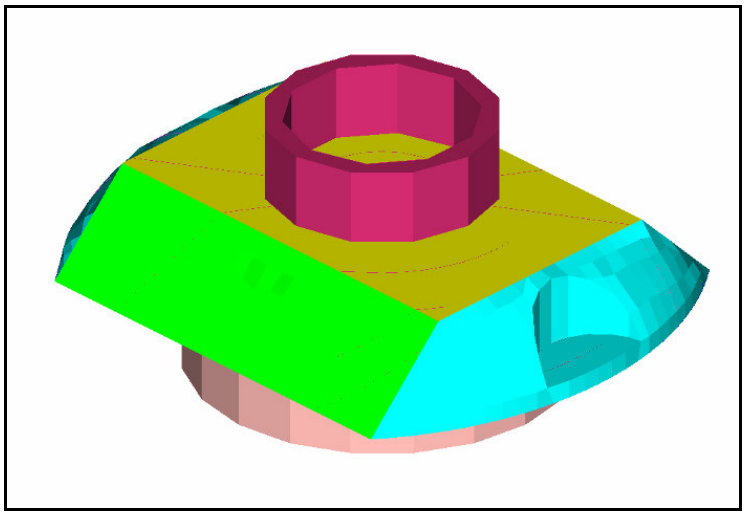

FIGURE 51 Finite element model of the cylindrical compression test.

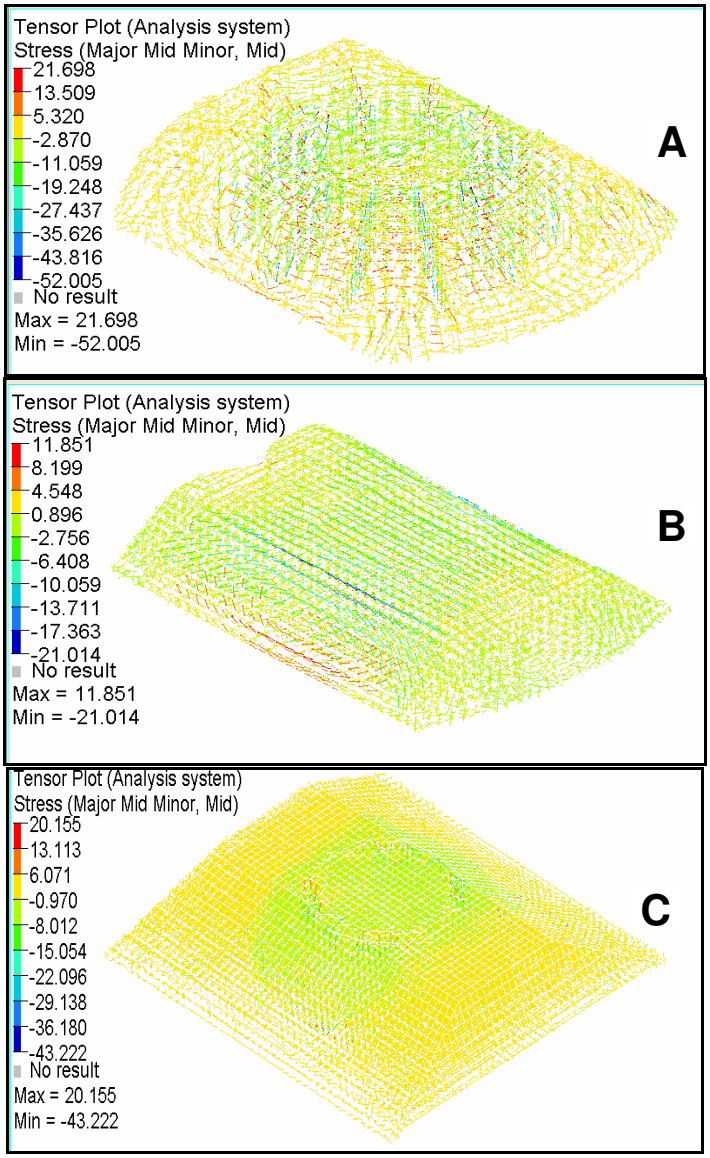

FIGURE 52 Stress tensor plots (in MPa) for RRPM Types A, B, and C (cylindrical compression test).

Figure 52 shows stress tensor plots from the test simulations for the RRPM Types A, B, and C. From the figures it is seen that there are large compressive stresses around the top cylinder while large tensile stresses at the bottom of marker (mostly around the bottom cylinder's contacts with the marker).The maximum compressive stresses were -68.992, -55.087, and -62.657 MPa for the RRPM Types A, B, and C respectively as opposed to the maximum tensile stresses 21.698, 11.851, and 20.155 MPa respectively. The locations and magnitudes of the principal stresses from this test are similar to the stage 2 of the tire-marker impact simulation.

Figure 53 shows percentage differences between maximum von Mises stresses (in the finite elements 1-6) from the cylindrical compression test and the three stages of the base tire-marker impact simulation. The von Mises stresses in the elements 1-4 were comparable with the stage 2 of the tire-marker impact simulation for the RRPM Type A, B, and C. The percentage differences varied from -79 to -82 MPa for the RRPM Type A, from -43 to -66 MPa for the RRPM Type B, and -83 to -92 MPa for the RRPM Type C respectively. The percentage differences varied much for the elements 1-4 for the other stages. They were higher for the elements 5-6 for all the stages (Appendix H).

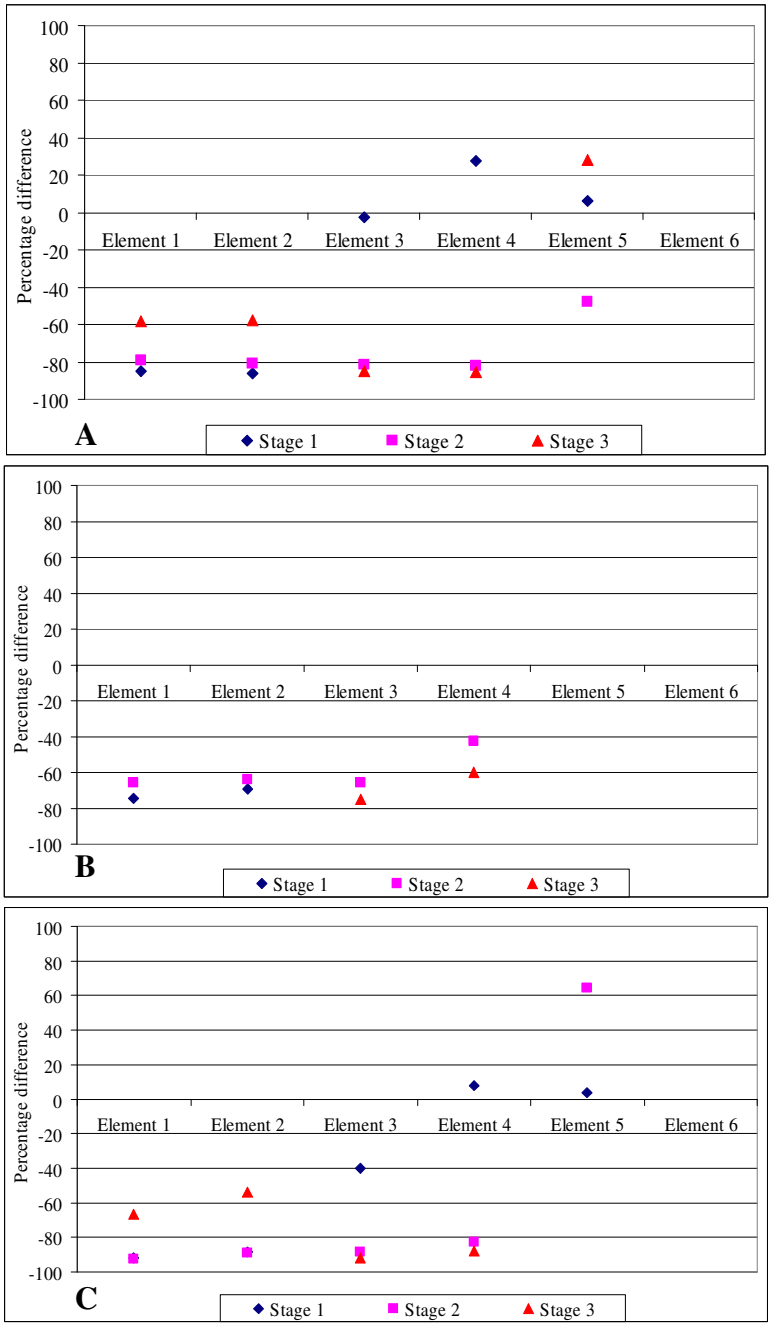

FIGURE 53 Percentage differences between maximum von Mises stresses from the three stages of the base tire-marker impact simulation and the cylindrical compression test simulation in the finite elements 1-6 (RRPM Types A, B, and C).

Offset Compression Test (Lower Loading Rate)

The researcher designed, modeled and simulated a new test and called it the Offset Compression Test. It was similar to the ASTM compression test except that there was no loading steel plate. Instead, there was a steel bar (12.7 mm or 0.5 inches wide and as long as the marker), which was placed along one of the retroreflective edges of the marker. This was done in an attempt to produce compression in one of retroreflective sides of the marker and tension in other parts of the marker. There were no elastomeric pads as in the ASTM test. The rate of loading was kept at 2.54 mm (0.1 inches) per minute as in the ASTM test. Figure 54 shows finite element model of the test.

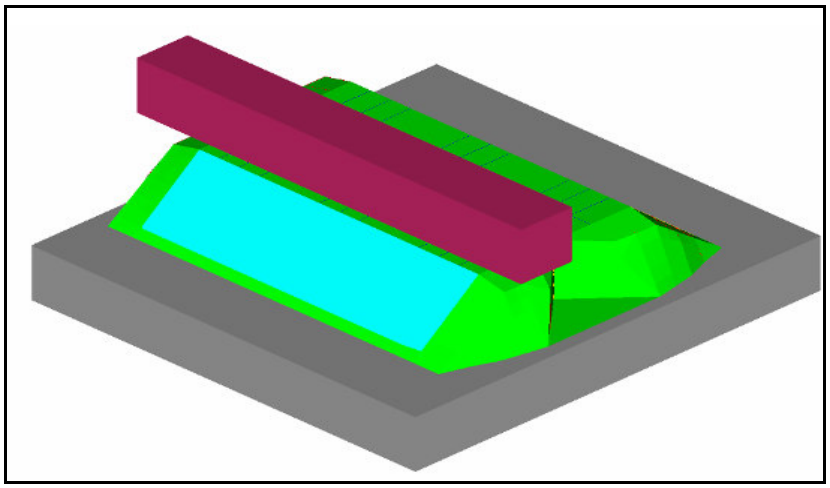

FIGURE 54 Finite element model of the offset compression test.

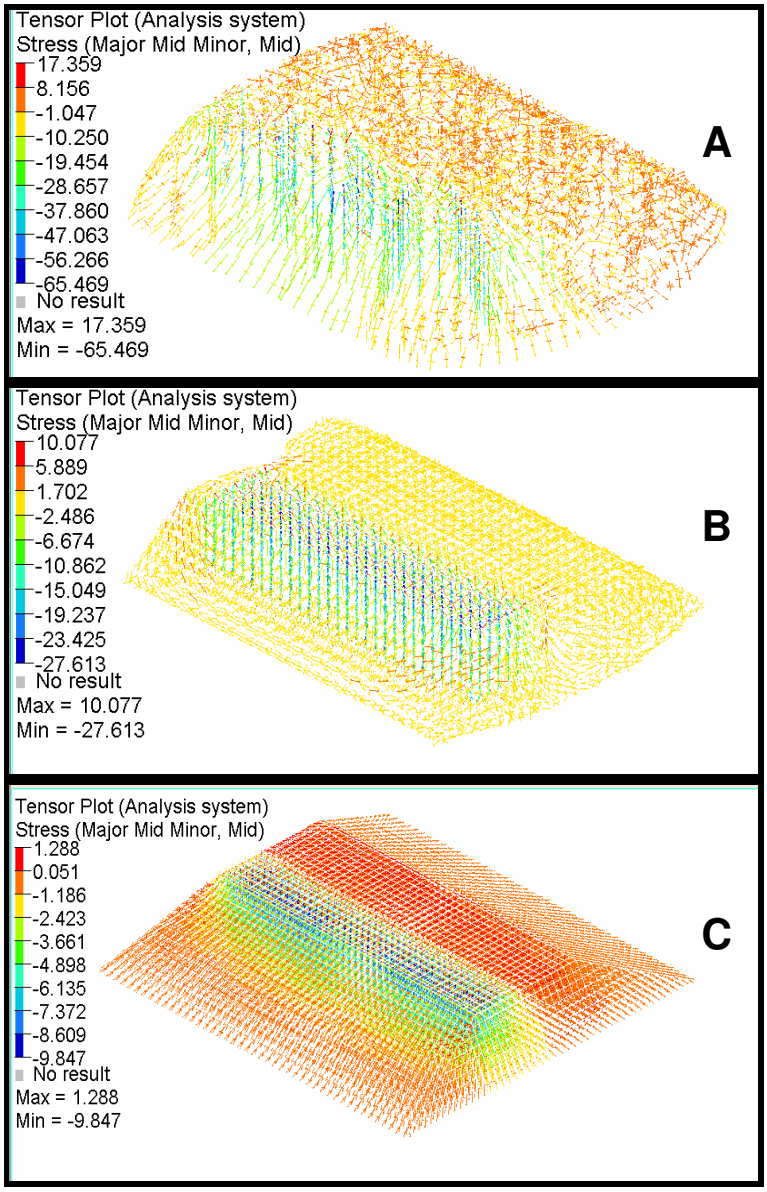

FIGURE 55 Stress tensor plots (in MPa) for RRPM Types A, B, and C (Offset compression test; lower loading rate).

Figure 55 shows the stress tensor plots for the RRPM Types (A, B, and C). The simulation caused major compression in areas around the place on the marker where loading bar was placed and in the retroreflective surface. It caused tension in other areas although magnitudes of the tensile stresses were not large especially in the RRPM Type

B and C. The maximum compressive stresses for the RRPM Types A, B, and C are 65.469, 27.613, and 9.847 MPa respectively. The major tensile stresses for these markers are 17.359, 10.077, and 1.288 MPa respectively.

Figure 56 shows percentage differences between maximum von Mises stresses (in the finite elements 1-6) from the offset compression test (lower loading rate) and the three stages of the base tire-marker impact simulation. For all the RRPM Types, the differences were less between the test simulation and the stages 1 and 2 of the tire-marker impact simulation. For the stage 1, the percent differences in the elements 1-4 varied from -50 to -66 percent for the RRPM Type A, -61 to -87 percent for the RRPM Type B, and -89 to -95 percent for the RRPM Type C respectively. For the stage 2, the percent differences in the elements 1-4 varied from -52 to -93 percent for the RRPM Type A, -52 to -97 percent for the RRPM Type B, and -89 to -99 percent for the RRPM Type C respectively. The von Mises stresses did not favor comparably for the stage 3 (Refer Appendix G).

Another variation of this test could be to apply the load in such a way that the edge of the loading bar parallel to the retroreflective side protrudes beyond the edgeline of the retroreflective side (say by 2.54 mm or 1/10 inches).

One of the challenges while developing this test would be to constrain the marker in such a way that it does not tip off when loading is applied. This is because the loading would be applied at an offset from centerline of the marker that would cause a moment about it. Hence, an arrangement is needed which can nullify the moment.

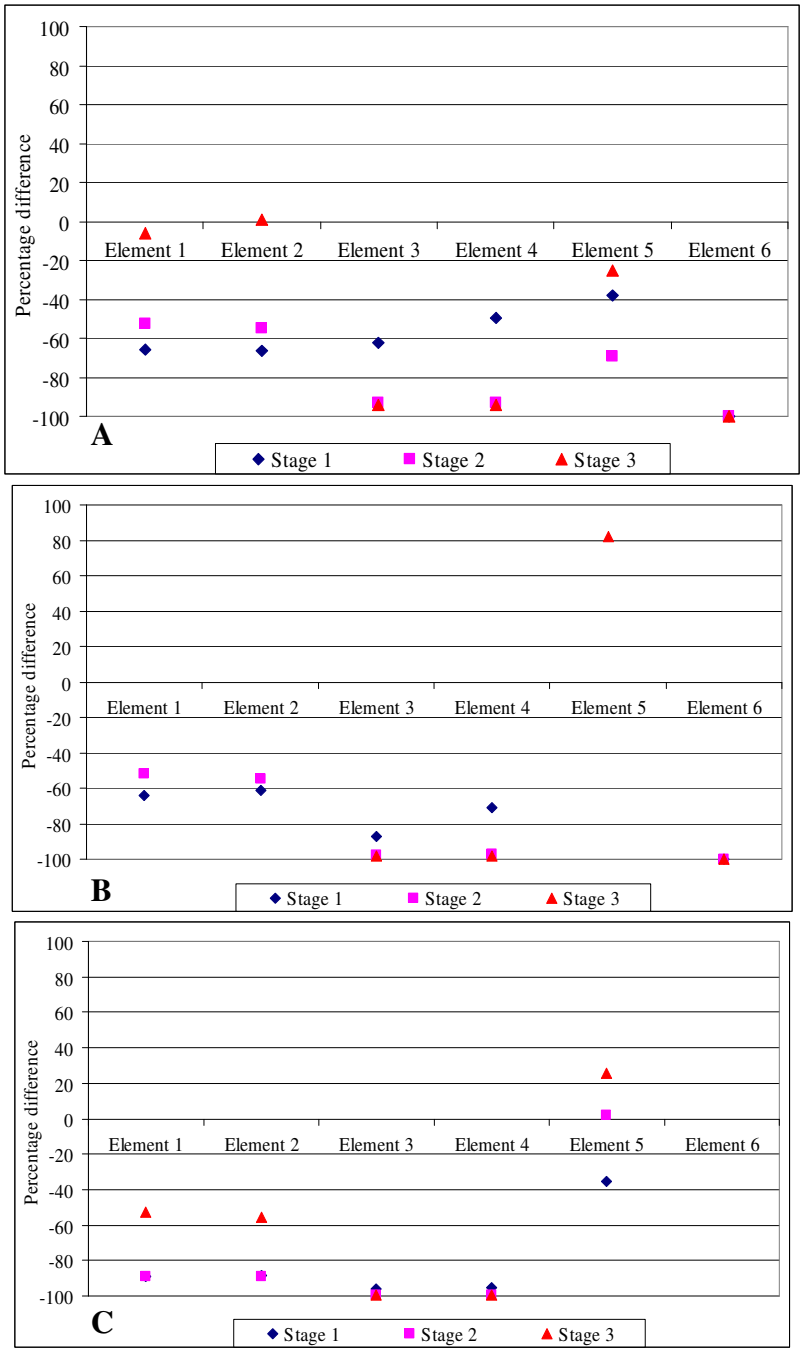

FIGURE 56 Percentage differences between maximum von Mises stresses from the three stages of the base tire-marker impact simulation and the offset compression test (lower loading rate) simulation in the finite elements 1-6 (RRPM Types A, B, and C).

Offset Compression Test (Higher Loading Rate)

The researcher modeled and simulated a slightly different version of the previous test. This time the load was applied at a rate of 5.08 mm (0.2 inches) per minute. This was done to compare the stress magnitudes for different loading rates.

Figure 57 shows the stress tensor plots for the RRPM Types A, B, and C. The stress locations were same as from the previous test. However, this test caused larger stresses, especially in the RRPM Types B and C. The RRPM Type B had a larger tensile stress (18.732 MPa as compared to 10.077 MPa in the previous test) and a larger compressive stress (-53.978 MPa as compared to 27.613 MPa in the previous test). Similarly, the RRPM Type C had a larger tensile stress (2.582 MPa as compared to 1.288 MPa in the previous test) and a larger compressive stress (19.599 MPa as compared to 9.847 MPa in the previous test). The maximum compressive and tensile stresses for the RRPM Type A were -68.813 and 24.554 MPa respectively. The results implied that the rate of loading could make difference to the stress magnitudes in the markers.

Figure 58 shows percentage differences between maximum von Mises stresses (in the finite elements 1-6) from the offset compression test (higher loading rate) and the three stages of the base tire-marker impact simulation. As in the case of the previous test, the differences are less in the elements 1-4, for the stages 1 and 2 of the tire-marker impact simulation (Refer Appendix G).

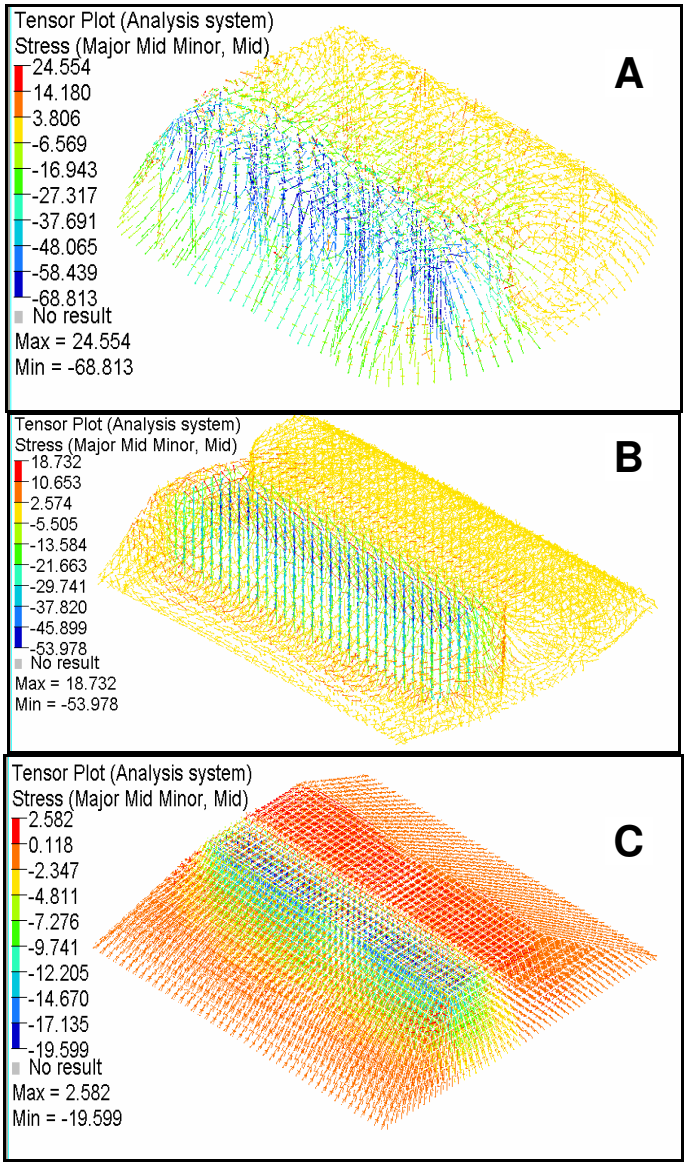

FIGURE 57 Stress tensor plots (in MPa) for RRPM Types A, B, and C (Offset compression test; higher loading rate).

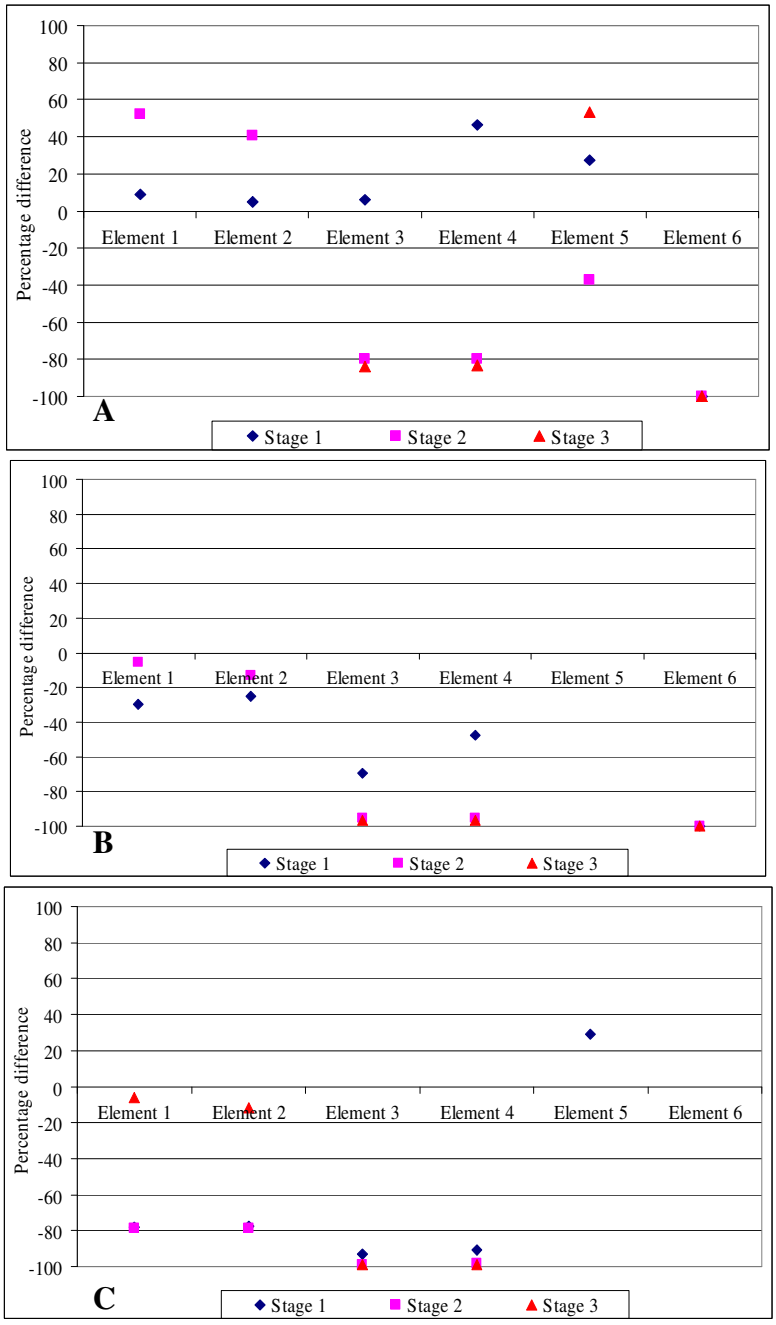

FIGURE 58 Percentage differences between maximum von Mises stresses from the three stages of the base tire-marker impact simulation and the offset compression test (higher loading rate) simulation in the finite elements 1-6 (RRPM Types A, B, and C).

Reversed ASTM Flexural Test

The researcher designed, modeled, and simulated one more laboratory procedure (Figure 59). This was similar to the ASTM flexural test. The only difference was that there were two loading steel bars at the top and just one at the bottom. The top steel bars were kept as far apart as possible in a direction perpendicular to traffic direction of the marker without protruding beyond top of the marker. The bottom bar was placed at the center of the marker perpendicular to the traffic direction. The loading rate was 5.08 mm (0.2 inches) per minute as in the ASTM flexural test. There were no elastomeric pads as in the ASTM test.

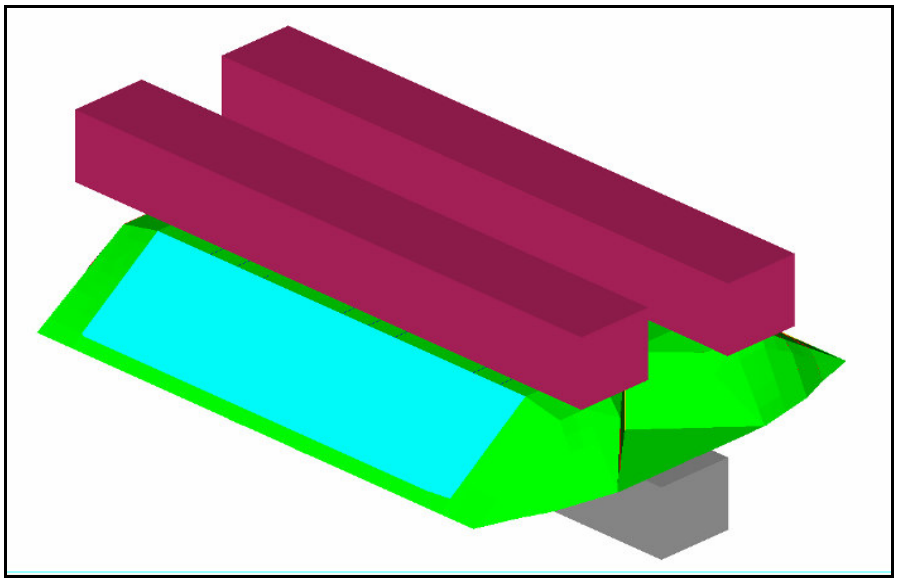

FIGURE 59 Finite element model of the reversed ASTM flexural test.

Figure 60 shows stress tensor plots for the RRPM Types A, B, and C. RRPM Type A had large compressive stresses at the top while other Types also had the same,

although lower in magnitude. There were major tensile stresses at the center-top surface of the RRPM Type A. The maximum tensile stresses were comparable to the maximum compressive stresses. The maximum compressive stresses in the RRPM Types A, B, and C were -69.011, -31.862, and -40.251 MPa respectively. The maximum tensile stresses in the RRPM Types A, B, and C were 68.127, 34.753, and 43.846 MPa respectively.

Figure 61 shows percentage differences between maximum von Mises stresses (in the finite elements 1-6) from the reversed ASTM flexural test and the three stages of the base tire-marker impact simulation. The differences varied much among the elements for the stages 1 and 3. For the stage 2, however, the percentage differences did not vary much. The percent differences in the elements 1-4 for this stage were from -23 to -33 percent for the RRPM Type A, -47 to -67 percent for the RRPM Type B, and -42 and -83 percent for the RRPM Type C respectively. The percent differences varied much for the elements 5-6 for all the stages.

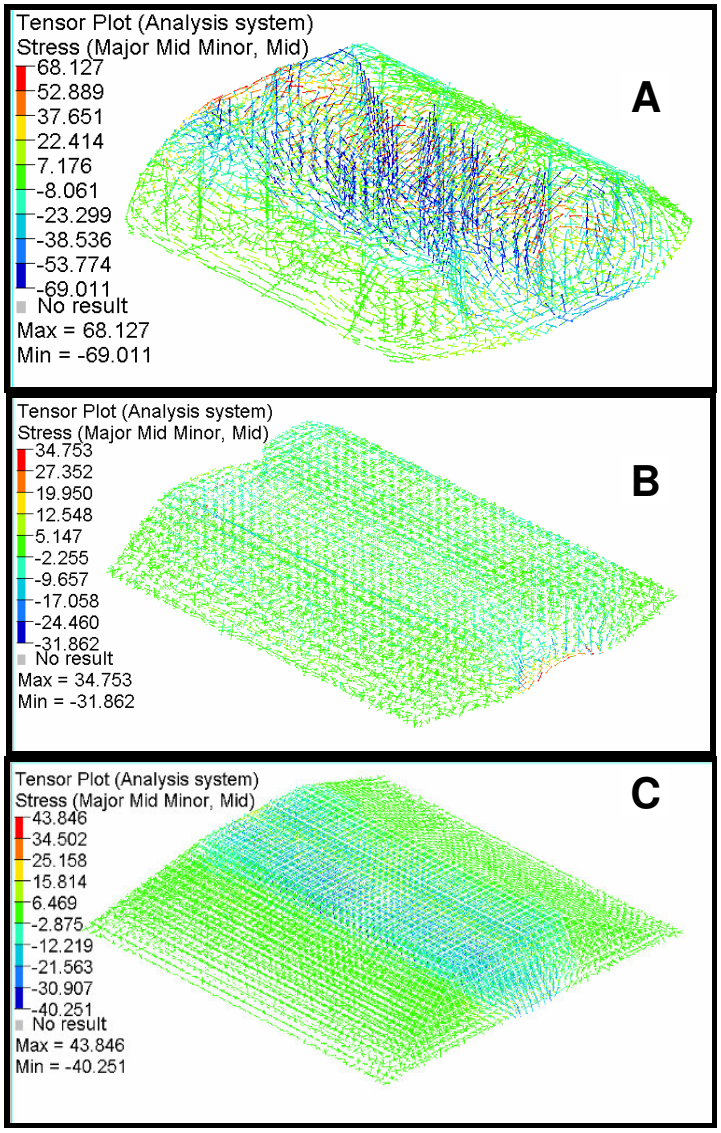

FIGURE 60 Stress tensor plots (in MPa) for RRPM Types A, B, and C (reversed ASTM flexure test).

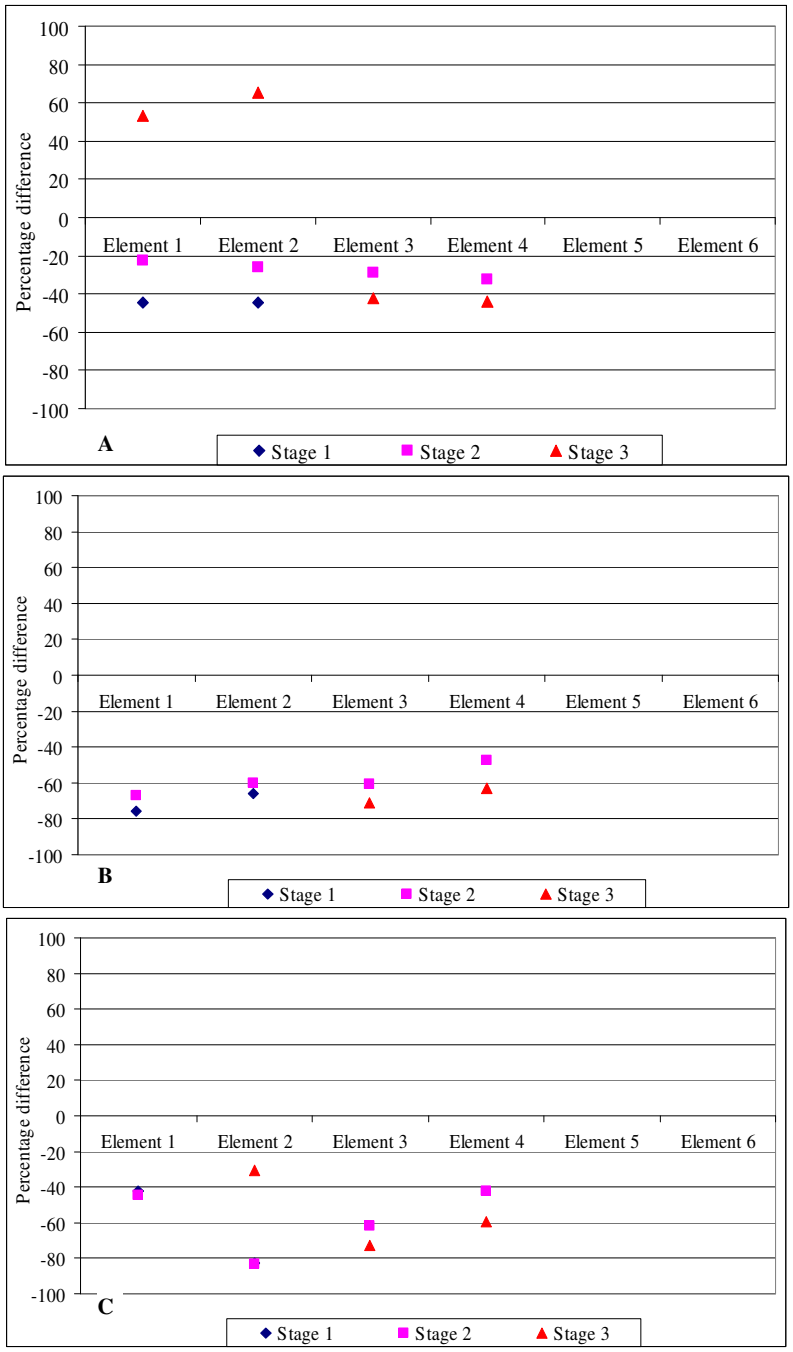

FIGURE 61 Percentage differences between maximum von Mises stresses from the three stages of the base tire-marker impact simulation and the reversed ASTM flexural test simulation in the finite elements 1-6 (RRPM Types A, B, and C).

Laboratory Tests Comparisons

The researcher used the previous analysis, where he compared the von Mises stresses from different laboratory testing simulations with the three stages of the tire-marker impact simulation, to compare the effectiveness of the six laboratory testing simulations. Appendix H provides the comparisons of the six laboratory tests simulation results (The points in the plots are connected by dotted curves, which is not appropriate as the data is discrete and not continuous; however, this is done to illustrate the comparisons better). The figures in the Appendix H are another representation of the analysis that the researcher did earlier. However, comparing all the laboratory tests together makes it easy to visualize the bigger picture.

From Figure 100 (page 170), Figure 101 (page 171), and Figure 102 (page 172), it is clear that the ASTM compression test, the cylindrical compression test and both the offset compression tests replicate the stage 2 of the tire-marker impact well. This is because for these tests, the percentage differences in von Mises stresses were lower in the chosen finite elements (except 5 and 6) of all the RRPM Types. The percent differences also did not vary much. The offset compression test simulates stage 1 of the tire-marker impact better than others do (Figure 97, page 167; Figure 98, page 168; and Figure 99, page 169). In the offset compression test, a higher loading rate makes a difference to the percentage differences. Figure 103 (page 173) and Figure 104 (page 174) show clearly that none of the laboratory tests simulations simulates stage 3 of the tire-marker impact simulation, as there is much variation among the elements for all the tests.

To better identify which laboratory test better simulated the tire-marker impact, the researcher compiled the percentage differences for all the tests in one single chart. Figure 62 shows this compilation. The figure has percent differences in von Mises stresses between the laboratory test simulations and the three stages of the tire-marker impacts simulations for all the possible cases. The yellow colored cells in the chart represent percentage differences lying between 0 and +100. The peach colored cells represent percentage differences lying between -100 and 0.The chart also has average of the percentage differences for every stage individually and across all the stages combined. The blue colored cells in the chart represent the averages of percent differences between -50 and 50.

The researcher sought to compare every laboratory test with every stage (1-3) of the tire-marker impact simulation. Since the researcher thought of stages 1, 2, and 3 of the tire-marker impact simulation as separate activities, he looked for the laboratory tests which could simulate any of these stages. He defined a few objective criteria to identify a good test:

1. The percentage differences across all the elements should be either positive or negative when comparing a laboratory test and any stage of the tire-marker impact simulation,
2. The percentage differences should lie within ±100 percent, and

RRPM Type	Laboratory test	Stage 1						Stage 2						Stage 3						Average (stage 1)	Average (stage 2)	Average (stage 3)	Average (across three stages)
		E1	E2	E3	E4	E5	E6	E1	E2	E3	E4	E5	E6	E1	E2	E3	E4	E5	E6				
RRPM Type A	ASTM compression test	-61	-62	178	233	-64	77	-45	-49	-48	-53	-82	209	9	13	-57	-61	-57	132	50	-11	-4	12
	ASTM flexural test	-42	-45	279	394	476	731	-19	-27	-29	-31	184	1355	61	63	-42	-43	595	991	299	239	271	270
	Cylindrical compression test	-85	-86	-3	27	6	103	-79	-81	-82	-82	-48	255	-58	-58	-85	-85	28	166	-6	-19	-15	-14
	Offset compression test (lower loading rate)	-66	-66	-62	-50	-38	-100	-52	-55	-93	-93	-69	-100	-6	1	-94	-94	-25	-100	-64	-77	-53	-65
	Offset compression test (higher loading rate)	9	5	6	46	27	-100	52	40	-80	-80	-37	-100	201	212	-84	-83	54	-100	-1	-34	33	-1
	Reversed ASTM flexural test	-45	-44	277	383	476	731	-23	-26	-29	-33	184	1355	53	65	-42	-44	595	991	296	238	270	268
RRPM Type B	ASTM compression test	-82	-78	84	405	87	306	-76	-75	-70	-54	108	267	182	244	-78	-68	45	394	120	16	120	85
	ASTM flexural test	-3	3	830	1650	1068	2476	31	20	50	59	1198	2226	1452	1545	9	12	807	3035	1004	597	1143	915
	Cylindrical compression test	-75	-69	114	529	187	344	-66	-64	-66	-43	218	301	305	393	-75	-60	123	440	172	47	188	135
	Offset compression test (lower loading rate)	-64	-61	-87	-71	134	-100	-52	-55	-98	-97	160	-100	473	517	-98	-98	82	-100	-42	-40	129	16
	Offset compression test (higher loading rate)	-30	-25	-70	-48	362	-100	-6	-13	-95	-95	413	-100	1019	1093	-96	-97	259	-100	15	17	346	126
	Reversed ASTM flexural test	-75	-66	144	476	188	393	-67	-60	-61	-47	220	346	291	447	-71	-63	124	500	177	55	205	145
RRPM Type C	ASTM compression test	74	70	103	152	1	700	75	71	61	60	60	700	10	18	72	72	97	517	183	171	131	162
	ASTM flexural test	28	37	967	1186	1725	10560	23	32	103	104	2786	10559	444	441	44	44	3467	8124	2417	2268	2094	2260
	Cylindrical compression test	-92	-88	-40	8	4	512	-92	-89	-89	-83	64	512	-67	-54	-92	-88	103	372	50	37	29	39
	Offset compression test (lower loading rate)	-89	-89	-96	-95	-36	341	-89	-89	-99	-99	2	341	-53	-56	-99	-99	26	241	-11	-6	-7	-8
	Offset compression test (higher loading rate)	-78	-78	-93	-91	29	785	-79	-78	-99	-99	104	785	-6	-12	-99	-99	153	583	79	89	87	85
	Reversed ASTM flexural test	-42	-82	101	264	900	2079	-44	-83	-62	-42	1481	2079	145	-30	-73	-59	1855	1581	537	555	570	554

FIGURE 62 Percentage differences in von Mises stresses from the laboratory tests simulations and the tire-marker impact in the elements 1-6 for all the possible cases.

3. The average percentage differences for any stage of the laboratory test should be within ±50 percent.

From the Figure 62, the researcher could not obtain any test that satisfied the above criteria. Hence, the researcher relaxed the criteria from elements 1-6 to elements 1-4. This was done because the percentage differences for the elements 5 and 6 were too high and thus, unreasonable for some cases (as seen in the Figure 62). Figure 63 shows the percentage differences and their averages without considering elements 5 and 6. After dropping elements 5 and 6 from the analysis, the researcher analyzed the new results and obtained a list of the tests that satisfied the criteria defined above. These are given in Table 10.

TABLE 10 Short Listed Laboratory Tests

<table>
<tr><td rowspan="2">RRPM Type</td><td colspan="3">Tire-marker impact simulation</td></tr>
<tr><td>Stage 1</td><td>Stage 2</td><td>Stage 3</td></tr>
<tr><td rowspan="3">A</td><td rowspan="3">offset compression test (higher loading rate)</td><td>ASTM compression test</td><td rowspan="3">Not applicable</td></tr>
<tr><td>ASTM flexural test</td></tr>
<tr><td>Reversed ASTM flexural test</td></tr>
<tr><td>B</td><td>offset compression test (higher loading rate)</td><td>ASTM flexural test</td><td>Not applicable</td></tr>
<tr><td>C</td><td>Not applicable</td><td>Not applicable</td><td>ASTM compression test</td></tr>
</table>

RRPM Type	Laboratory test	Stage 1				Stage 2				Stage 3				Average (stage 1)	Average (stage 2)	Average (stage 3)	Average (across three stages)
		E1	E2	E3	E4	E1	E2	E3	E4	E1	E2	E3	E4				
RRPM Type A	ASTM compression test	-61	-62	178	233	-45	-49	-48	-53	9	13	-57	-61	72	-49	-24	0
	ASTM flexural test	-42	-45	279	394	-19	-27	-29	-31	61	63	-42	-43	146	-26	10	43
	Cylindrical compression test	-85	-86	-3	27	-79	-81	-82	-82	-58	-58	-85	-85	-36	-81	-72	-63
	Offset compression test (lower)	-66	-66	-62	-50	-52	-55	-93	-93	-6	1	-94	-94	-61	-73	-48	-61
	Offset compression test (higher)	9	5	6	46	52	40	-80	-80	201	212	-84	-83	17	-17	62	20
	Reversed ASTM flexural test	-45	-44	277	383	-23	-26	-29	-33	53	65	-42	-44	143	-27	8	41
RRPM Type B	ASTM compression test	-82	-78	84	405	-76	-75	-70	-54	182	244	-78	-68	82	-69	70	28
	ASTM flexural test	-3	3	830	1650	31	20	50	59	1452	1545	9	12	620	40	755	472
	Cylindrical compression test	-75	-69	114	529	-66	-64	-66	-43	305	393	-75	-60	125	-60	141	69
	Offset compression test (lower)	-64	-61	-87	-71	-52	-55	-98	-97	473	517	-98	-98	-71	-75	198	17
	Offset compression test (higher)	-30	-25	-70	-48	-6	-13	-95	-95	1019	1093	-96	-97	-43	-52	480	128
	Reversed ASTM flexural test	-75	-66	144	476	-67	-60	-61	-47	291	447	-71	-63	120	-59	151	71
RRPM Type C	ASTM compression test	74	70	103	152	75	71	61	60	10	18	72	72	100	67	43	70
	ASTM flexural test	28	37	967	1186	23	32	103	104	444	441	44	44	554	66	243	288
	Cylindrical compression test	-92	-88	-40	8	-92	-89	-89	-83	-67	-54	-92	-88	-53	-88	-75	-72
	Offset compression test (lower)	-89	-89	-96	-95	-89	-89	-99	-99	-53	-56	-99	-99	-92	-94	-77	-88
	Offset compression test (higher)	-78	-78	-93	-91	-79	-78	-99	-99	-6	-12	-99	-99	-85	-89	-54	-76
	Reversed ASTM flexural test	-42	-82	101	264	-44	-83	-62	-42	145	-30	-73	-59	60	-58	-4	-1

FIGURE 63 Percentage differences in von Mises stresses from the laboratory tests simulations and the tire-marker impact in the elements 1-4 for all the possible cases.

Hence, the researcher limited the analysis to the laboratory tests listed in the above table. The researcher needed to validate the findings as listed in the above table with the qualitative analysis of principal stresses as done for all the laboratory tests. It was mentioned that the offset compression test (both loading rates) simulated the stage 1 of the tire-marker impact simulation only and the ASTM compression test simulated the stage 2 of the tire-marker impact only. As the ASTM flexural test produces major tensile stresses at the bottom center of the marker, it did not simulate any stage of the tire-marker impact. Similarly, as the reversed flexural test produced major tensile stresses at the top center of the marker, it did not simulate any stage of the tire-marker impact.

Hence, considering both the qualitative and quantitative analysis that the researcher did for comparing the six laboratory tests in their effectiveness to simulate the tire-marker impacts, he found the offset compression test (higher loading rate) to be a good test for simulating stage 1 of the tire-marker impact. He found the ASTM compression test to be a good test for simulating stage 2 of the tire-marker impact. He found no test to replicate stage 3 of the tire-marker impact. However, the researcher hypothesizes that a variation of the offset compression test, in which the loading bar is kept along the other retroreflective side's top edge of the marker, would replicate stage 3 of the tire-marker impact.

It should be mentioned here that these results would be more applicable for the tire-marker impacts on the rigid (concrete) pavements than on the flexible (asphalt) pavements. This is because the tire-marker-pavement model developed for this research did not have flexible pavement properties.

SUMMARY AND RECOMMENDATIONS

Retroreflective Raised Pavement Markers (RRPMs) supplement other pavement markings to provide information and guidance to road users. Previous research concerning durability of the RRPMs suggested that their performance had been degrading over the years. One of the main causes for underperformance of RRPMs was the lack of appropriate laboratory testing standards, which could test the adequacy of the RRPMs to perform in field conditions. There was a need to modify the existing standards or develop new testing procedures that could better simulate field conditions. The goal of this research was to identify critical magnitudes and locations of the stresses in RRPMs during tire-marker impacts by doing the FEM and simulation of the impacts, and use the information to recommend laboratory testing procedures that could simulate real-world conditions.

The researcher modeled the tire-marker impacts using the finite element tools Hypermesh and LS-DYNA. He calibrated the material properties of the marker models to improve the tire-marker model. He then used the model to simulate tire-impact forces on markers and find the critical locations and magnitudes of stresses inside the markers during the tire-marker impacts. In the process, he analyzed the effect of varying loads, velocities, and angles of impact on the locations and magnitudes of stresses in the markers. In accordance with the main objective of the research, the researcher then modeled a few laboratory-testing procedures that could simulate the field performance of RRPMs.

This section summarizes the findings from this research work. The researcher also makes recommendations based on the findings and lists limitations of the research. He then lists a few things that may be done in future as a continuation of this research.

FINDINGS

Following are findings from the research. These results are more applicable for tire-marker impacts on the rigid pavements than on the flexible pavements.

- The tire-marker impact simulations revealed the locations and magnitudes of stresses inside the markers during the impacts. According to the simulations, there are different locations and magnitudes of stresses during different stages of the impact.
    - When a tire ascends over the marker, it causes major compression in the upper half of the corresponding retroreflective side of the marker it approaches and on the edge contacts of top surface with the retroreflective side. The same thing happens during the phase when the tire leaves the marker. During the stage when the tire sits over the marker, compressive stresses are concentrated at the top edges of the retroreflective surfaces.
    - Tensile stresses were observed throughout the marker during these stages of impact, mostly at bottom of the marker. The compressive stresses discussed earlier are concentrated and are large in magnitude compared to the tensile stresses.

- The researcher analyzed the effect of varying a few variables, namely tire load, tire velocity, and angle of impact that could influence the behavior of tire-marker impacts.
    - The researcher found an effect of varying the angle of impact on the locations and magnitudes of stresses in the markers. There was a clear indication from the simulation results that the angle of impact is a critical factor in the tire-marker impacts. The stresses increased as the tire hit the marker at a greater angle, with higher stresses at the corners of the markers.
    - Although not very explicit, there was a relationship between the tire load and the magnitudes of stresses in the markers. Higher tire loads may lead to higher stresses. However, there is a need for further research to look into this aspect.
    - The researcher did not find any systematic effect of tire velocity on the locations and magnitudes of stresses inside the markers.
- The researcher got an estimate of interface forces between the RRPM and the pavement surface from the simulation results. These forces are in the range of 11,000-15,000 N based on the simulation results. There is an effect of variation in angles of impact and tire velocities on the interface forces. A higher angle of impact leads to higher interface forces. Higher tire velocities may lead to higher interface forces. No effect of varying tire load was seen on the interface forces.

- The researcher simulated six laboratory testing procedures that could simulate the stress conditions that were found during tire-marker impact simulations.
    - Based on the simulations, the ASTM compression test replicates stage 2 of the tire-marker impact.
    - The ASTM flexural test simulation did not produce the kind of stresses in the marker as were shown from the tire-marker impact simulations. However, it should be kept in mind that this research is more applicable to the tire-marker impacts on the rigid pavements than the flexible pavements. Hence, there is a need for further research in this aspect.
    - The researcher found that a test that could produce compressive stresses on one retroreflective top edge of the marker while producing tensile stresses in the other areas of the marker would be a good test to simulate ascent or descent of the tire over marker. The offset compression test discussed earlier (page 95) was found to be such a test. Based on the simulations, the offset compression test with a higher loading rate replicates the stage 1 of the tire-marker impact.

LIMITATIONS

Following are a few limitations that might have affected accuracy of the results.

- The major limitation of the tire-marker model was that it did not incorporate the pavement properties. Thus, the researcher could not replicate the phenomenon of a RRPM separating from the pavement. Additionally, the results from this work would be more applicable to tire-marker impacts on the rigid (concrete) pavements than the flexible (asphalt) pavements.
- The model was not perfectly calibrated, largely because the researcher could not get material properties or stress-strain curves for the RRPM materials. He relied on the manufacturers and online databases for these properties. This might have affected the simulation results and hence, these results must be viewed with some caution.
- The finite element solvers themselves have their limitations, which can reduce the model accuracy.
- None of the laboratory tests modeled to simulate the stresses in RRPMs as caused from the tire-marker impacts had elastomeric pads. In reality, the ASTM laboratory standards consist of the elastomeric pads. This might have limited accuracy of the results.

The researcher was also limited by the time-frame of this research work and limited resources. However, he believes that the methodology adopted here holds

much significance. Hence, it should be used for future research with improvements wherever required.

RECOMMENDATIONS

Following are the recommendations based on the simulation results: This research work is more applicable to the tire-marker impacts on the rigid pavements than on the flexible pavements. Hence, it is recommended that further research be pursued with consideration of the flexible pavement properties before taking any decision based on these recommendations.

- The ASTM compression test for testing RRPMs' structural performance or a similar test would be a good test to replicate the field conditions. Hence, either the ASTM test should be continued or a similar test be developed.
- There is a need to review the ASTM flexural test, as it did not provide the similar stresses in the markers as the tire-marker impact simulations did. Based on the simulation results in this research work, ASTM flexural test should be eliminated.
- A test similar to the offset compression test discussed in this research (page 95) should be developed. The loading rate for the test should be decided only after doing further simulations with different loading rates.

FUTURE WORK

The researcher recommends pursuing the following tasks as a continuation of this research.

- The laboratory procedures simulated in this research are not exhaustive. There are other scenarios that could be tested. Especially, one needs to further evaluate tests with different loading rates, (e.g. impact loading) as the researcher found out from the simulations that different loading rates led to different magnitudes of stresses inside the markers.
- The tire-marker model developed in the research did not consider pavement properties. That could be an important factor and future models should be developed to include that.
- The researcher did not analyze any laboratory test that could simulate tires hitting RRPMs at a non-zero angle. Since, it was found in this research that angle of impact is a critical external variable in the tire-marker impacts; hence the researcher recommends that work should be directed towards developing tests that consider this aspect. The researchers may also look into developing tests with forces that are not directly vertical in nature.
- The tire-marker model developed in this research was not calibrated perfectly. It would be better if the marker model were calibrated with material properties found from appropriate respective laboratory testing procedures.

- There is a need to develop a fatigue-loading model from the tire-marker model developed in this research. It would be interesting to note the effect of repetitive impacts of tires over markers, as happens in the field, by simulating the fatigue loading.
- One can further evaluate the effect of variation in external factors, e.g. tire inflation pressures, locations of impact, etc. on stresses inside the markers.
- There is a need to evaluate further the effect of tire loads on the stresses inside markers during the tire-marker impacts. This research indicated, although not very clearly, that higher tire loads may lead to higher stresses inside markers.
- There is a need to measure the interface forces between the markers and the pavement during the tire-marker impacts. This could be a good way of validating the tire-marker model developed for this research.
- There is a need to develop the tire-marker model used here to include the estimation of interface forces between a tire and different faces of a marker (e.g. top, front, and back surfaces etc.).
- The researcher did not perform a sensitivity analysis on doing the finite element modeling of the tire-marker impacts by different ways. In the future, researchers can look at this aspect.

REFERENCES

1. *Manual on Uniform Traffic Control Devices for Streets and Highways.* Federal Highway Administration, U.S. Department of Transportation, Washington D.C., 2003.

2. McNees, R. and J. S. Noel. *State-of-the-art and Objectives of Reflective Raised Pavement Markers*. Report No. 322-1. Texas Transportation Institute, College Station, Texas, 1986.

3. Tielking, J. T. and J. S. Noel. *On the Retention of Reflective Raised Pavement Markers*. Report No. 477-1F. Texas Transportation Institute, College Station, Texas 1988.

4. Pezoldt, V. J. *Raised Pavement Marker Retroreflectivity*. Report No. 1151-1F. Texas Transportation Institute, College Station, Texas, 1990.

5. Ullman, G. L. *Retroreflective Raised Pavement Markers: A Two-year Field Evaluation in Texas.* Report No. 1946-3. Texas Transportation Institute, College Station, Texas, 1994.

6. ASTM International. *Standard Specification for Extended Life Type, Nonplowable, Raised Retroreflective Pavement Markers*. Publication ASTM D4280-03. West Conshohocken, Pennsylvania, 2003.

7. Migletz, J., J. K. Fish, and J. L. Graham. *Roadway Delineation Practices Handbook*. Report No. FHWA-SA-93-001. Federal Highway Administration, U.S. Department of Transportation, Washington D.C., 1993.

8. Pline, J. L. *Traffic Control Devices Handbook*. Institute of Transportation Engineers, Washington D.C., 2001.

9. Grant, A.R. and J. R. Bloomfield. *Guidelines for the Use of Raised Pavement Markers*. Report No. FHWA-RD-97-152. Federal Highway Administration, U.S. Department of Transportation, Washington D.C., 1998.

10. Rushing, H.B., J. O. Burt, and E. J. LeBlanc. *Evaluation of Raised Pavement Markers.* Report No. 68-1T. Louisiana Department of Highways, Baton Rouge, Louisiana, 1968.

11. Pigman, J.G., K. R. Agent, and R. L. Rizenbergs. *Evaluation of Raised Pavement Markers.* Kentucky Department of Transportation, Lexington, Kentucky, 1975.

12. Kidd, S.Q. *An Evaluation of Reflective Markers: Final Report*. Report No. MSHD-RD-90-67-4. Mississippi State Highway Department, Jackson, Mississippi, 1990.

13. McNees, R, and J. S. Noel. *Retroreflectivity Retention of Reflective Raised Pavement Markers.* Report No. 322-2. Texas Transportation Institute, College Station, Texas, 1986.

14. McNees, R. and J. S. Noel. *Retention of Reflective Raised Pavement Markers.* Report No. 322-3. Texas Transportation Institute, College Station, Texas, 1986.

15. McNees, R. and J. S. Noel. *Executive Summary, Significant Results and Assorted Tests and Procedures for Reflective Raised Pavement Markers.* Report No. 322-4F. Texas Transportation Institute, College Station, Texas, 1986.

16. Ullman, G. L. *Retroreflective Raised Pavement Marker Field Testing: Initial Interim Report*. Report No. 1946-1. Texas Transportation Institute, College Station, Texas, 1992.

17. Ullman, G. L. *Retroreflective Raised Pavement Marker Field Testing: Results of the First Year Evaluation*. Report No. 1946-2. Texas Transportation Institute, College Station, Texas, 1994.

18. California Department of Transportation Engineering Services. *Method of Testing for Specification Compliance of Non-reflective and Retroreflective Pavement Markers.* California Department of Transportation, Sacramento, 2003.

19. National Transportation Product Evaluation Program (NTPEP). *Project Work Plan for the Field and Laboratory Evaluations Raised Pavement Markers and Adhesives.* American Association of State Highway and Transportation, Washington D. C., 2004.

20. Marshek, K. M., W. R. Hudson, R. B. Connell, H. H. Chen, and C. L. Saraf. *Experimental Investigation of Truck Tire Inflation Pressure on Pavement-Tire Contact Area and Pressure Distribution.* Report No. 386-1. Center for Transportation Research, University of Texas at Austin, Austin, Texas, 1985.

21. Roberts, F. L., J. T. Tielking, D. Middleton, R. L. Lytton, and K. Tseng. *Effects of Tire Pressures on Flexible Pavements*. Report No. 372-1F, College Station, Texas, 1986.

22. Cebon, D. *Handbook of Vehicle-road Interaction*. Swets and Zieitlinger Publications, Lisse, Netherlands, 1999.

23. Xu, Y., L. Jia, and J. Zhang. Modeling Tire/road Contact Using Piecewise Ritz Procedure. In *Journal of Terramechanics*, Vol. 2, 2005, Elsevier, Amsterdam, Netherlands, pp. 99-113.

24. Rothert, H., H. Idelberger, W. Jacobi, and G Laging, On the Finite Element Solution of the Three-Dimensional Tire Contact Problem. In *Nuclear Engineering and Design*, Vol. 78, Amsterdam, Netherlands, 1984, pp. 363-375.

25. Abeels, P. F. J. Tire Deflection and Contact Studies. In *Journal of Terramechanics*, Vol. 13, Elsevier, Amsterdem, Netherlands, 1976, pp. 183-196.

26. Mousseau, C. W. and G. M. Hulbert. An Efficient Tire Model for the Analysis of Spindle Forces Produced by a Tire Impacting Large Obstacles. In *Computer Methods in Applied Mechanics and Engineering*, Vol. 135, Elsevier, Amsterdem, Netherlands, 1996, pp. 15-34.

27. Pesterev, A.V., L. A. Bergman, C. A. Tan, and B. Yang. Assessing Tire Forces Due to Roadway Unevenness by the Pothole Dynamic Amplification Factor Method. In *Journal of Sound and Vibration*, Vol. 279, Elsevier, Amsterdem, Netherlands, 2005, pp. 817-841.

28. Bonse, R. P. H. and S. H. Kuhn. Dynamic Forces Exerted by Moving Vehicles on a Road Surface. In *Flexible Pavement Design Research*, Vol. 233, Highway Research Board, Washington D.C., 1959, pp. 9-32.

29. Hansen, R. W., C. Bertrand, K.M. Marshek, and W. R. Hudson. *Truck Tire Pavement Contact Pressure Distribution Characteristics for Super Single 18-22.5 and Smooth 11R24.5 Tires.* Report No. 1190-1. Center for Transportation Research, University of Texas at Austin, 1989.

30. Philips, D.A. *Finite Element Analysis of a Shaft-rotor System*. Master's thesis, Virginia Polytechnic and State University, Blacksburg, Virginia, 2001.

31. Lecture Notes. Finite Element Methods. http://www.st.bv.tum.de/content/teaching/ifem/ifem.html#notes. Accessed 8 Jan 2006.

32. Rao, S. S. *Finite Element Method in Engineering, First Edition.* Pergamon Press, Oxford, 1982.

33. Livesley, R. K. *Finite Elements: an Introduction for Engineers, First Edition*. Cambridge University Press, Cambridge, 1983.

34. Finite Element Analysis. Wikipedia, The Free Encyclopedia. http://en.wikipedia.org/wiki/Finite_element_analysis. Accessed 30 May 2005.

35. Altair Hypermesh. http://www.altair.com/software/hw_hm.htm. Accessed 20 June 2005.

36. LS-DYNA. http://www.lstc.com/. Accessed 20 June 2005.

37. Altair Hyperview. http://www.altair.com/software/hw_hv.htm. Accessed 20 June 2005.

38. Von Mises Stress. Wikipedia, The Free Enyclopedia. http://en.wikipedia.org/wiki/Von_Mises_stress. Accessed 10 February 2006.

APPENDIX A

DISTRICT SURVEY ON RETROREFLECTIVE RAISED PAVEMENT MARKERS

District_____
District Engineer_____
Traffic/Maintenance Engineer_____
Phone_____
Address_____
Phone_____

1. Are RRPMs used in your district?

Yes_____
No_____
(If the answer is yes, follow to next questions)

2. What are the RRPM brands that you use?

3. Do you have any specific tests for RRPMs? If yes, then explain.

4. What are the application procedures?

5. What is the average maintenance period for markers? What percentages of markers do you replace on one section at a time? Do you have reports of the past and future maintenance schedules and details?

6. Do you have any mass failure experience with RRPMs (Large losses shortly after installation)? If yes, then where?

7. Have you had any markers with service life of 5 years? If yes, then where are they located? What are the traffic, geometric and environmental conditions there?

8. Does the performance of markers vary by these factors? Explain.

i. Volume
High volume roads _____
Low volume roads_____
ii. Pavement Surface
Asphalt_____
Concrete_____
Seal-coat surface treatment_____

iii. Environment
Rain_____
Heat_____
Cold weather_____

9. Has there been ever a survey of RRPM performance by the district office or by any agency? If yes, then do you have any reports of performance regarding retention of markers?

10. How would you rate these failure modes by frequency? (High/Average/Low)
    a. Marker loss in pavement
    b. Marker break
    c. Marker-epoxy failure
    d. Epoxy failure
    e. Epoxy-pavement bond failure
    f. Marker wear
    g. Retroreflective lenses broken/scratched
    h. Retroreflectivity loss

11. Have there been any complaints from the motorists regarding markers?

12. What suggestions do you have to improve the durability of markers?

13. Any comments_____

APPENDIX B

CALIBRATION RESULTS

The Appendix provides Figure 64 to Figure 75. The figures show the comparisons between experimental and simulation results. There are two kinds of results:

1. Displacement of top surface of the marker in mm, and
2. Strains in the strain gauges 1-6.

Figure 64 shows the comparison of displacements (in mm) of top surface of the marker from the experiment and the simulation for the RRPM Type A. Figures 65-67 show the comparisons of strains in the strain gauges 1-6 for the RRPM Type A. Figure 68 shows the comparison of displacements (in mm) of top surface of the marker from the experiment and the simulation for the RRPM Type B. Figures 69-71 show the comparisons of strains in the strain gauges 1-6 for the RRPM Type B. Figure 72 shows the comparison of displacements (in mm) of top surface of the marker from the experiment and the simulation for the RRPM Type C. Figures 73-75 show the comparisons of strains in the strain gauges 1-6 for the RRPM Type C.

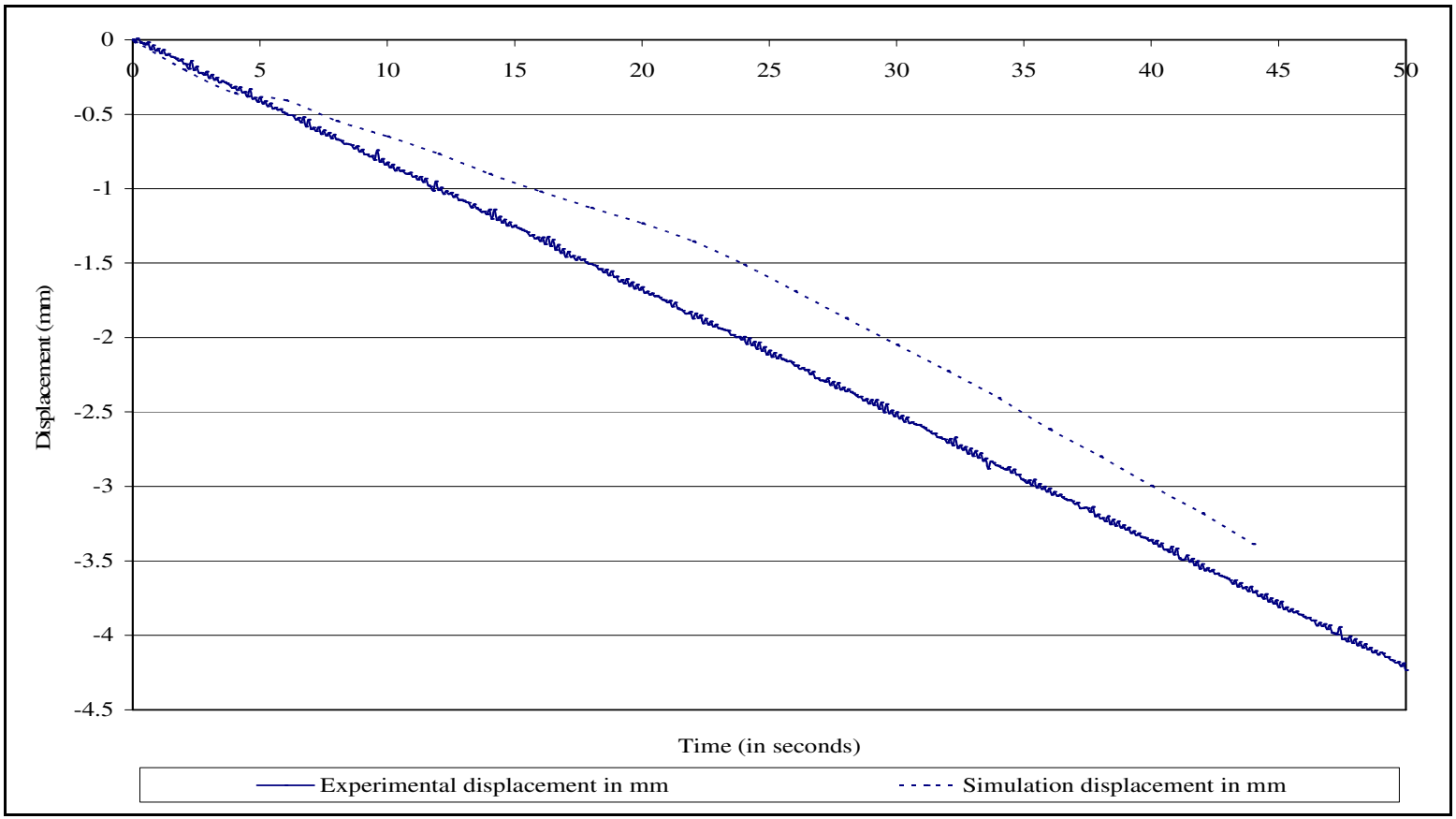

FIGURE 64 Experiment versus simulation for RRPM Type A- displacement of top surface of the marker in mm.

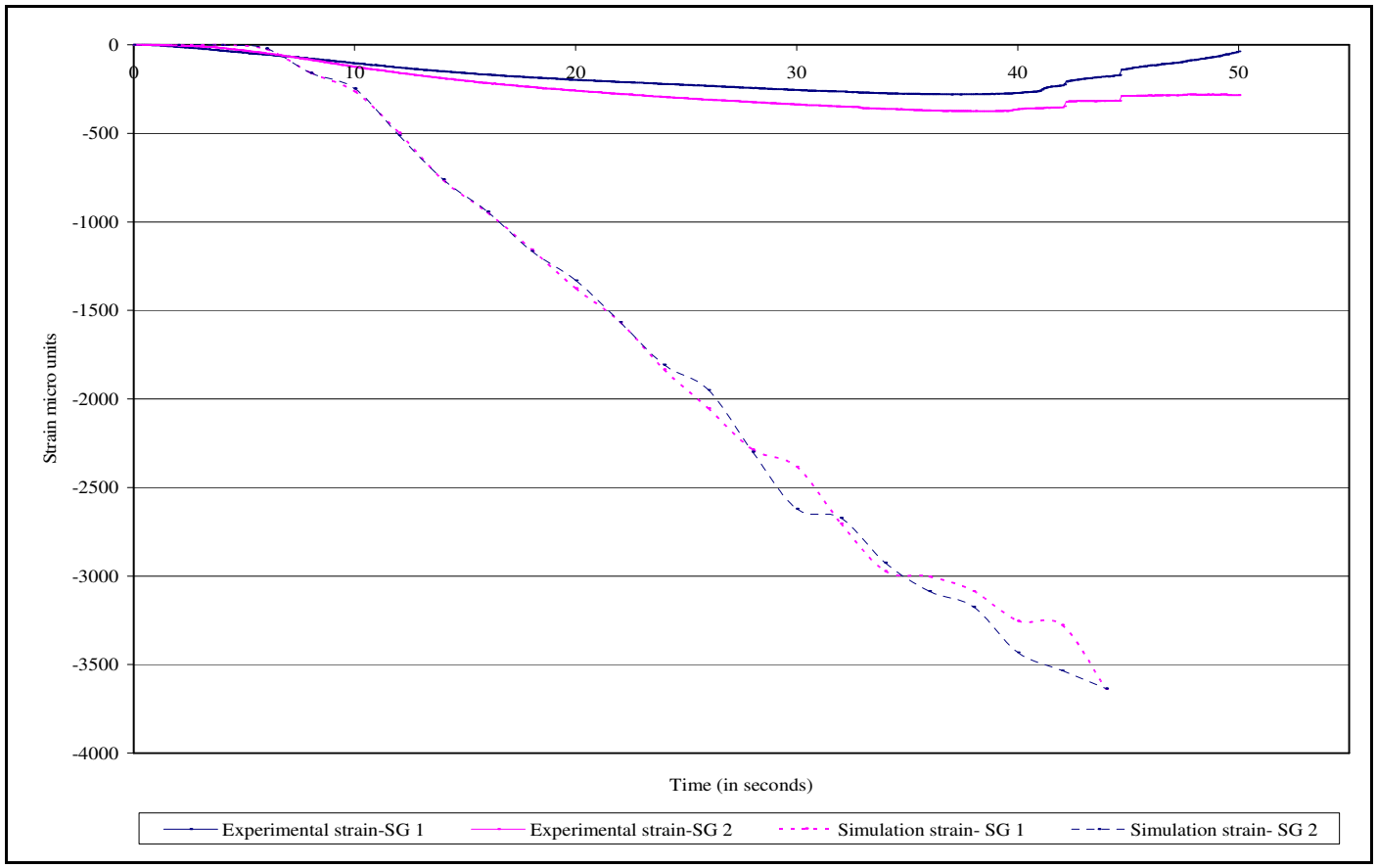

FIGURE 65 Experiment versus simulation for RRPM Type A- strains from strain gauges 1 and 2.

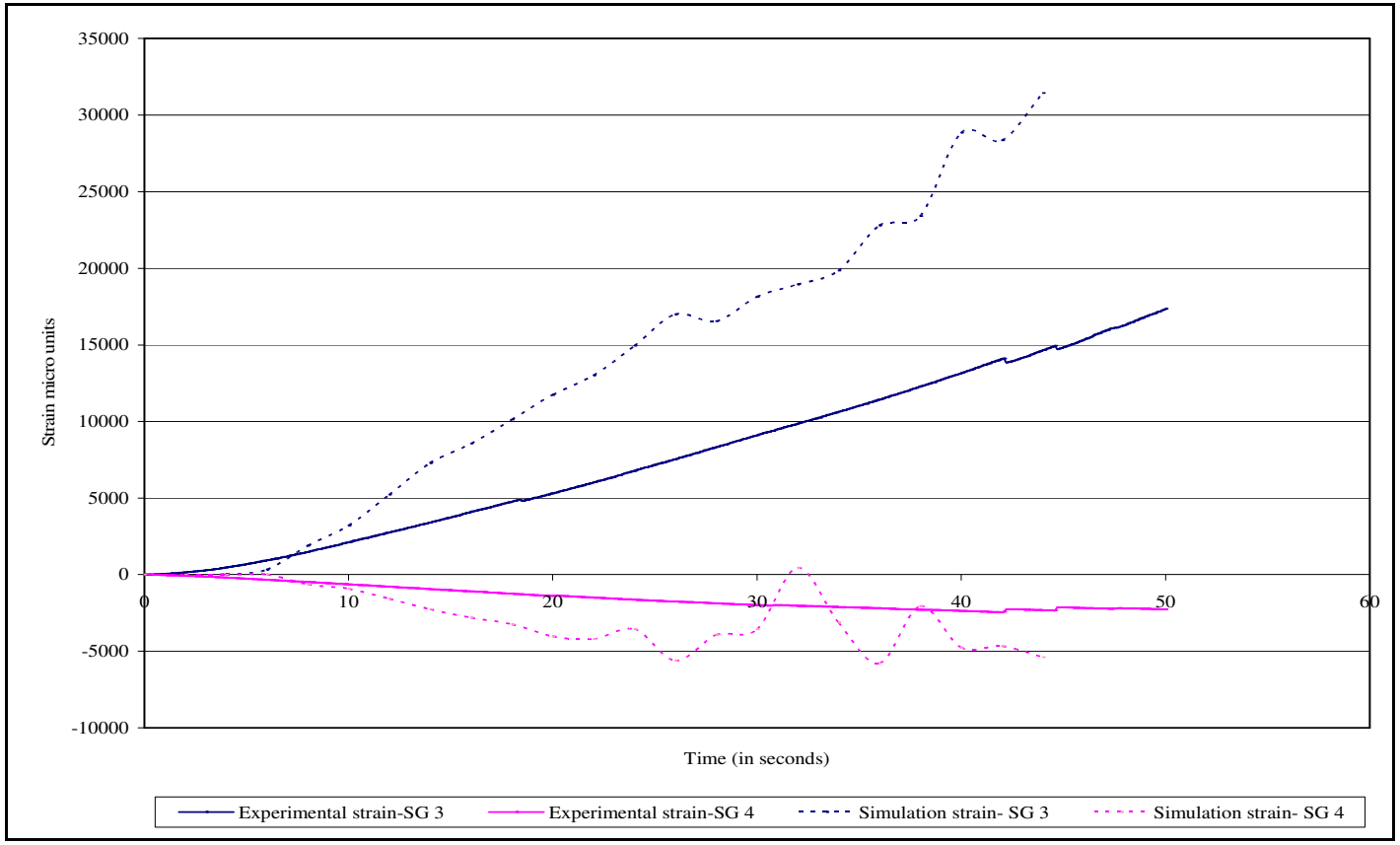

FIGURE 66 Experiment versus simulation for RRPM Type A- strains from strain gauges 3 and 4.

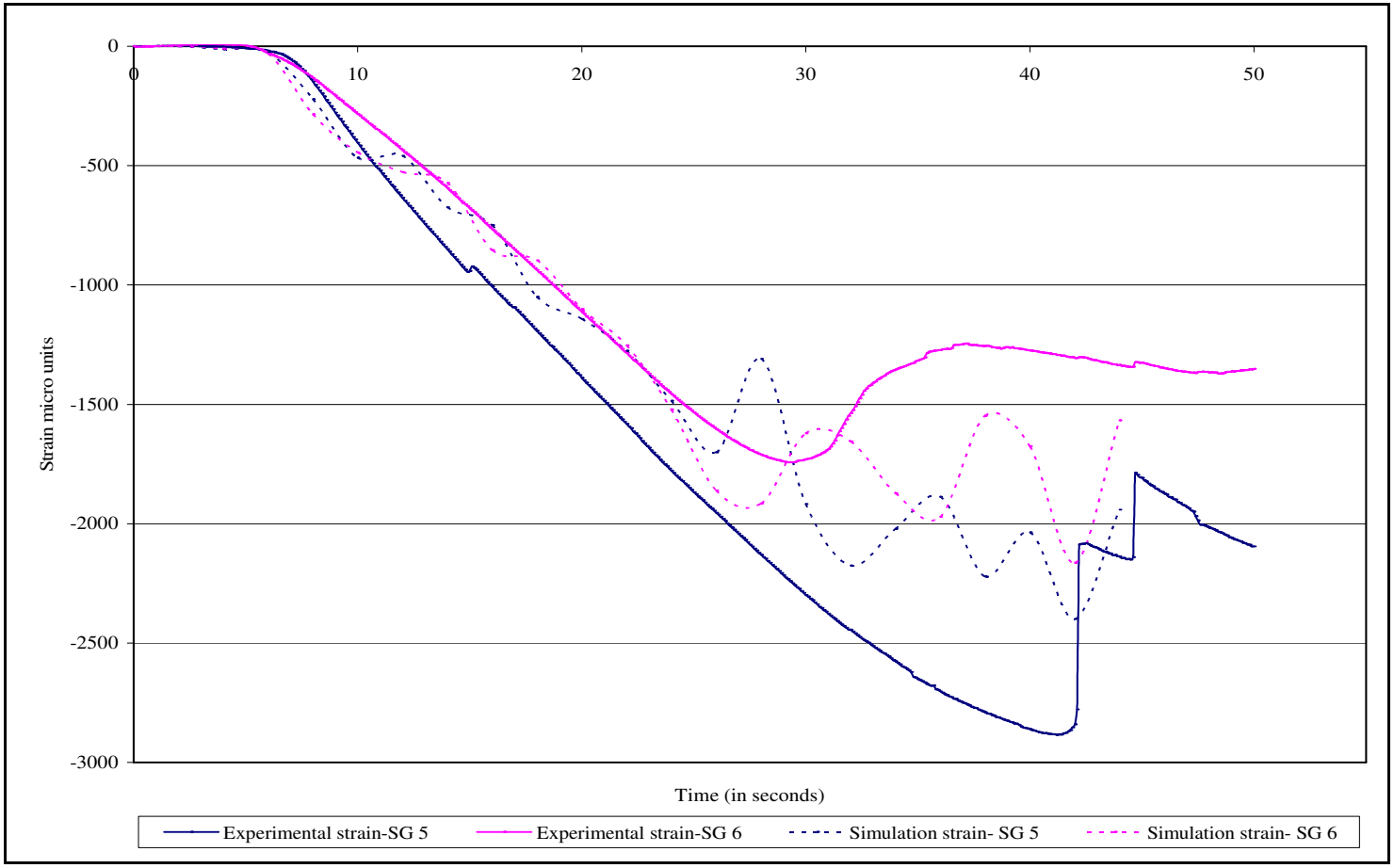

FIGURE 67 Experiment versus simulation for RRPM Type A- strains from strain gauges 5 and 6.

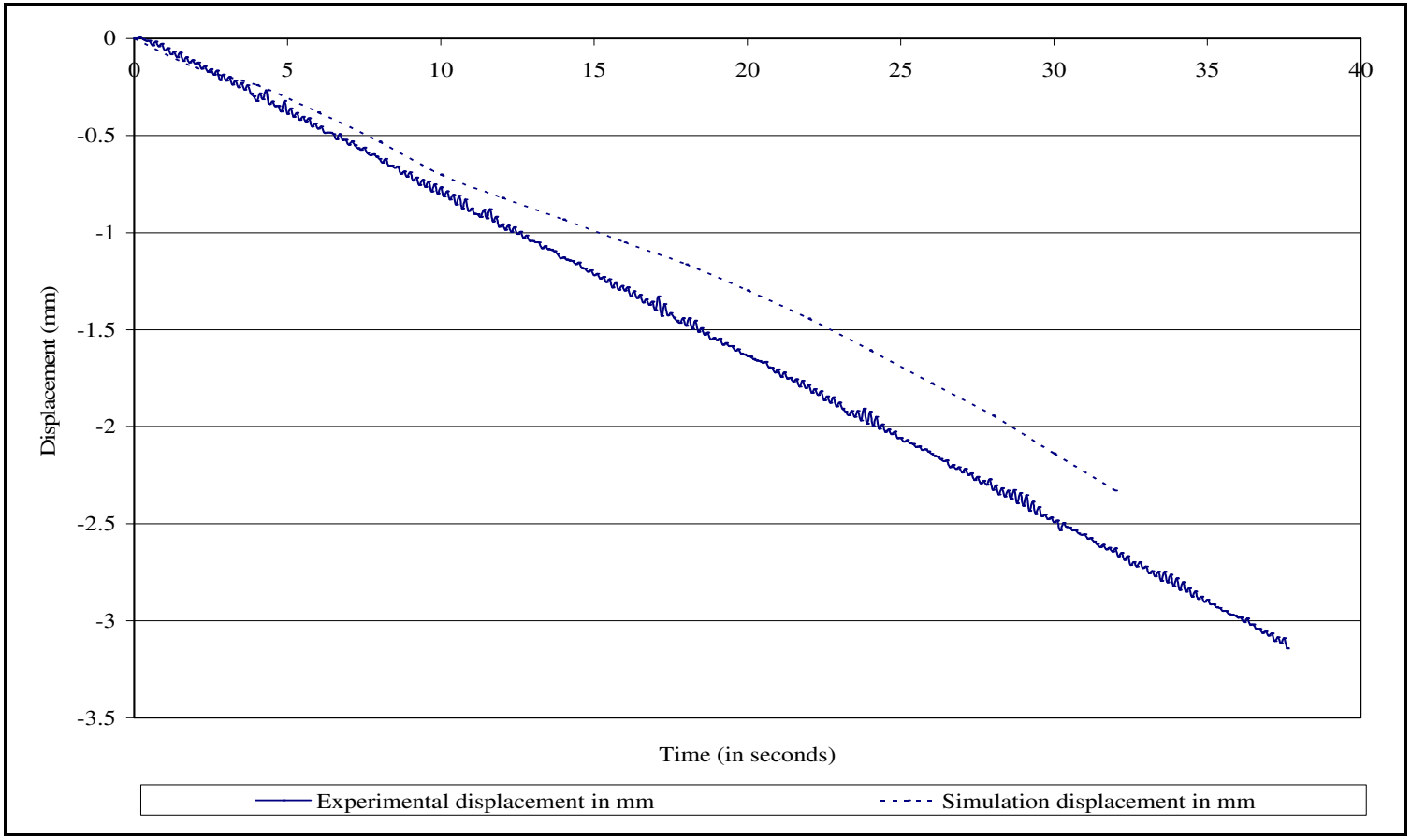

FIGURE 68 Experiment versus simulation for RRPM Type B- displacement of top surface of the marker in mm.

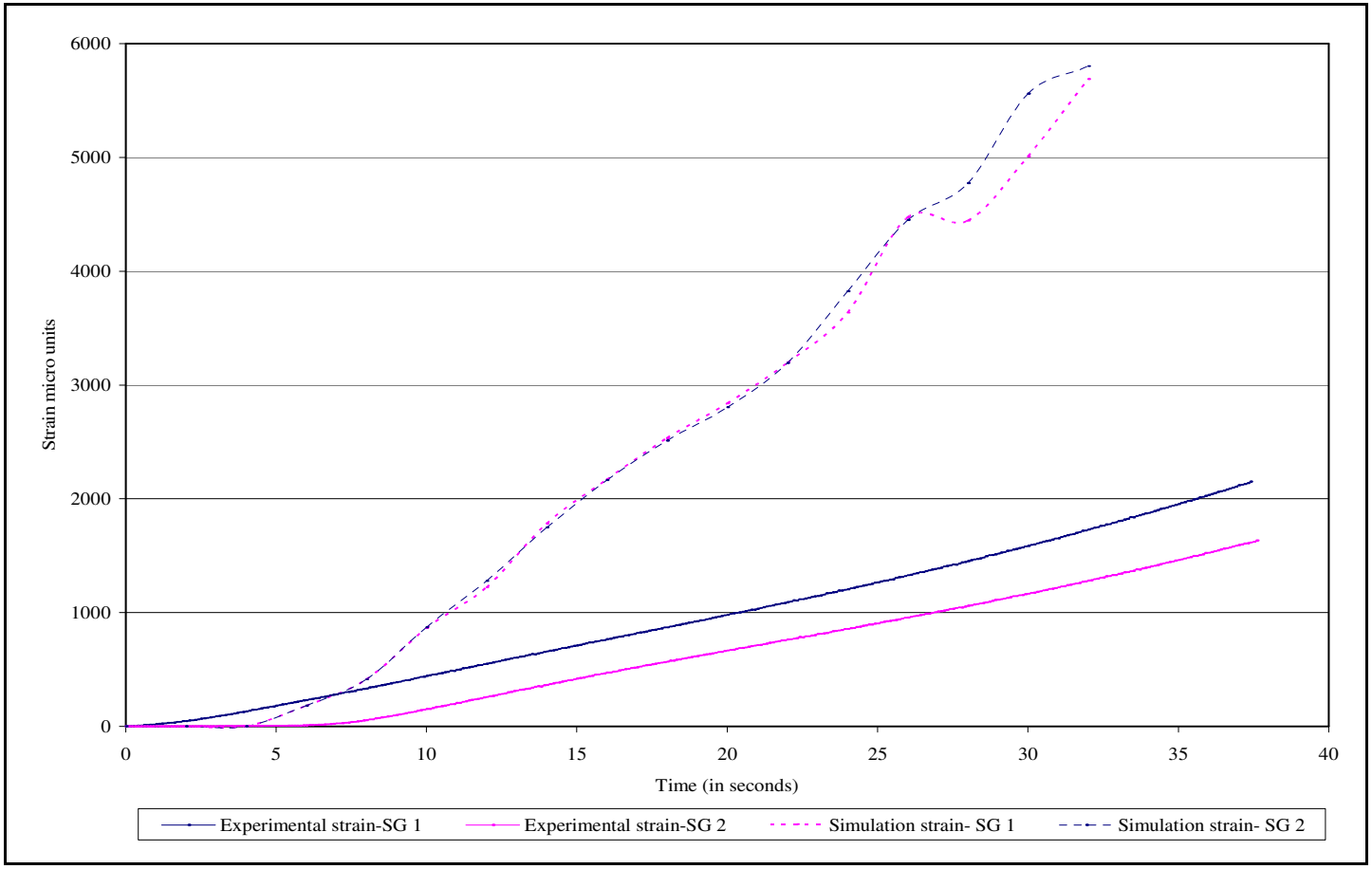

FIGURE 69 Experiment versus simulation for RRPM Type B- strains from strain gauges 1 and 2.

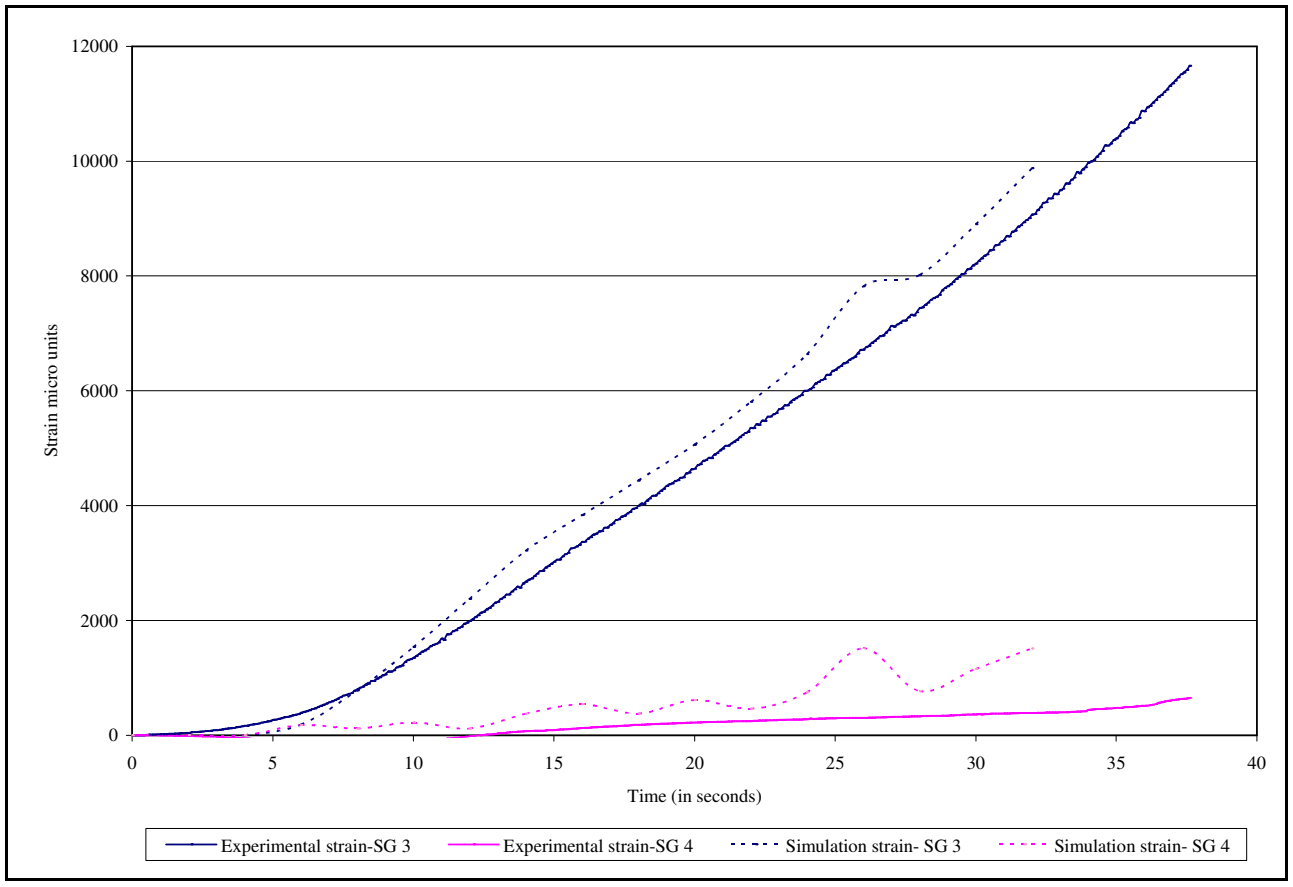

FIGURE 70 Experiment versus simulation for RRPM Type B - strains from strain gauges 3 and 4.

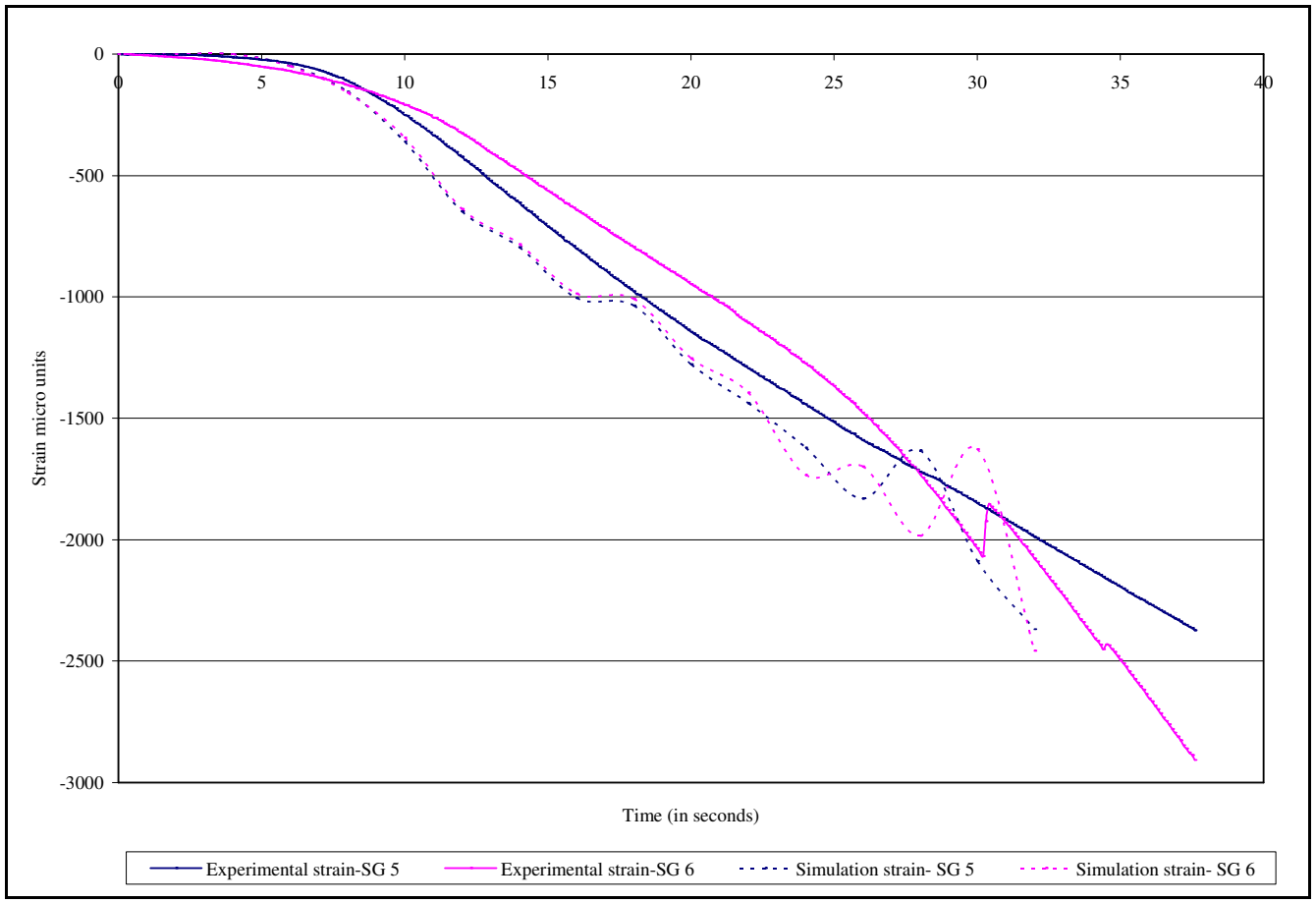

FIGURE 71 Experiment versus simulation for RRPM Type B- strains from strain gauges 5 and 6.

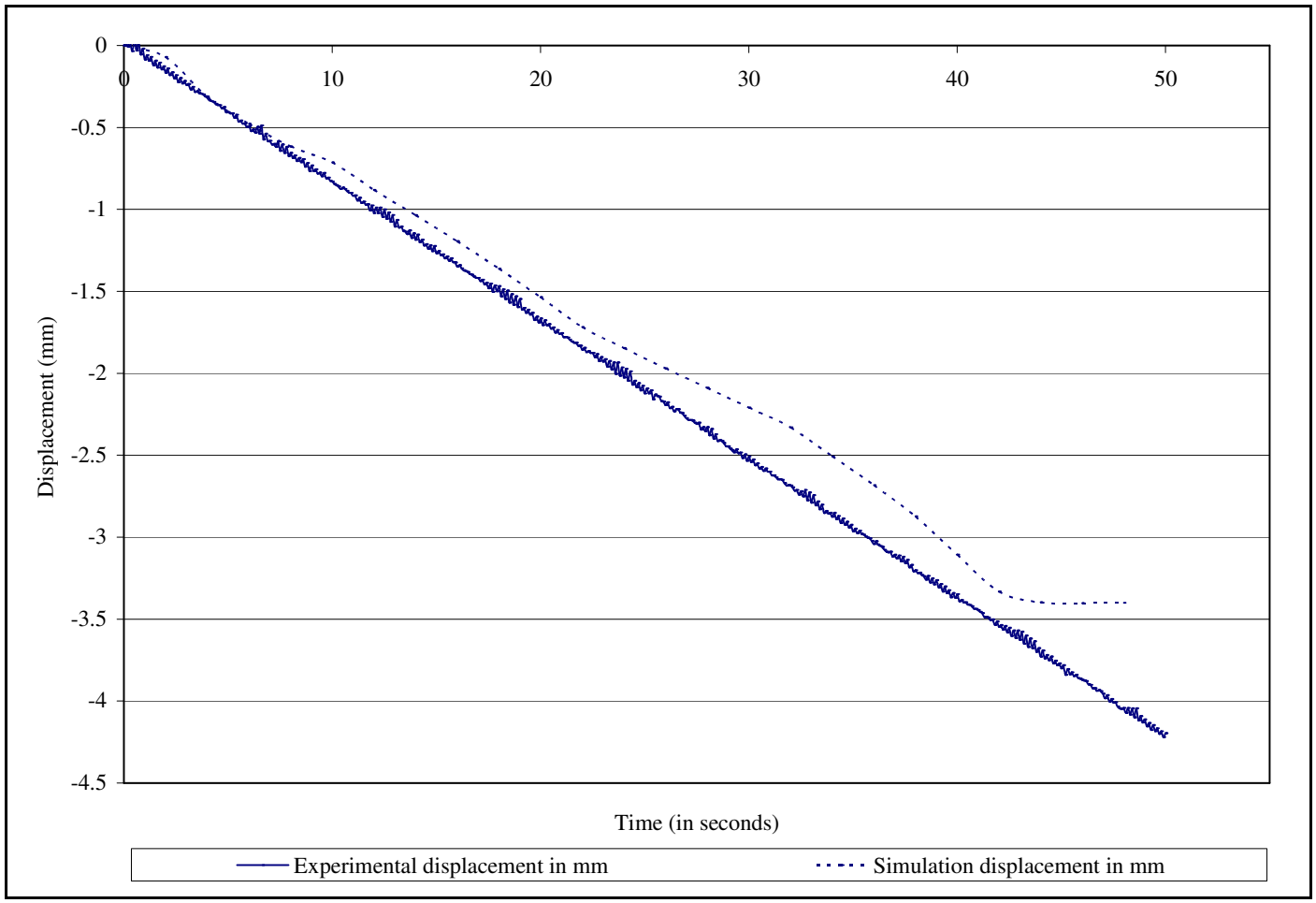

FIGURE 72 Experiment versus simulation for RRPM Type C- displacement of top surface of the marker in mm.

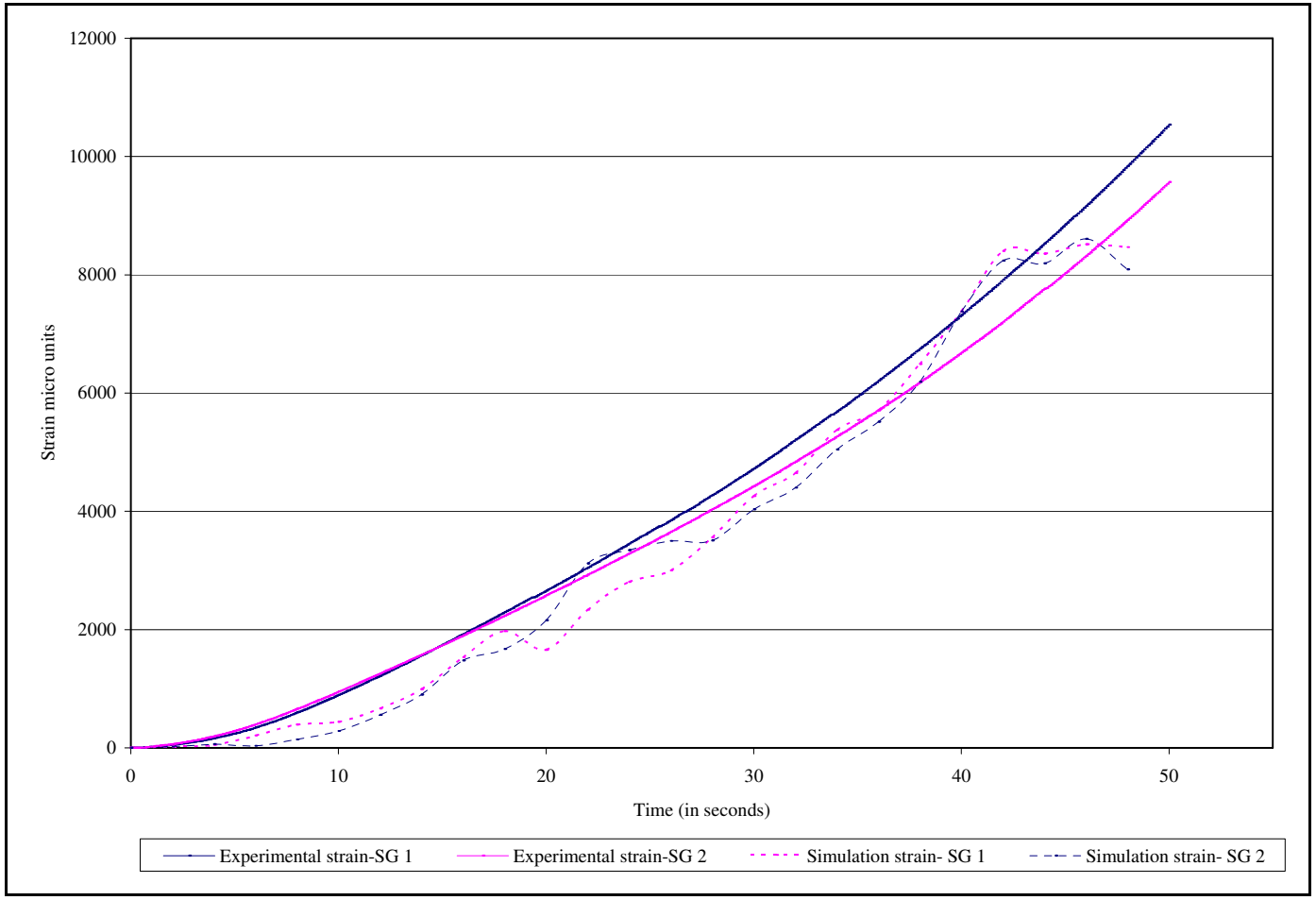

FIGURE 73 Experiment versus simulation for RRPM Type C- strains from strain gauges 1 and 2.

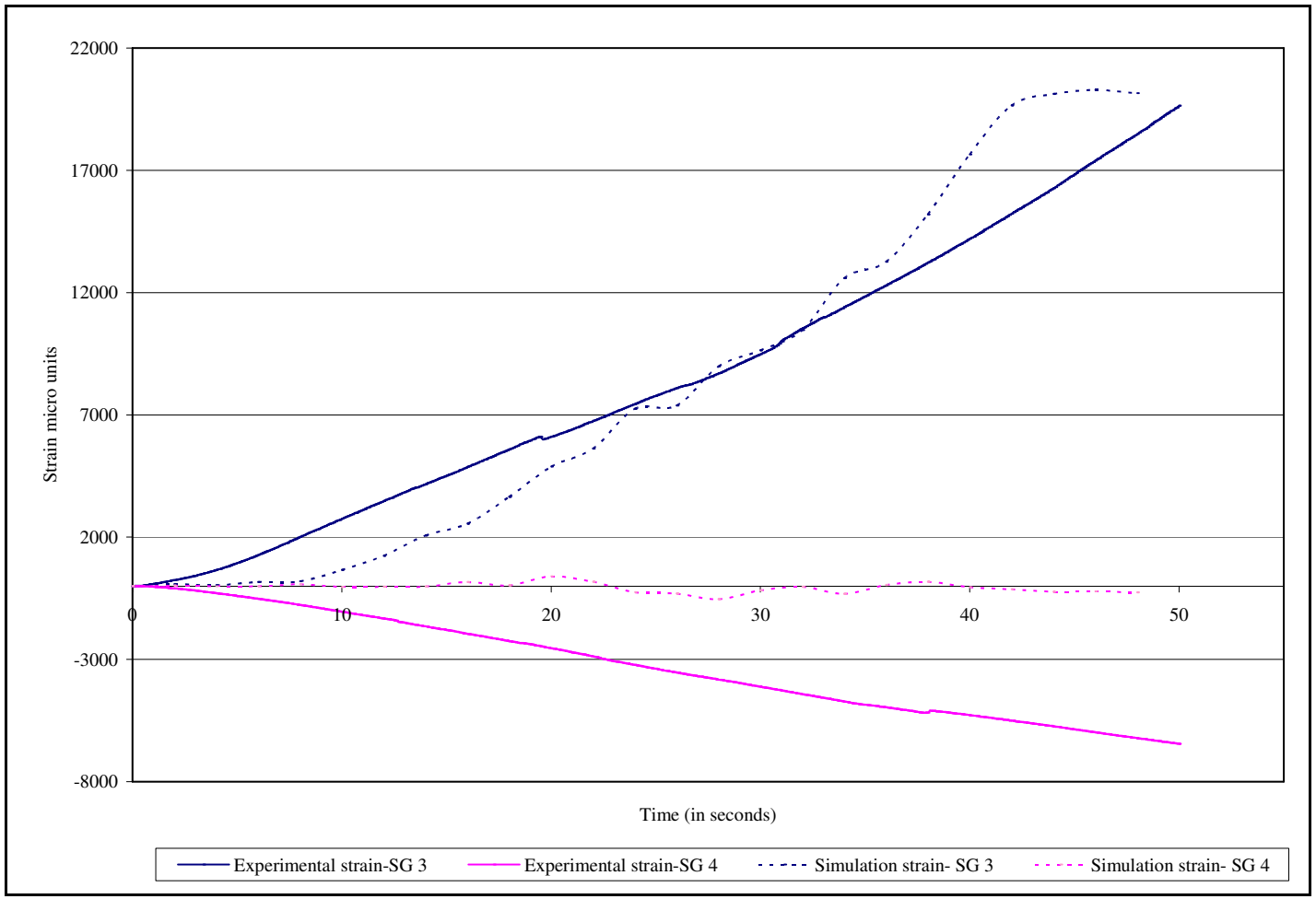

FIGURE 74 Experiment versus simulation for RRPM Type C- strains from strain gauges 3 and 4.

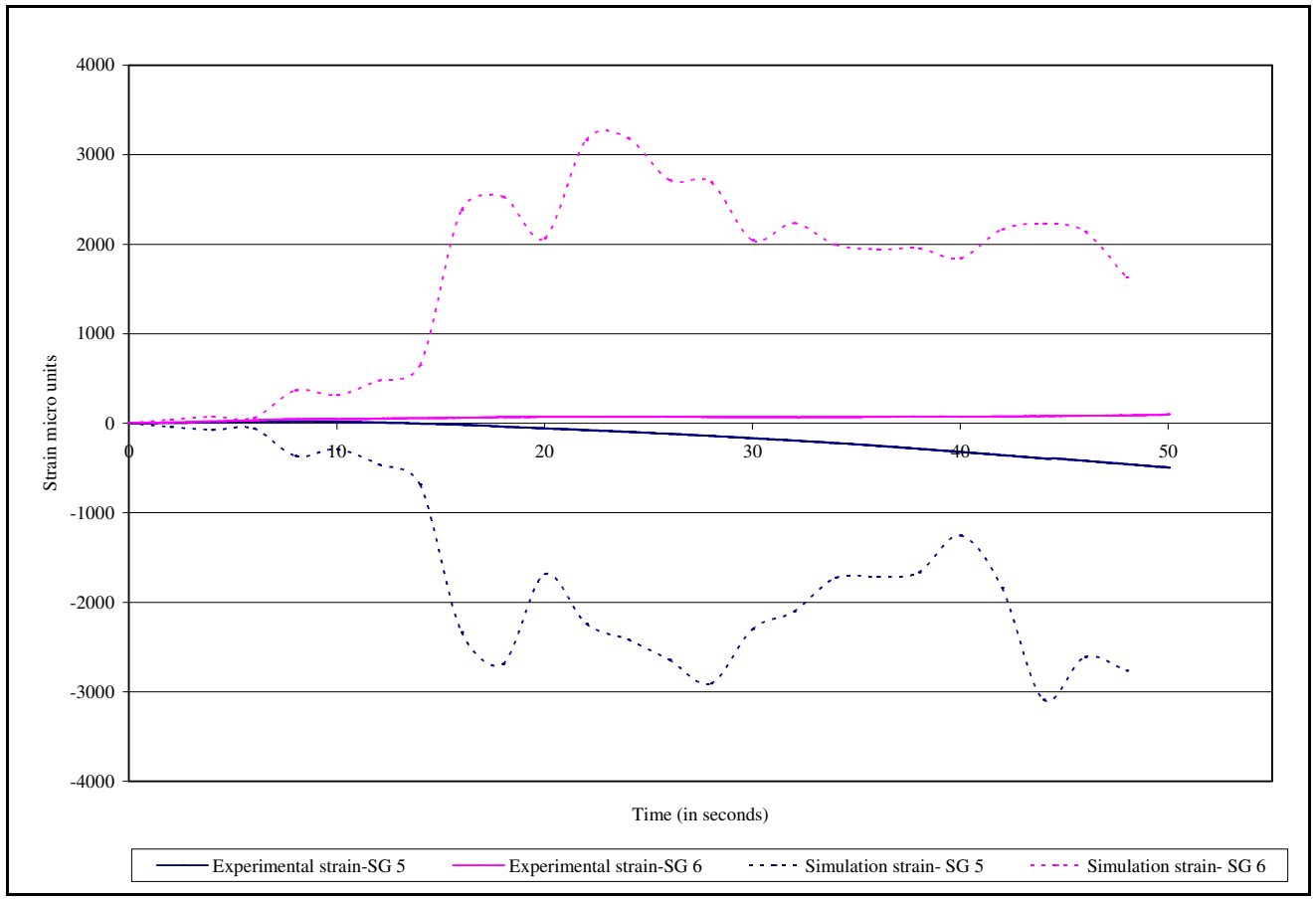

FIGURE 75 Experiment versus simulation for RRPM Type C- strains from strain gauges 5 and 6.

APPENDIX C

RRPM TYPE A RESULTS

TABLE 11 Variation in Maximum Stresses in MPa for Three Stages (RRPM Type A)

		Maximum stresses in MPa		
		Stage 1	Stage 2	Stage 3
Tire load in N	13,345 N	55.525	42.406	58.484
	22,241 N	59.608	54.520	60.000
	31,138 N	56.961	59.283	55.346
Tire velocity in m/s	17.9 m/s	50.181	58.377	50.410
	26.8 m/s	56.842	59.999	54.461
	35.8 m/s	54.525	54.211	56.859
Angle of impact in degrees	0 degree	59.608	54.520	60.000
	10 degrees	60.000	55.262	60.000
	20 degrees	59.922	60.000	60.000

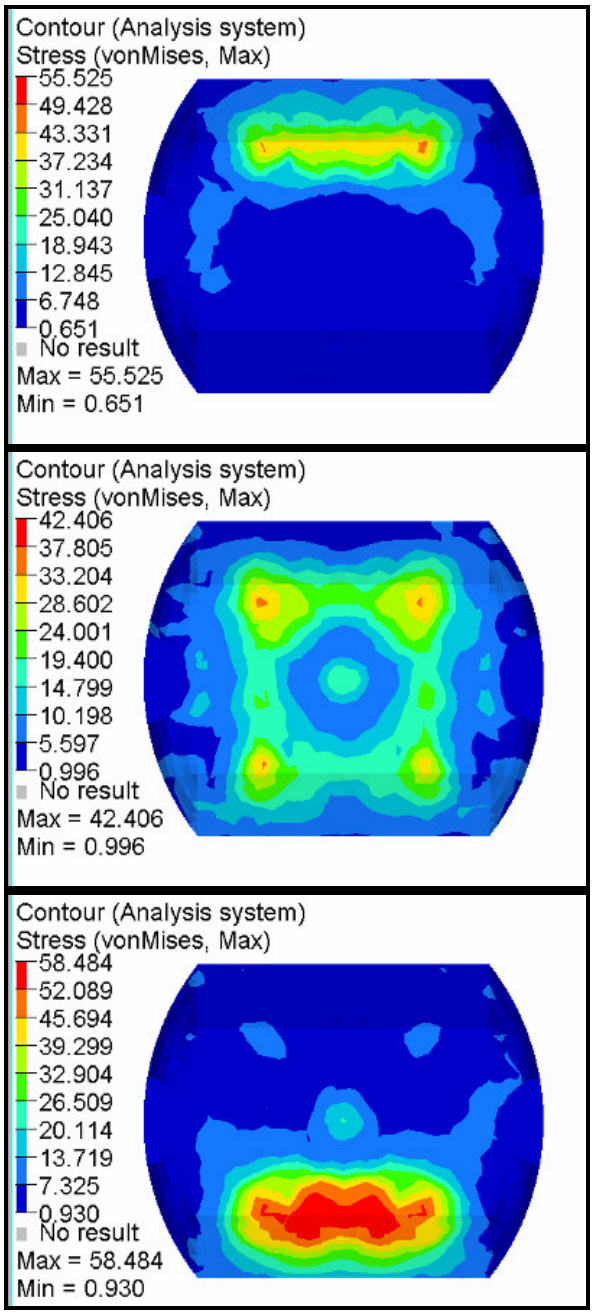

FIGURE 76 RRPM Type A von Mises stresses in MPa (tire load= 13,345 N).

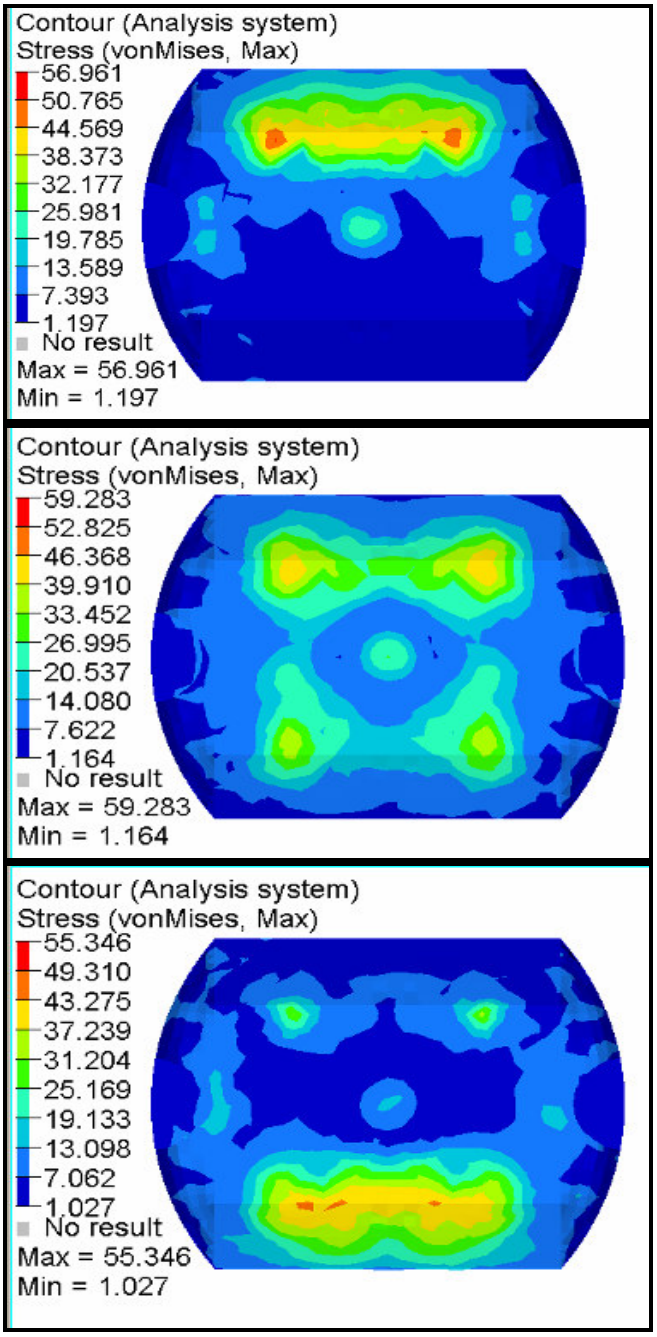

FIGURE 77 RRPM Type A von Mises stresses in MPa (tire load= 31,138 N).

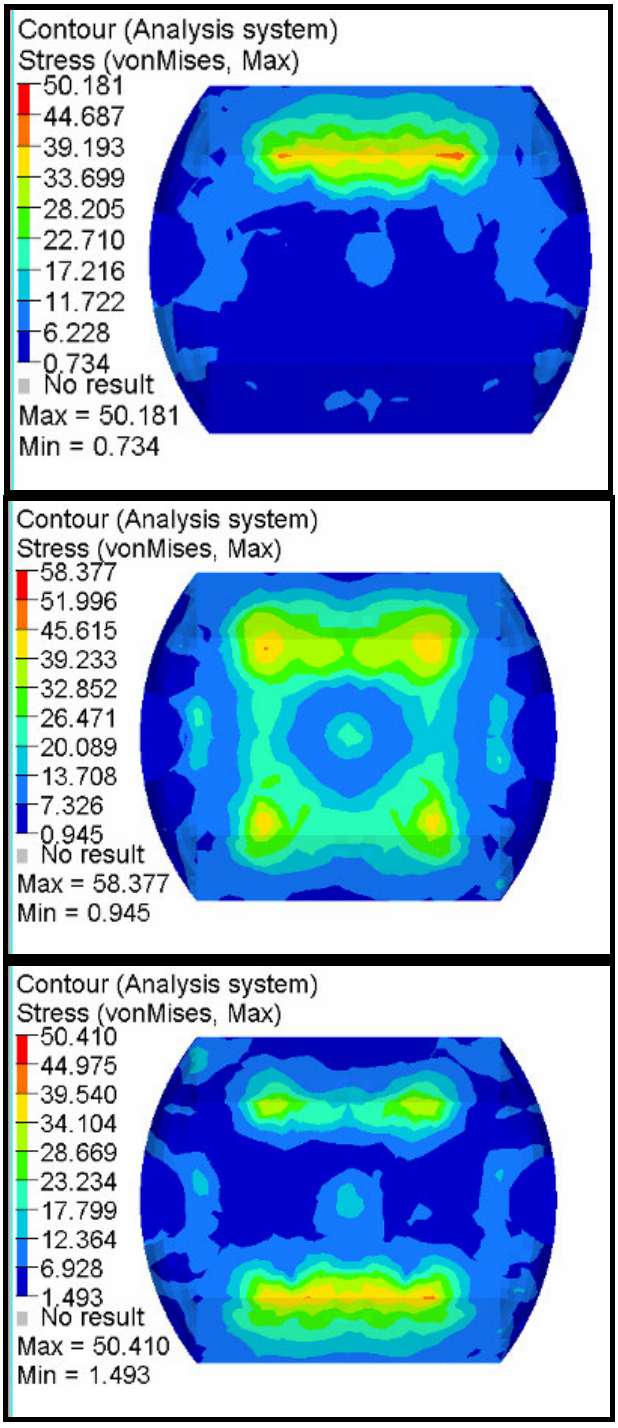

FIGURE 78 RRPM Type A von Mises stresses in MPa (tire velocity= 17.9 m/s).

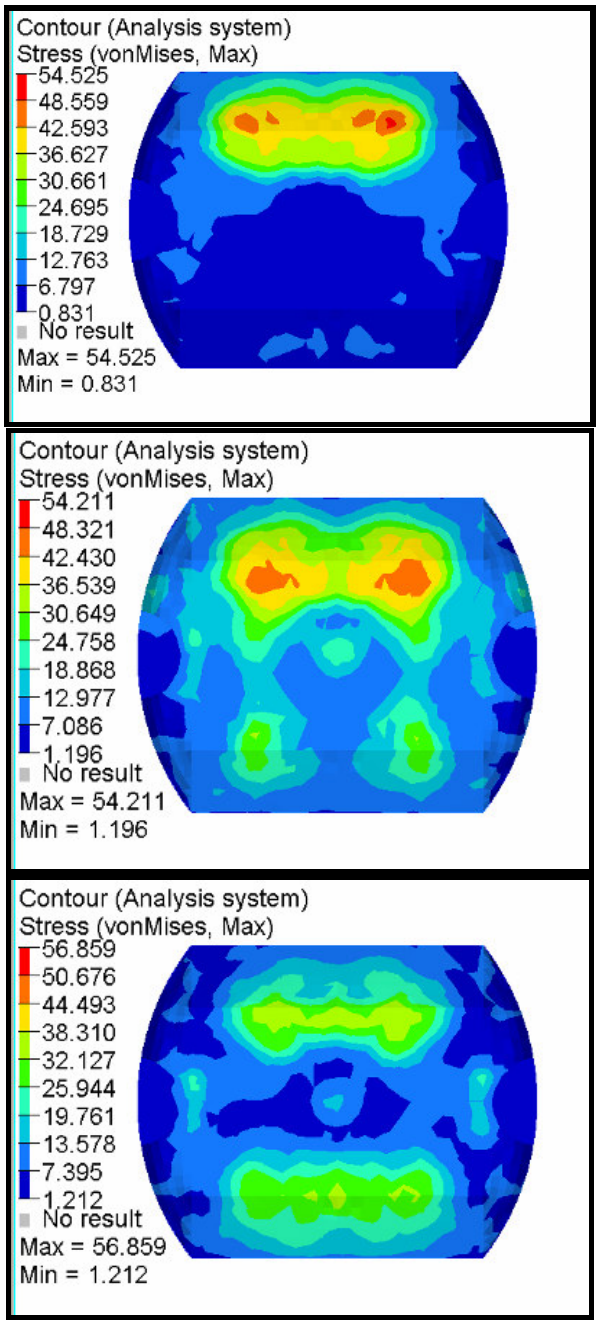

FIGURE 79 RRPM Type A von Mises stresses in MPa (tire velocity= 35.8 m/s).

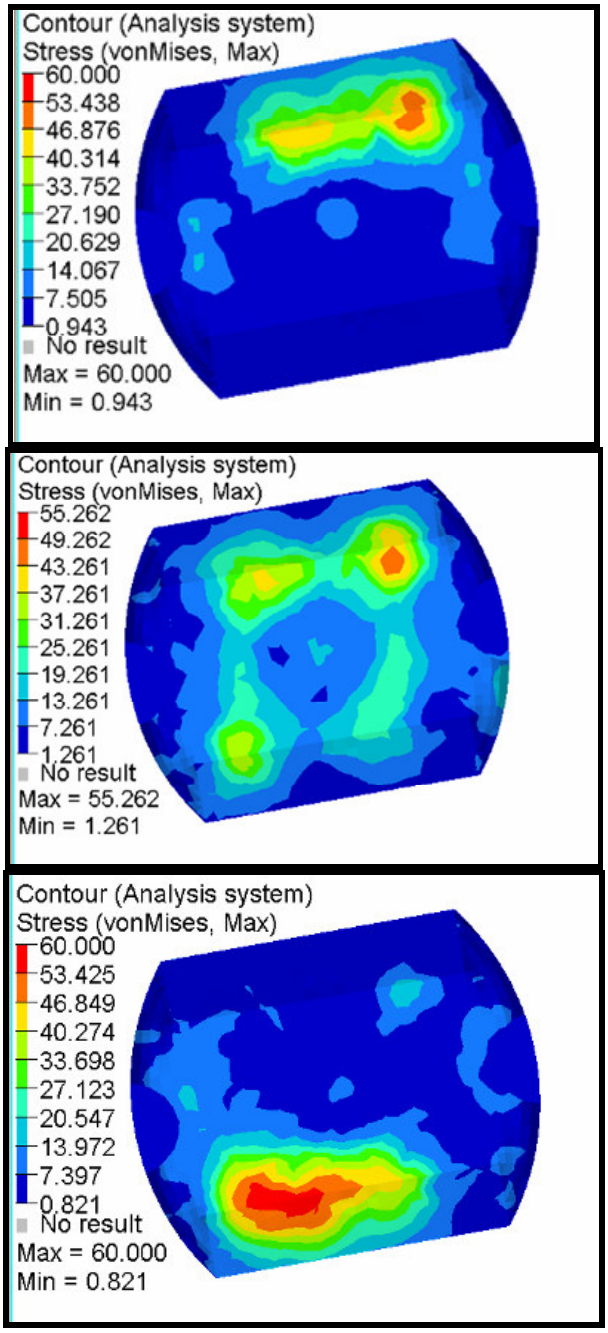

FIGURE 80 RRPM Type A von Mises stresses in MPa (angle of impact=10 degrees).

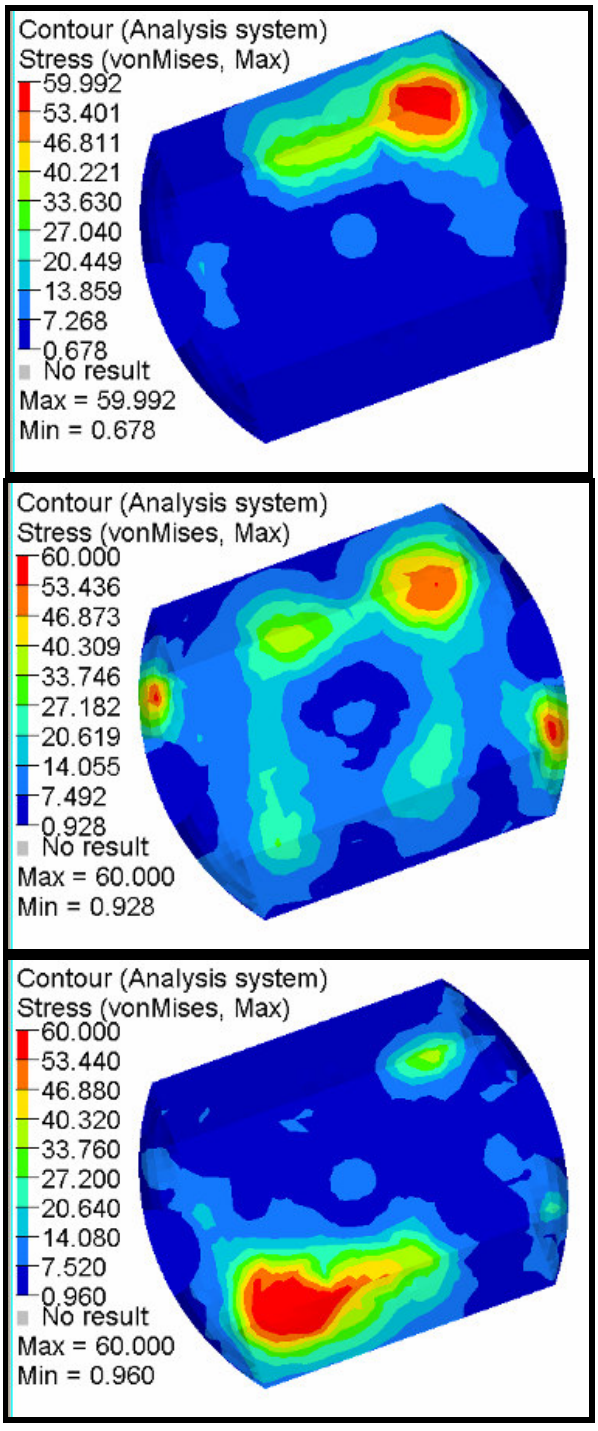

FIGURE 81 RRPM Type A von Mises stresses in MPa (angle of impact=20 degrees).

APPENDIX D

RRPM TYPE B RESULTS

TABLE 12 Variation in Maximum Stresses in MPa for Three Stages (RRPM Type B)

		Maximum stresses in MPa		
		Stage 1	Stage 2	Stage 3
Tire load in N	13,345 N	20.218	25.962	32.974
	22,241 N	26.300	26.718	31.649
	31,138 N	29.800	29.161	29.384
Tire velocity in m/s	17.9 m/s	32.647	45.866	49.999
	26.8 m/s	26.300	26.718	31.649
	35.8 m/s	24.921	27.224	23.349
Angle of impact in degrees	0 degree	26.300	26.718	31.649
	10 degrees	28.591	50.000	34.572
	20 degrees	36.669	50.000	39.204

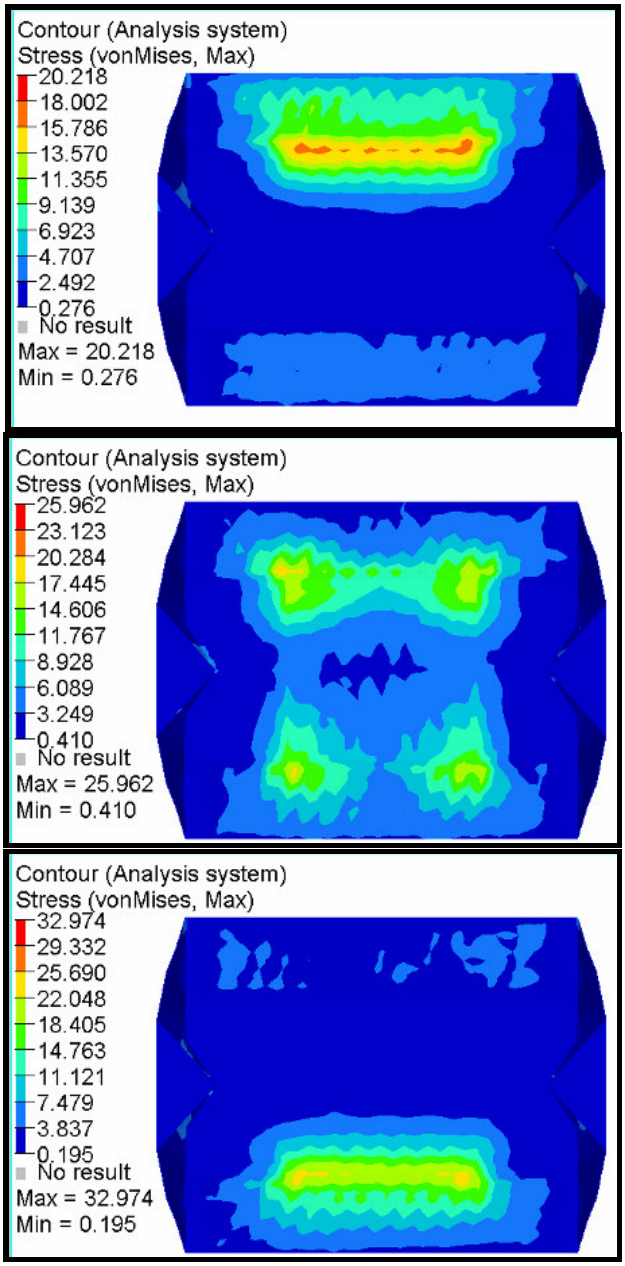

FIGURE 82 RRPM Type B von Mises stresses in MPa (tire load= 13,345 N).

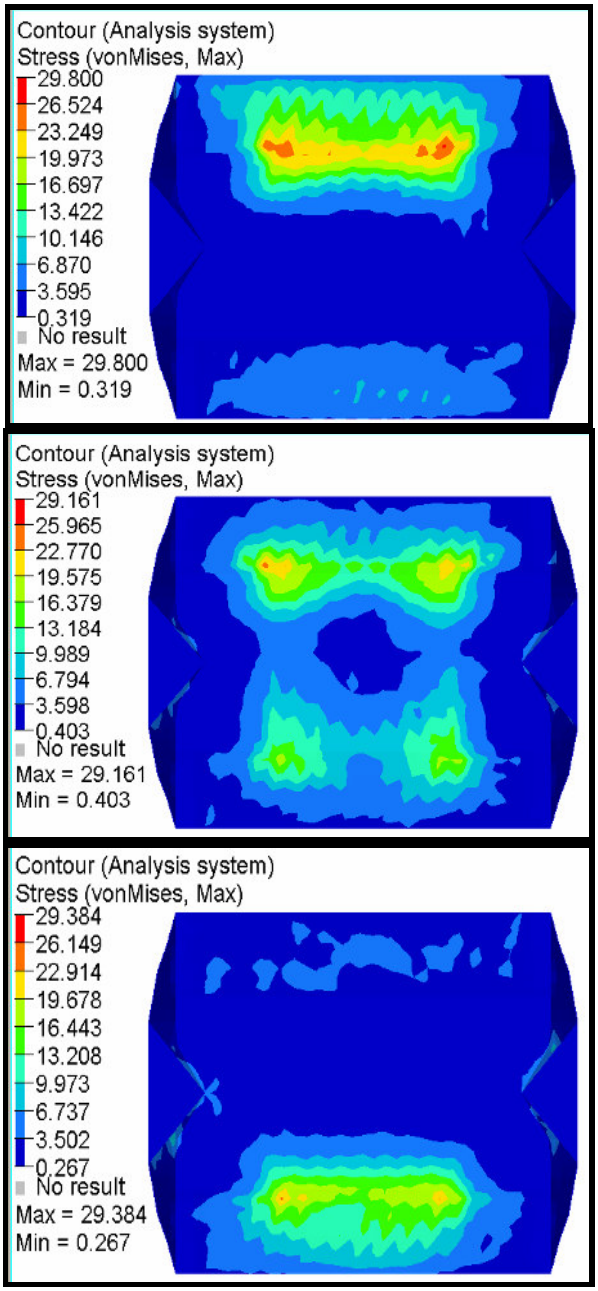

FIGURE 83 RRPM Type B von Mises stresses in MPa (tire load= 31,138 N).

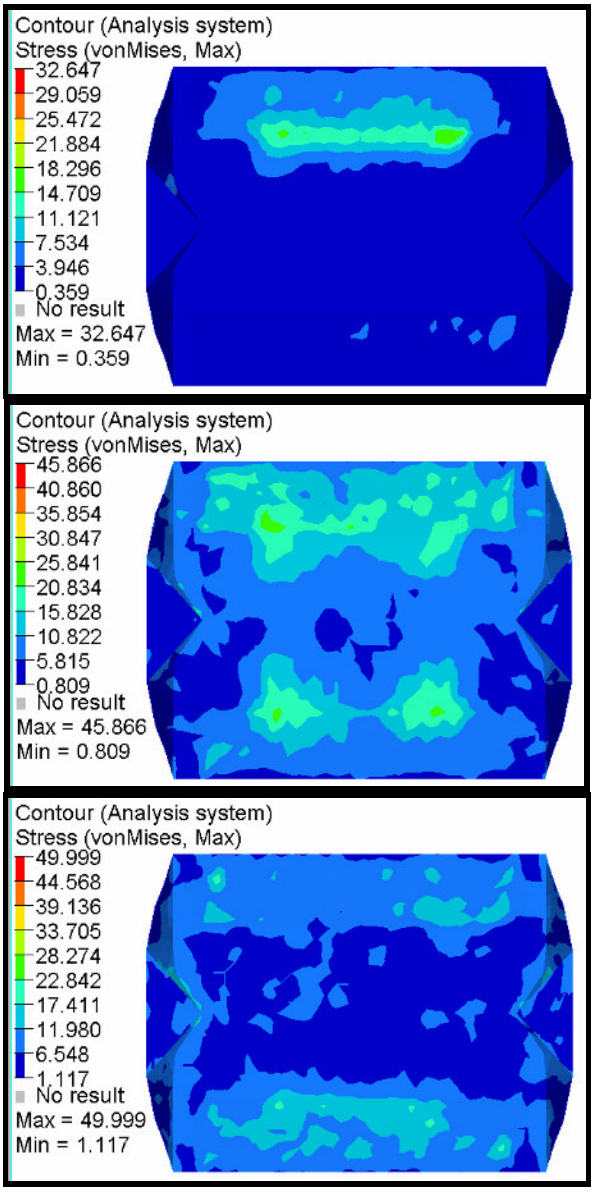

FIGURE 84 RRPM Type B von Mises stresses in MPa (tire velocity= 17.9 m/s).

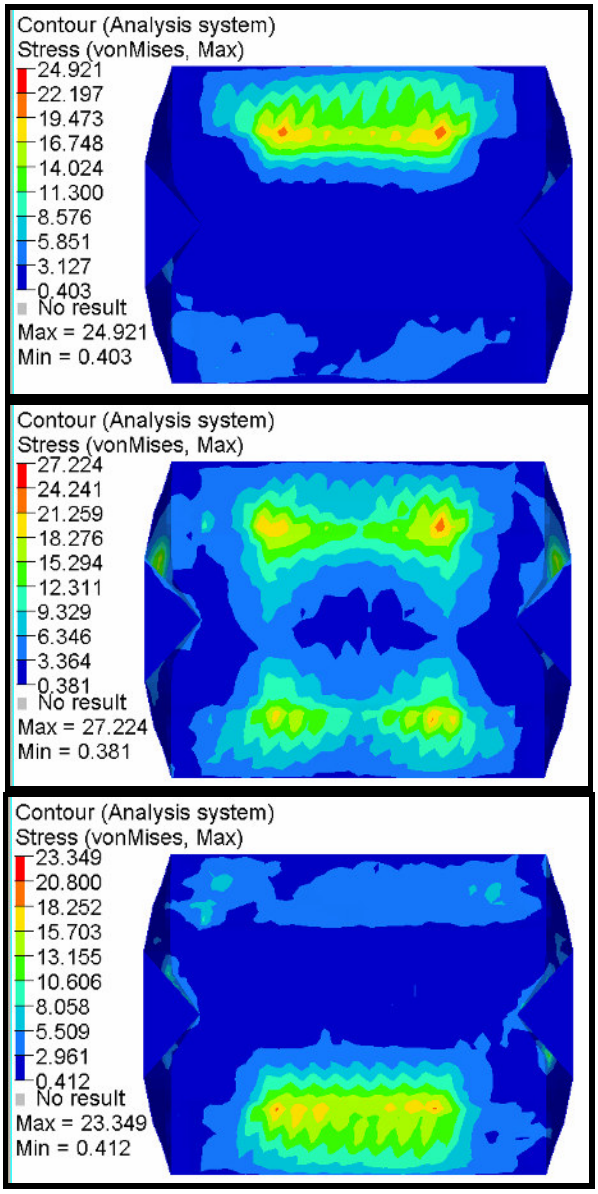

FIGURE 85 RRPM Type B von Mises stresses in MPa (tire velocity= 35.8 m/s).

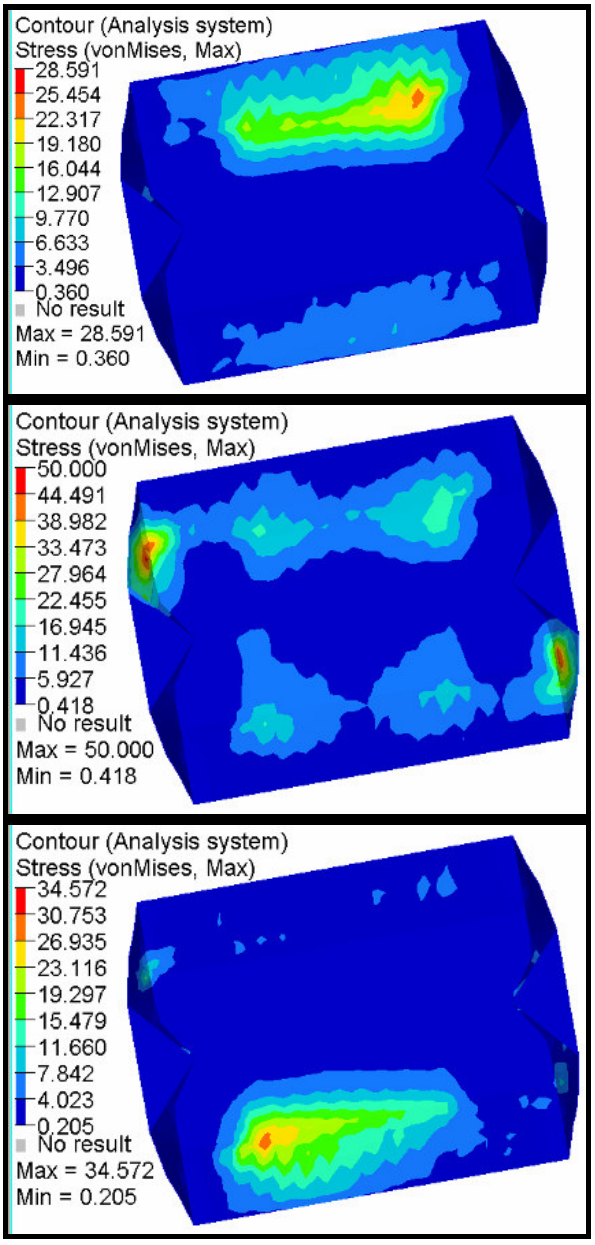

FIGURE 86 RRPM Type B von Mises stresses in MPa (angle of impact= 10 degrees).

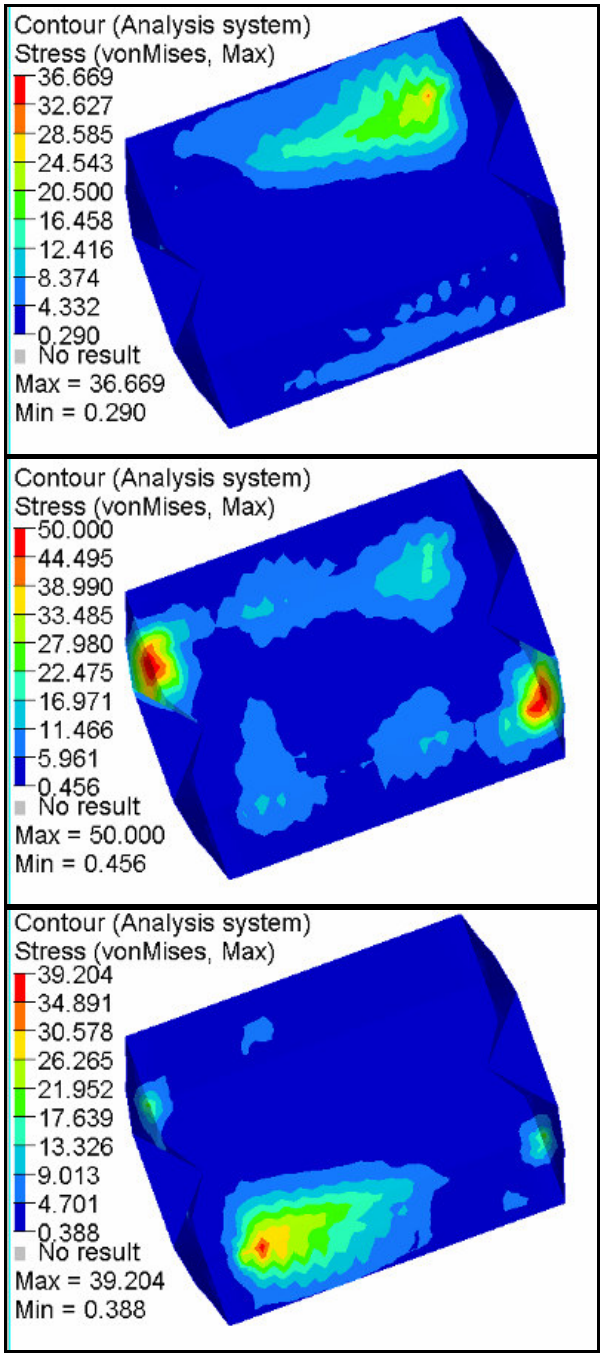

FIGURE 87 RRPM Type B von Mises stresses in MPa (angle of impact= 20 degrees).

APPENDIX E

RRPM TYPE C RESULTS

TABLE 13 Variation in Maximum Stresses in MPa for Three Stages (RRPM Type C)

		Maximum stresses in MPa		
		Stage 1	Stage 2	Stage 3
Tire load in N	13,345 N	28.806	27.547	29.377
	22,241 N	29.464	30.624	29.260
	31,138 N	32.973	28.757	29.671
Tire velocity in m/s	17.9 m/s	17.633	25.301	19.099
	26.8 m/s	29.464	30.624	29.260
	35.8 m/s	24.852	11.595	26.960
Angle of impact in degrees	0 degree	29.464	30.624	29.260
	10 degrees	34.395	75.232	41.075
	20 degrees	35.588	80.000	55.367

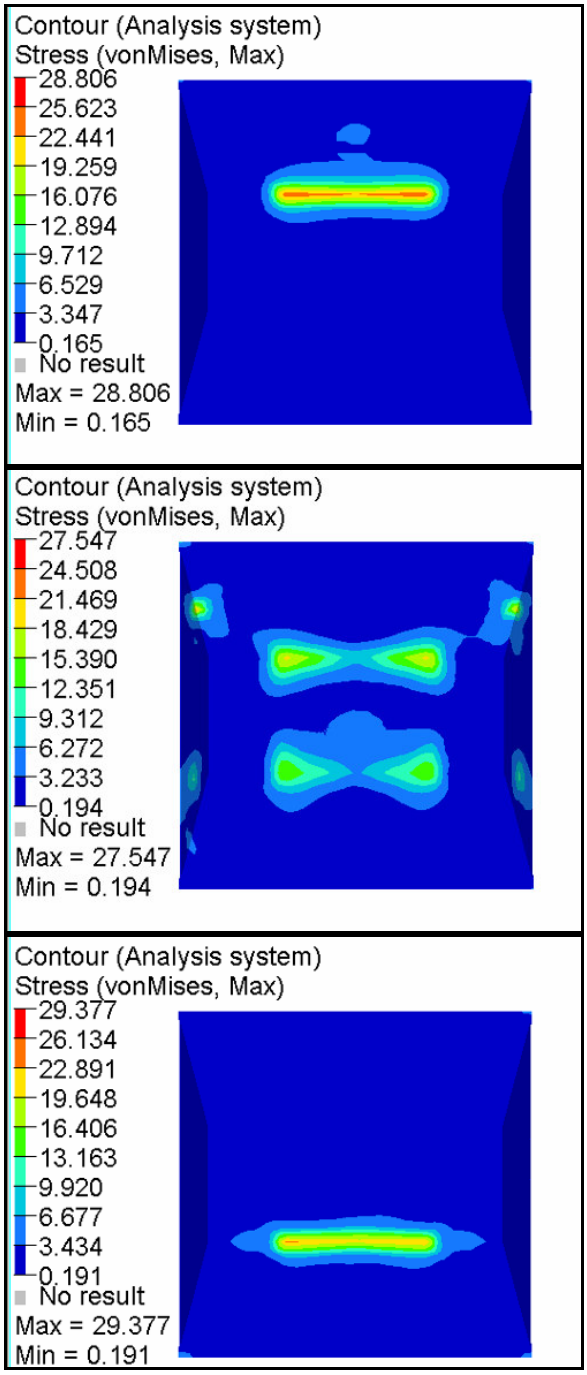

FIGURE 88 RRPM Type C von Mises stresses in MPa (tire load=13,345 N).

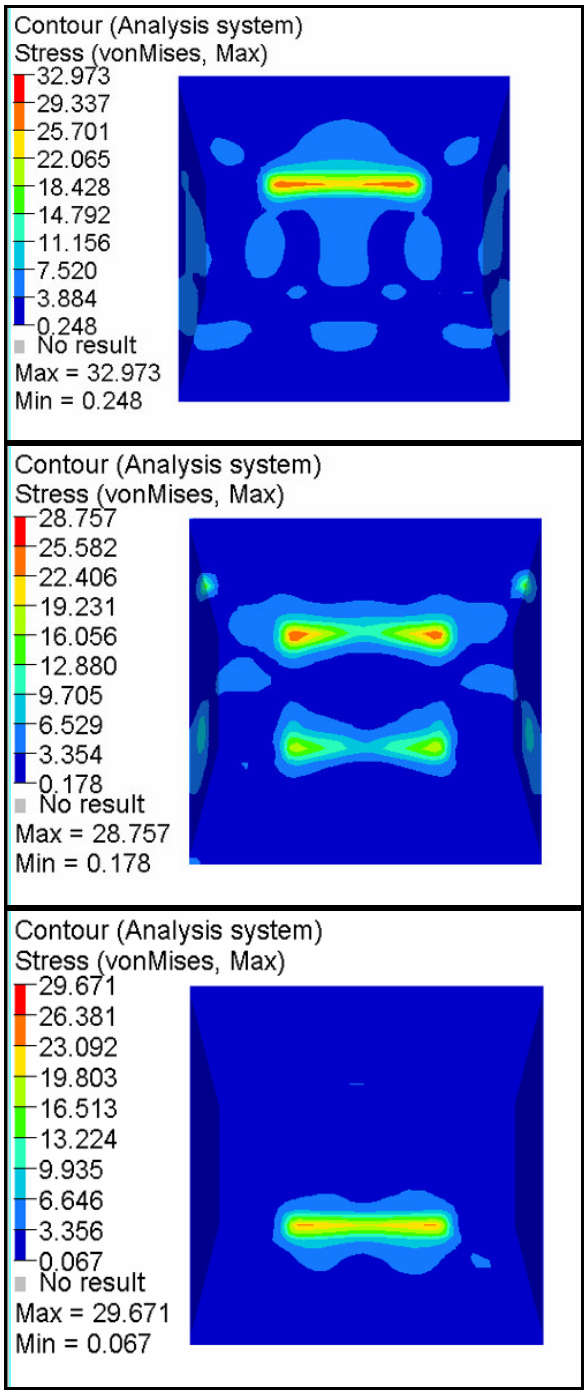

FIGURE 89 RRPM Type C von Mises stresses in MPa (tire load=31,138 N).

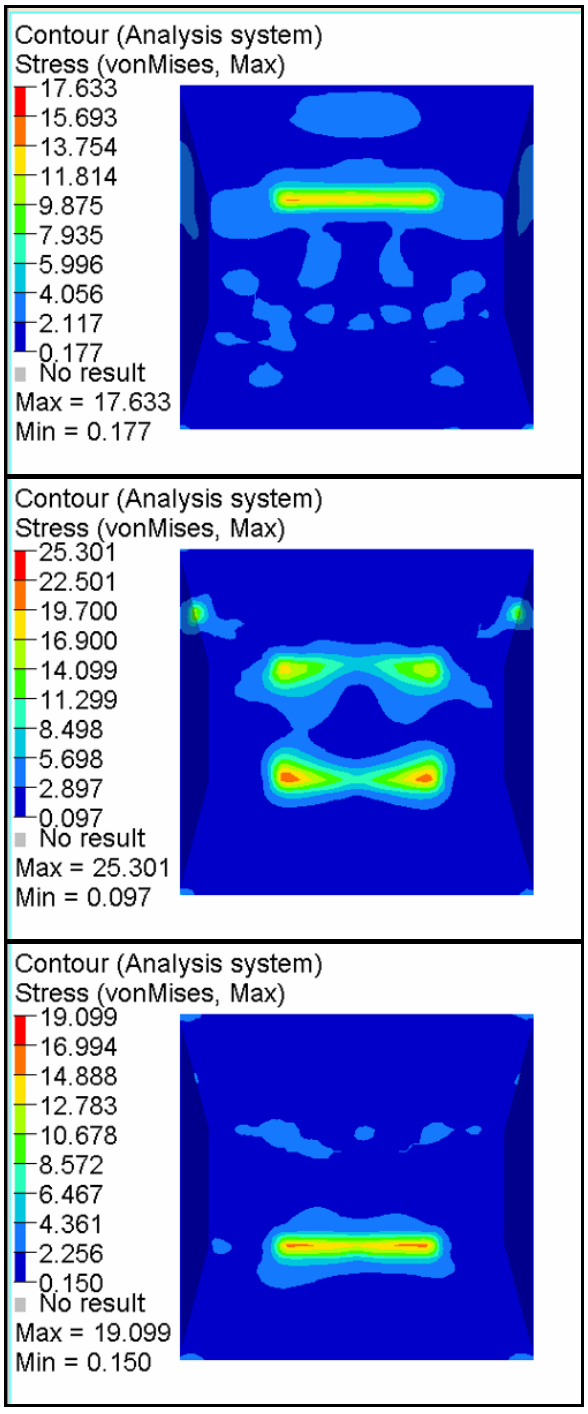

FIGURE 90 RRPM Type C von Mises stresses in MPa (tire velocity= 17.9 m/s).

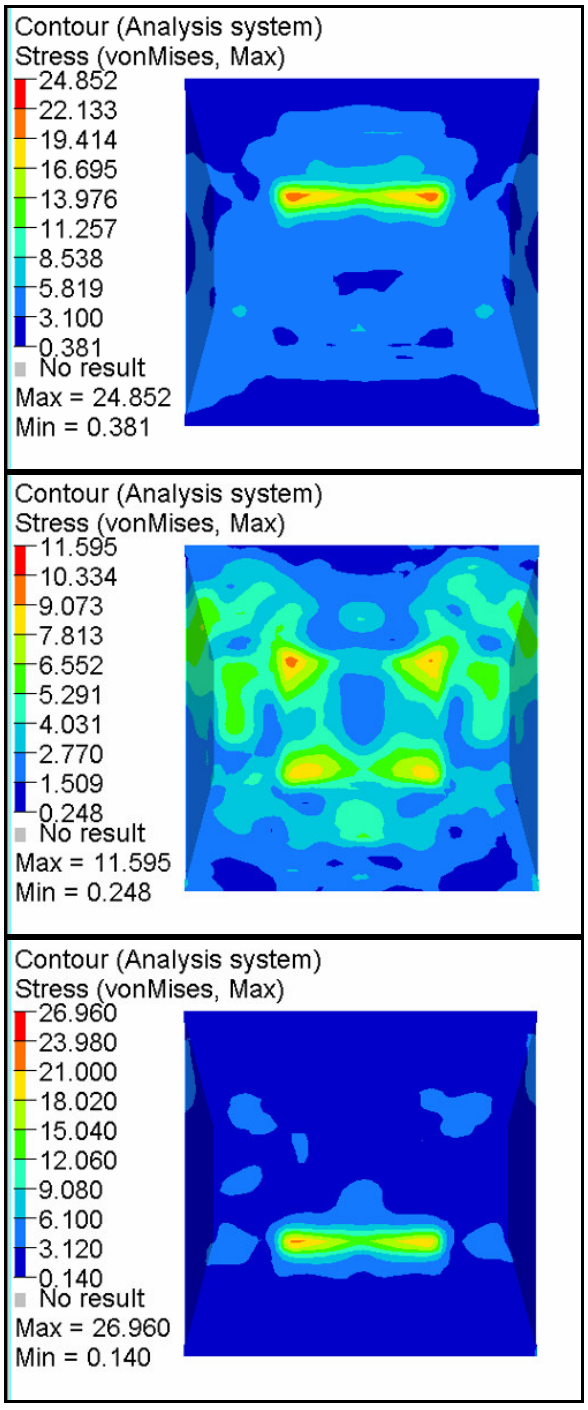

FIGURE 91 RRPM Type C von Mises stresses in MPa (tire velocity= 35.8 m/s).

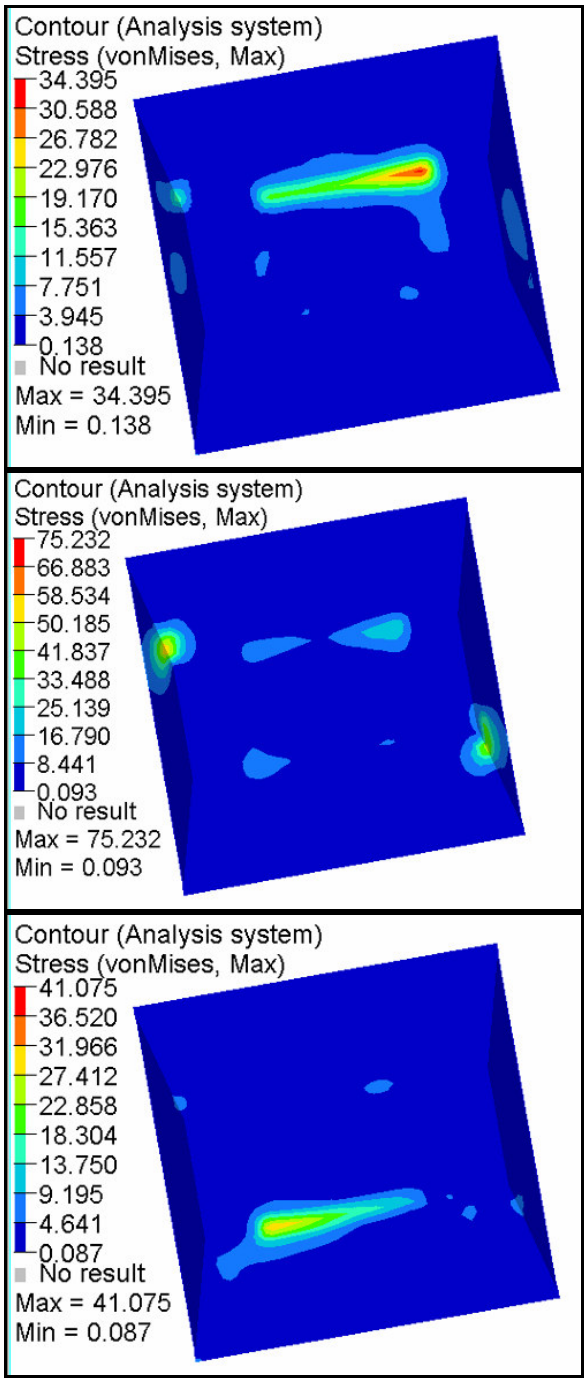

FIGURE 92 RRPM Type C von Mises stresses in MPa (angle of impact=10 degrees).

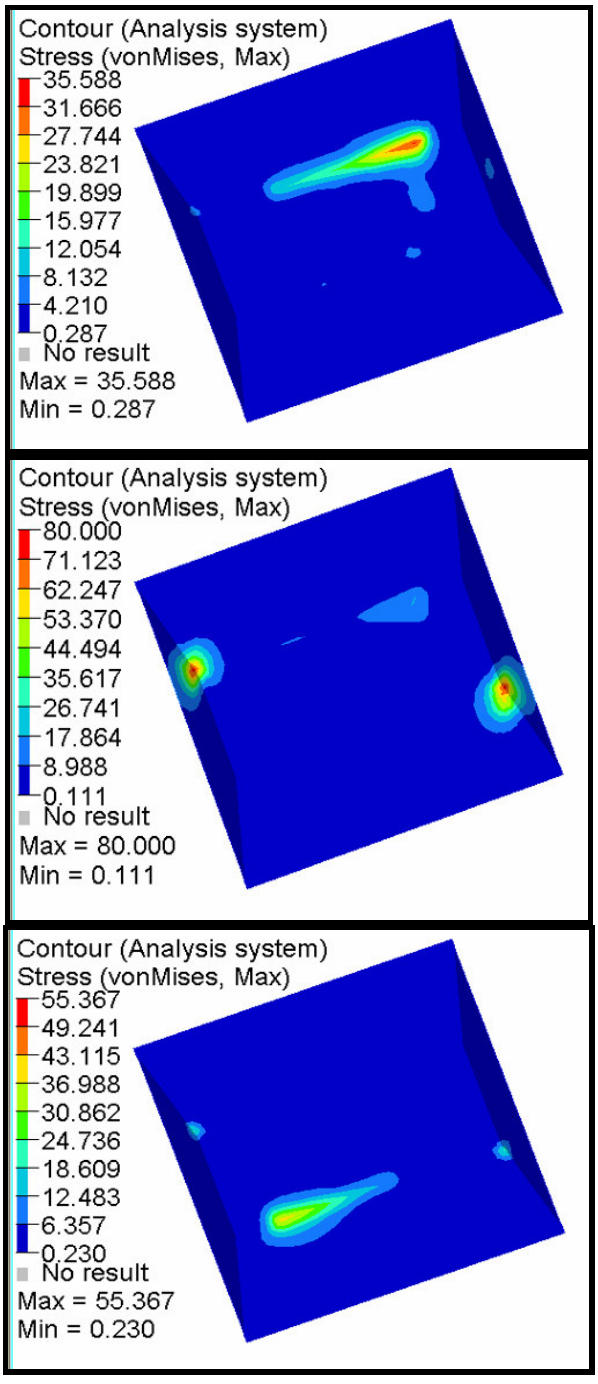

FIGURE 93 RRPM Type C von Mises stresses in MPa (angle of impact=20 degrees).

APPENDIX F

RRPM-GROUND INTERFACE FORCES

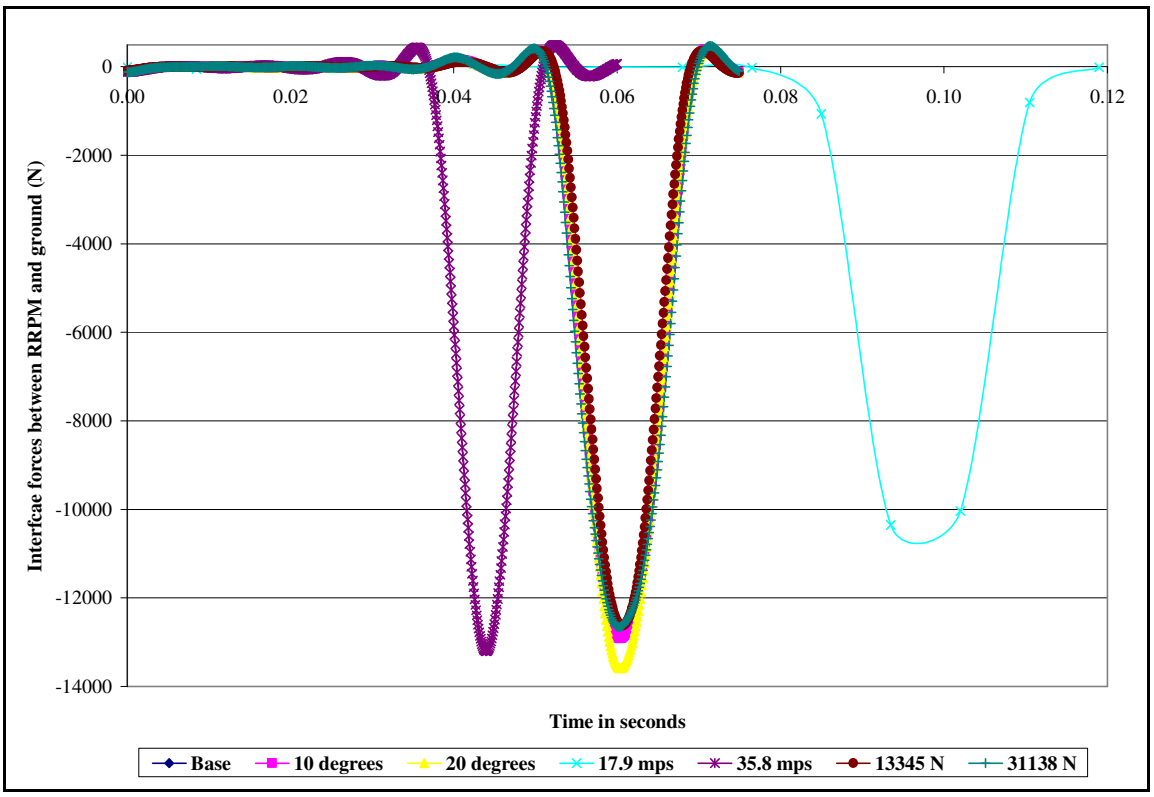

FIGURE 94 RRPM-ground interface forces for RRPM Type A.

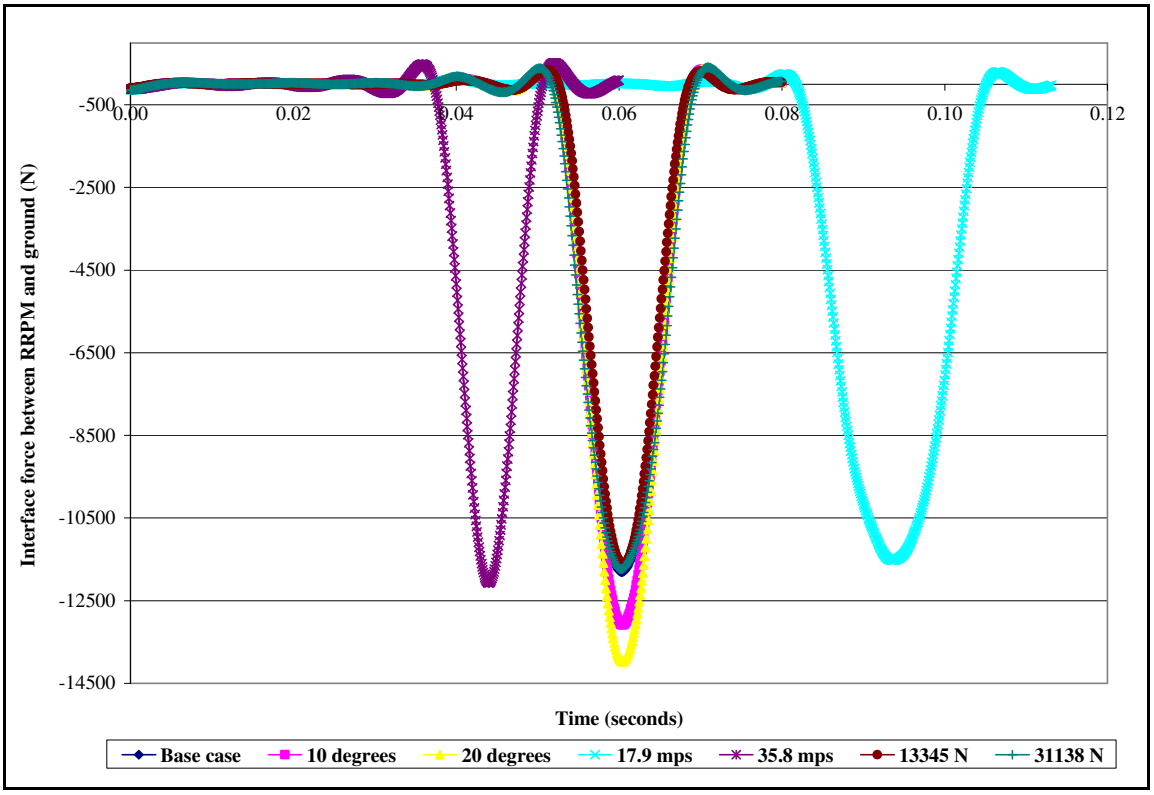

FIGURE 95 RRPM-ground interface forces for RRPM Type B.

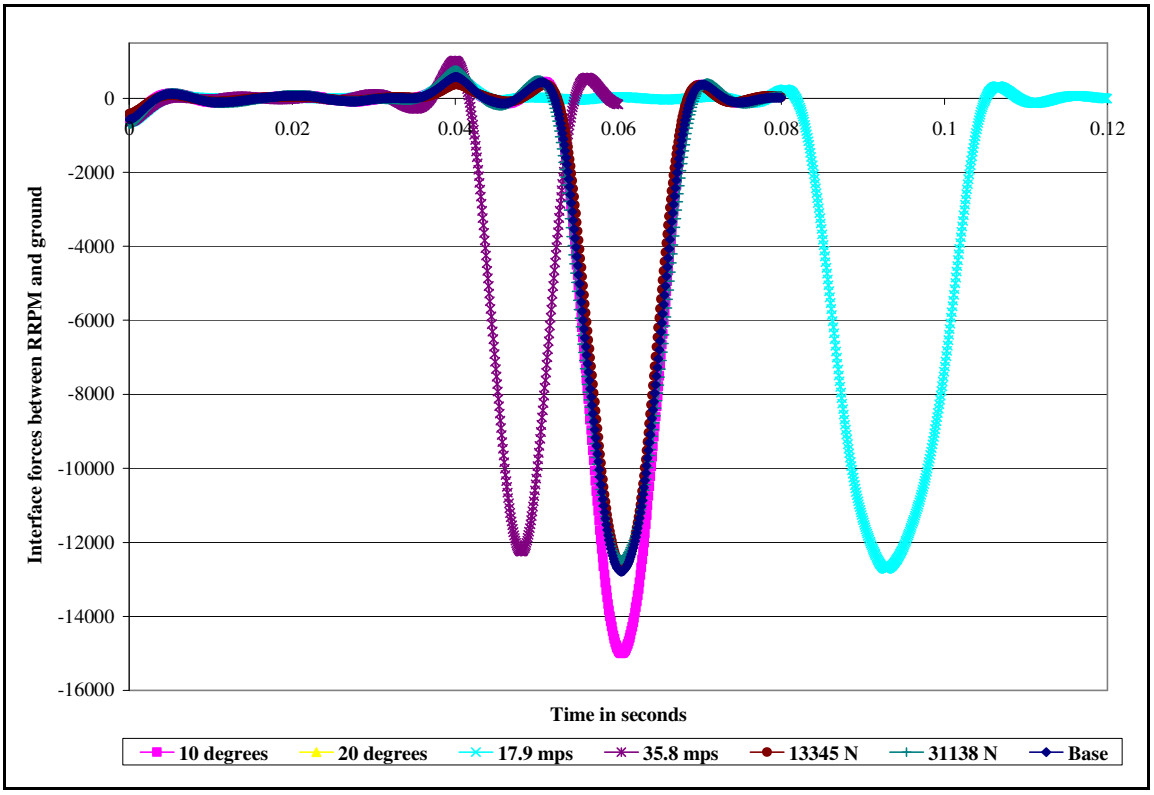

FIGURE 96 RRPM-ground interface forces for RRPM Type C.

APPENDIX G

COMPARISONS OF VON MISES STRESSES BETWEEN TIRE MARKER IMPACTS AND LABORATORY TESTS SIMULATIONS

TABLE 14 Percentage Differences between Maximum Von Mises Stresses from the Three Stages of the Base Tire-Marker Impact Simulation and the ASTM Compression Test in the Finite Elements 1-6 (RRPM Types A, B, and C)

	Tire-marker impact simulation			ASTM compression test simulation	Differences in percent		
	Stage 1	Stage 2	Stage 3		Stage 1	Stage 2	Stage 3
	RRPM Type A						
Element 1	54.20	38.73	19.61	21.36	-61	-45	9
Element 2	55.80	41.71	18.75	21.10	-62	-49	13
Element 3	8.10	42.95	52.90	22.54	178	-48	-57
Element 4	6.41	45.85	55.30	21.36	233	-53	-61
Element 5	10.42	21.14	8.63	3.70	-64	-82	-57
Element 6	7.22	4.12	5.50	12.75	77	209	132
	RRPM Type B						
Element 1	21.70	16.12	1.36	3.83	-82	-76	182
Element 2	20.30	17.40	1.27	4.37	-78	-75	244
Element 3	2.25	13.96	19.10	4.13	84	-70	-78
Element 4	1.19	13.01	18.60	5.99	405	-54	-68
Element 5	2.34	2.10	3.01	4.37	87	108	45
Element 6	1.53	1.69	1.26	6.21	306	267	394
	RRPM Type C						
Element 1	26.25	27.22	6.17	6.78	74	75	10
Element 2	24.69	25.64	6.26	7.37	70	71	18
Element 3	3.17	16.64	23.44	6.45	103	61	72
Element 4	2.64	16.70	23.66	6.65	152	60	72
Element 5	3.23	2.04	1.65	3.26	1	60	97
Element 6	0.63	0.63	0.82	5.06	700	700	517

TABLE 15 Percentage Differences between Maximum Von Mises Stresses from the Three Stages of the Base Tire-Marker Impact Simulation and the ASTM Flexural Test in the Finite Elements 1-6 (RRPM Types A, B, and C)

	Tire-marker impact simulation			ASTM flexural test simulation	Differences in percent		
	Stage 1	Stage 2	Stage 3		Stage 1	Stage 2	Stage 3
	RRPM Type A						
Element 1	54.20	38.73	19.61	31.55	-42	-19	61
Element 2	55.80	41.71	18.75	30.65	-45	-27	63
Element 3	8.10	42.95	52.90	30.67	279	-29	-42
Element 4	6.41	45.85	55.30	31.63	394	-31	-43
Element 5	10.42	21.14	8.63	60.00	476	184	595
Element 6	7.22	4.12	5.50	60.00	731	1355	991
	RRPM Type B						
Element 1	21.70	16.12	1.36	21.09	-3	31	1452
Element 2	20.30	17.40	1.27	20.93	3	20	1545
Element 3	2.25	13.96	19.10	20.89	830	50	9
Element 4	1.19	13.01	18.60	20.74	1650	59	12
Element 5	2.34	2.10	3.01	27.29	1068	1198	807
Element 6	1.53	1.69	1.26	39.41	2476	2226	3035
	RRPM Type C						
Element 1	26.25	27.22	6.17	33.56	28	23	444
Element 2	24.69	25.64	6.26	33.87	37	32	441
Element 3	3.17	16.64	23.44	33.84	967	103	44
Element 4	2.64	16.70	23.66	34.00	1186	104	44
Element 5	3.23	2.04	1.65	58.93	1725	2786	3467
Element 6	0.63	0.63	0.82	67.44	10560	10559	8124

TABLE 16 Percentage Differences between Maximum Von Mises Stresses from the Three Stages of the Base Tire-Marker Impact Simulation and the Cylindrical Compression Test in the Finite Elements 1-6 (RRPM Types A, B, and C)

	Tire-marker impact simulation			Cylindrical compression test simulation	Absolute Differences in percent		
	Stage 1	Stage 2	Stage 3		Stage 1	Stage 2	Stage 3
	RRPM Type A						
Element 1	54.20	38.73	19.61	8.16	-85	-79	-58
Element 2	55.80	41.71	18.75	7.91	-86	-81	-58
Element 3	8.10	42.95	52.90	7.89	-3	-82	-85
Element 4	6.41	45.85	55.30	8.16	27	-82	-85
Element 5	10.42	21.14	8.63	11.07	6	-48	28
Element 6	7.22	4.12	5.50	14.65	103	255	166
	RRPM Type B						
Element 1	21.70	16.12	1.36	5.50	-75	-66	305
Element 2	20.30	17.40	1.27	6.27	-69	-64	393
Element 3	2.25	13.96	19.10	4.81	114	-66	-75
Element 4	1.19	13.01	18.60	7.45	529	-43	-60
Element 5	2.34	2.10	3.01	6.70	187	218	123
Element 6	1.53	1.69	1.26	6.79	344	301	440
	RRPM Type C						
Element 1	26.25	27.22	6.17	2.06	-92	-92	-67
Element 2	24.69	25.64	6.26	2.88	-88	-89	-54
Element 3	3.17	16.64	23.44	1.91	-40	-89	-92
Element 4	2.64	16.70	23.66	2.85	8	-83	-88
Element 5	3.23	2.04	1.65	3.35	4	64	103
Element 6	0.63	0.63	0.82	3.87	512	512	372

TABLE 17 Percentage Differences between Maximum Von Mises Stresses from the Three Stages of the Base Tire-Marker Impact Simulation and the Offset Compression Test (Lower Loading Rate) in the Finite Elements 1-6 (RRPM Types A, B, and C)

	Tire-marker impact simulation			Offset compression test simulation	Absolute Differences in percent		
	Stage 1	Stage 2	Stage 3		Stage 1	Stage 2	Stage 3
	RRPM Type A						
Element 1	54.20	38.73	19.61	18.45	-66	-52	-6
Element 2	55.80	41.71	18.75	18.92	-66	-55	1
Element 3	8.10	42.95	52.90	3.06	-62	-93	-94
Element 4	6.41	45.85	55.30	3.22	-50	-93	-94
Element 5	10.42	21.14	8.63	6.47	-38	-69	-25
Element 6	7.22	4.12	5.50	0.00	-100	-100	-100
	RRPM Type B						
Element 1	21.70	16.12	1.36	7.79	-64	-52	473
Element 2	20.30	17.40	1.27	7.85	-61	-55	517
Element 3	2.25	13.96	19.10	0.29	-87	-98	-98
Element 4	1.19	13.01	18.60	0.34	-71	-97	-98
Element 5	2.34	2.10	3.01	5.47	134	160	82
Element 6	1.53	1.69	1.26	0.00	-100	-100	-100
	RRPM Type C						
Element 1	26.25	27.22	6.17	2.91	-89	-89	-53
Element 2	24.69	25.64	6.26	2.78	-89	-89	-56
Element 3	3.17	16.64	23.44	0.13	-96	-99	-99
Element 4	2.64	16.70	23.66	0.13	-95	-99	-99
Element 5	3.23	2.04	1.65	2.08	-36	2	26
Element 6	0.63	0.63	0.82	2.79	341	341	241

TABLE 18 Percentage Differences between Maximum Von Mises Stresses from the Three Stages of the Base Tire-Marker Impact Simulation and the Offset Compression Test (Higher Loading Rate) in the Finite Elements 1-6 (RRPM Types A, B, and C)

	Tire-marker impact simulation			Offset compression test simulation	Absolute Differences in percent		
	Stage 1	Stage 2	Stage 3		Stage 1	Stage 2	Stage 3
	RRPM Type A						
Element 1	54.20	38.73	19.61	59.00	9	52	201
Element 2	55.80	41.71	18.75	58.57	5	40	212
Element 3	8.10	42.95	52.90	8.59	6	-80	-84
Element 4	6.41	45.85	55.30	9.37	46	-80	-83
Element 5	10.42	21.14	8.63	13.25	27	-37	54
Element 6	7.22	4.12	5.50	0.00	-100	-100	-100
	RRPM Type B						
Element 1	21.70	16.12	1.36	15.21	-30	-6	1019
Element 2	20.30	17.40	1.27	15.18	-25	-13	1093
Element 3	2.25	13.96	19.10	0.68	-70	-95	-96
Element 4	1.19	13.01	18.60	0.62	-48	-95	-97
Element 5	2.34	2.10	3.01	10.80	362	413	259
Element 6	1.53	1.69	1.26	0.00	-100	-100	-100
	RRPM Type C						
Element 1	26.25	27.22	6.17	5.78	-78	-79	-6
Element 2	24.69	25.64	6.26	5.53	-78	-78	-12
Element 3	3.17	16.64	23.44	0.23	-93	-99	-99
Element 4	2.64	16.70	23.66	0.24	-91	-99	-99
Element 5	3.23	2.04	1.65	4.17	29	104	153
Element 6	0.63	0.63	0.82	5.60	785	785	583

TABLE 19 Percentage Differences between Maximum Von Mises Stresses from the Three Stages of the Base Tire-Marker Impact Simulation and the Reversed ASTM Flexural Test Simulation in the Finite Elements 1-6 (RRPM Types A, B, and C)

	Tire-marker impact simulation			Reversed ASTM flexural test simulation	Differences in percent		
	Stage 1	Stage 2	Stage 3		Stage 1	Stage 2	Stage 3
	RRPM Type A						
Element 1	54.20	38.73	19.61	29.99	-45	-23	53
Element 2	55.80	41.71	18.75	30.97	-44	-26	65
Element 3	8.10	42.95	52.90	30.55	277	-29	-42
Element 4	6.41	45.85	55.30	30.94	383	-33	-44
Element 5	10.42	21.14	8.63	59.98	476	184	595
Element 6	7.22	4.12	5.50	60.00	731	1355	991
	RRPM Type B						
Element 1	21.70	16.12	1.36	5.32	-75	-67	291
Element 2	20.30	17.40	1.27	6.96	-66	-60	447
Element 3	2.25	13.96	19.10	5.48	144	-61	-71
Element 4	1.19	13.01	18.60	6.83	476	-47	-63
Element 5	2.34	2.10	3.01	6.73	188	220	124
Element 6	1.53	1.69	1.26	7.55	393	346	500
	RRPM Type C						
Element 1	26.25	27.22	6.17	15.12	-42	-44	145
Element 2	24.69	25.64	6.26	4.35	-82	-83	-30
Element 3	3.17	16.64	23.44	6.37	101	-62	-73
Element 4	2.64	16.70	23.66	9.63	264	-42	-59
Element 5	3.23	2.04	1.65	32.29	900	1481	1855
Element 6	0.63	0.63	0.82	13.79	2079	2079	1581

APPENDIX H

COMPARISON OF LABORATORY TESTS SIMULATIONS

This Appendix provides Figure 97 to Figure 105. Figures 97-99 show the percentage differences between von Mises stresses from the six laboratory tests simulations and each stage of the tire-marker impact simulation in the finite elements 1-6 for the RRPM Type A. Figures 100-102 show the percentage differences between von Mises stresses from the six laboratory tests simulations and each stage of the tire-marker impact simulation in the finite elements 1-6 for the RRPM Type B. Figures 103-105 show the percentage differences between von Mises stresses from the six laboratory tests simulations and each stage of the tire-marker impact simulation in the finite elements 1-6 for the RRPM Type C.

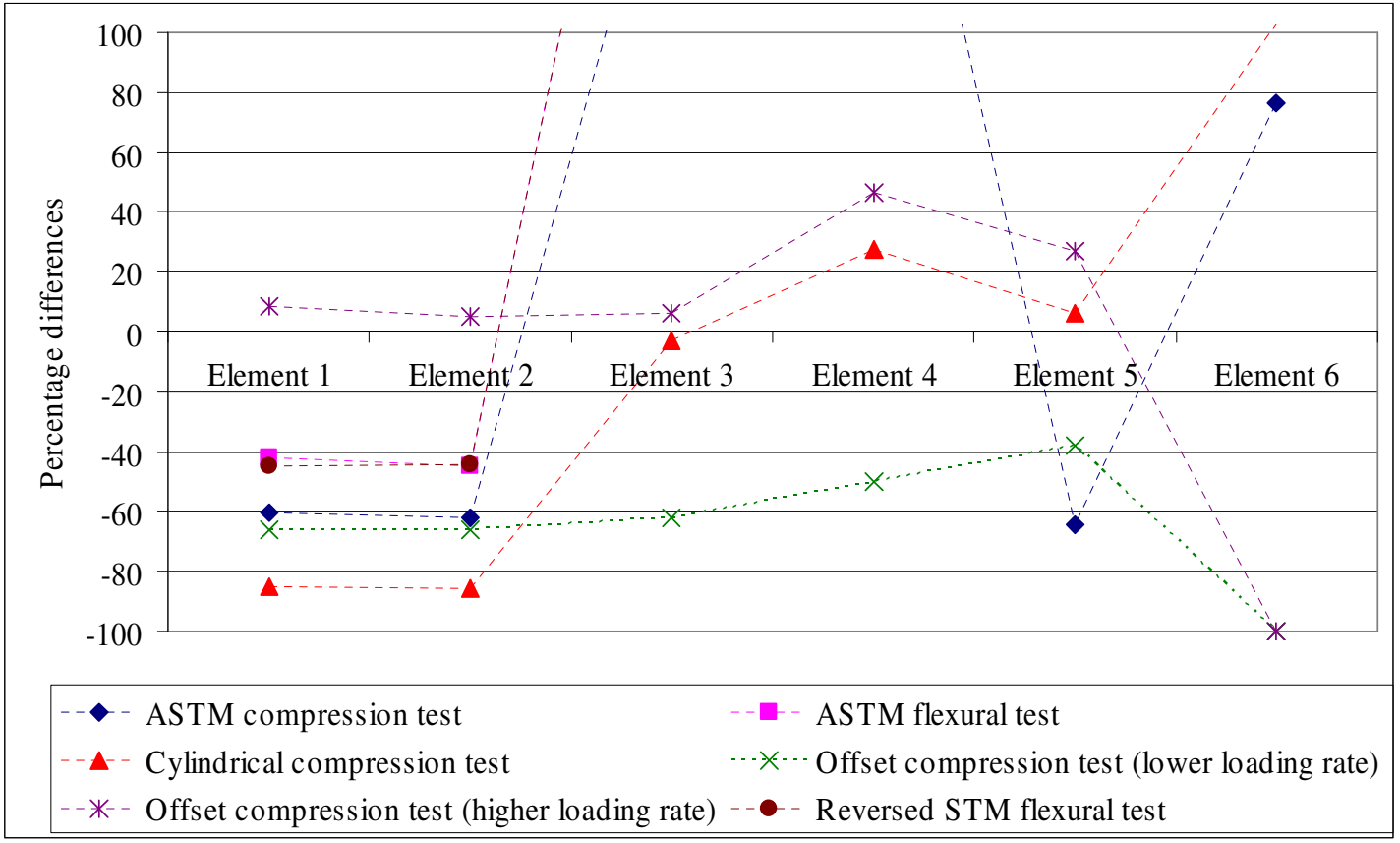

FIGURE 97 Percentage differences between von Mises stresses from the six laboratory tests simulations and the stage 1 of the tire-marker impact simulation in the finite elements 1-6 (RRPM Type A).

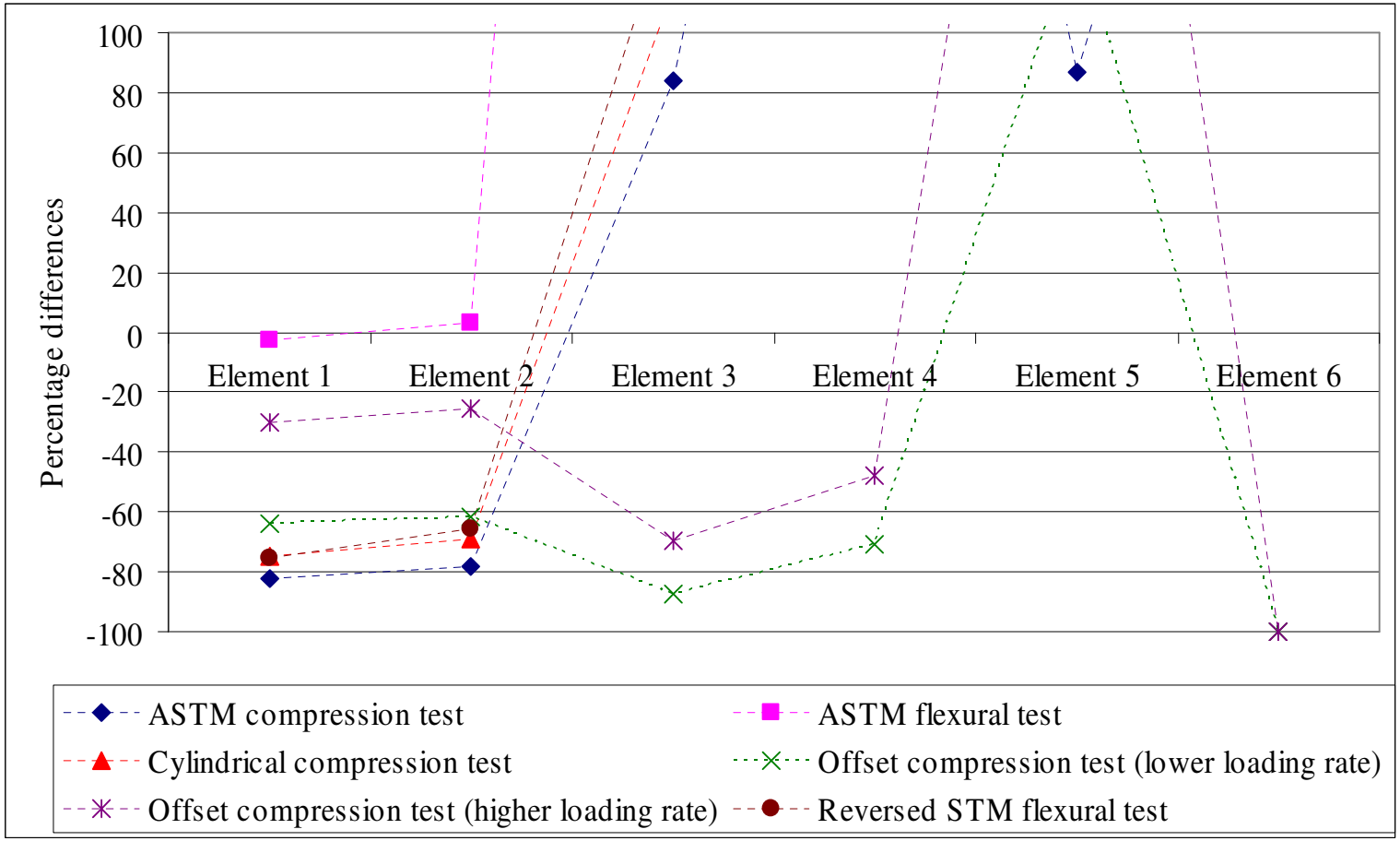

FIGURE 98 Percentage differences between von Mises stresses the six laboratory tests simulations and the stage 1 of the tire-marker impact simulation in the finite elements 1-6 (RRPM Type B).

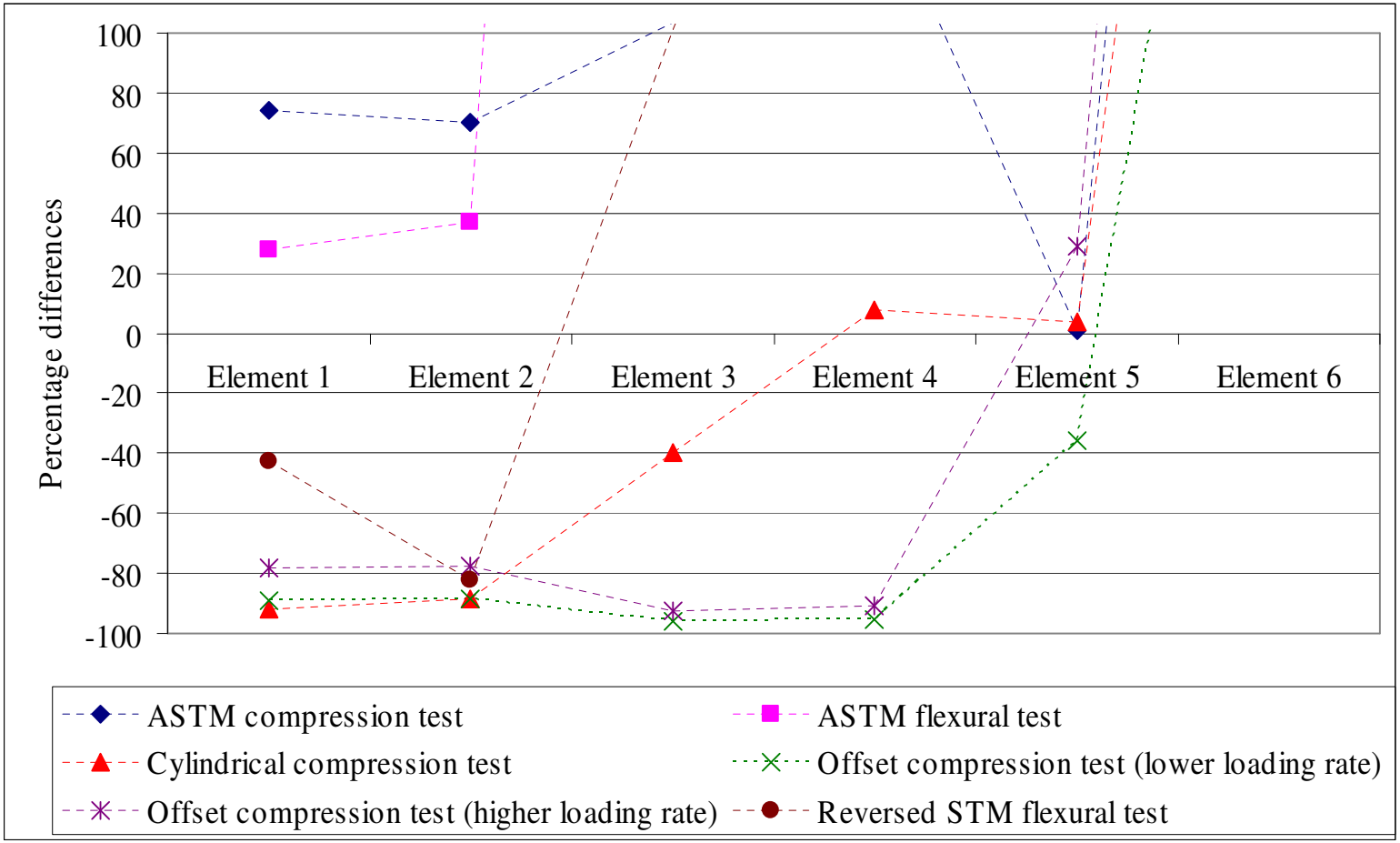

FIGURE 99 Percentage differences between von Mises stresses from the six laboratory tests simulations and the stage 1 of the tire-marker impact simulation in the finite elements 1-6 (RRPM Type C).

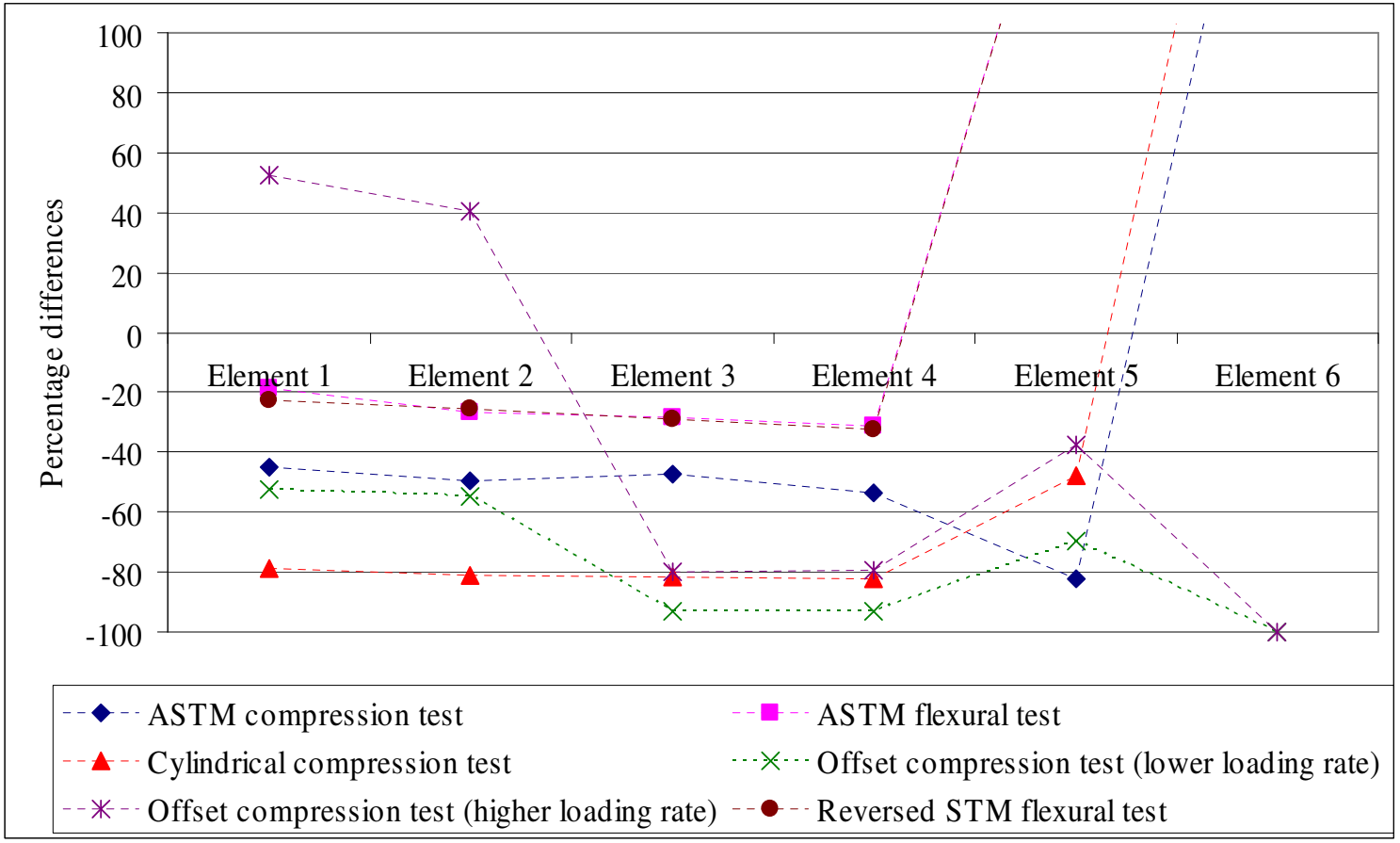

FIGURE 100 Percentage differences between von Mises stresses from the six laboratory tests simulations and the stage 2 of the tire-marker impact simulation in the finite elements 1-6 (RRPM Type A).

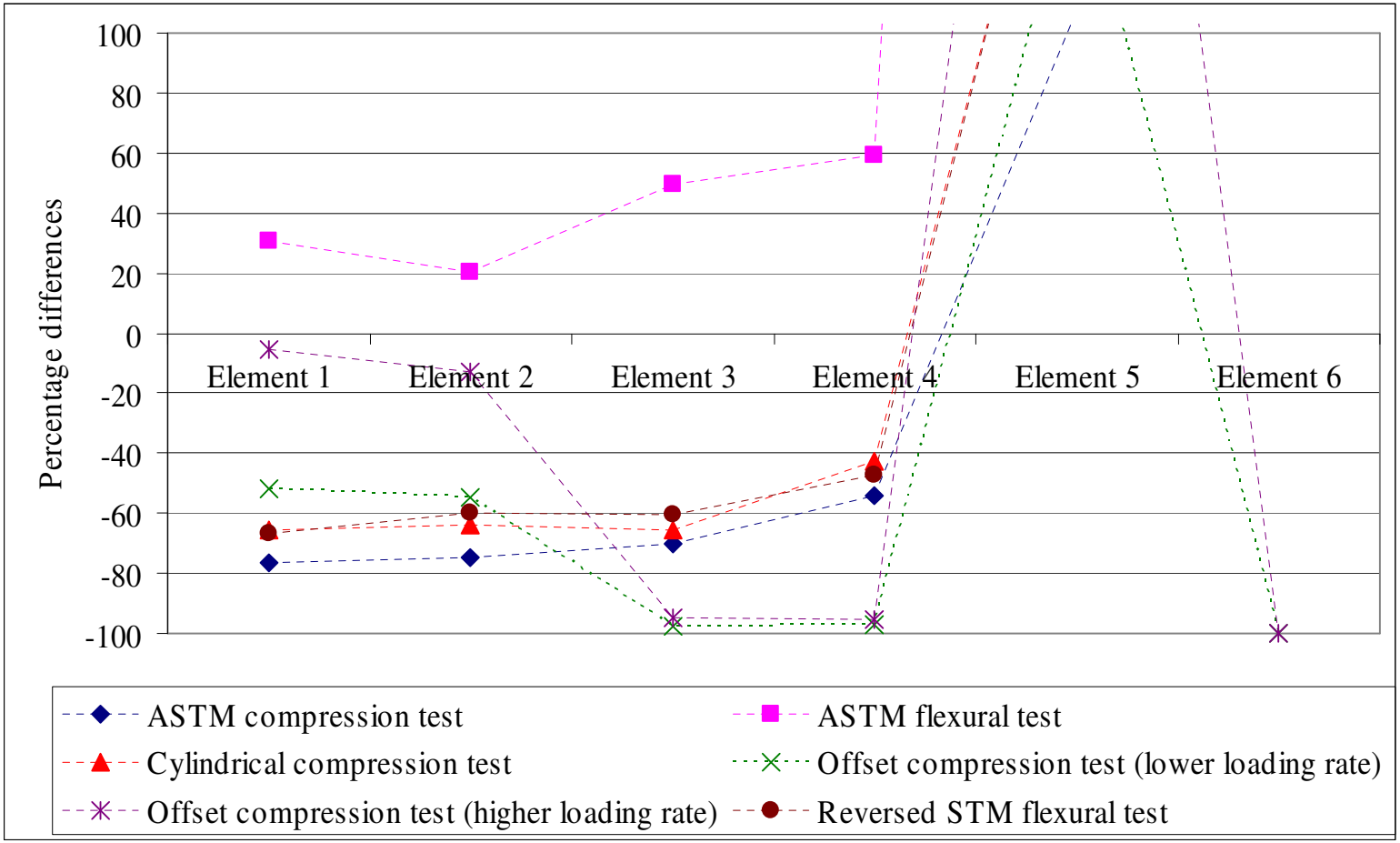

FIGURE 101 Percentage differences between von Mises stresses from the six laboratory tests simulations and the stage 2 of the tire-marker impact simulation in the finite elements 1-6 (RRPM Type B).

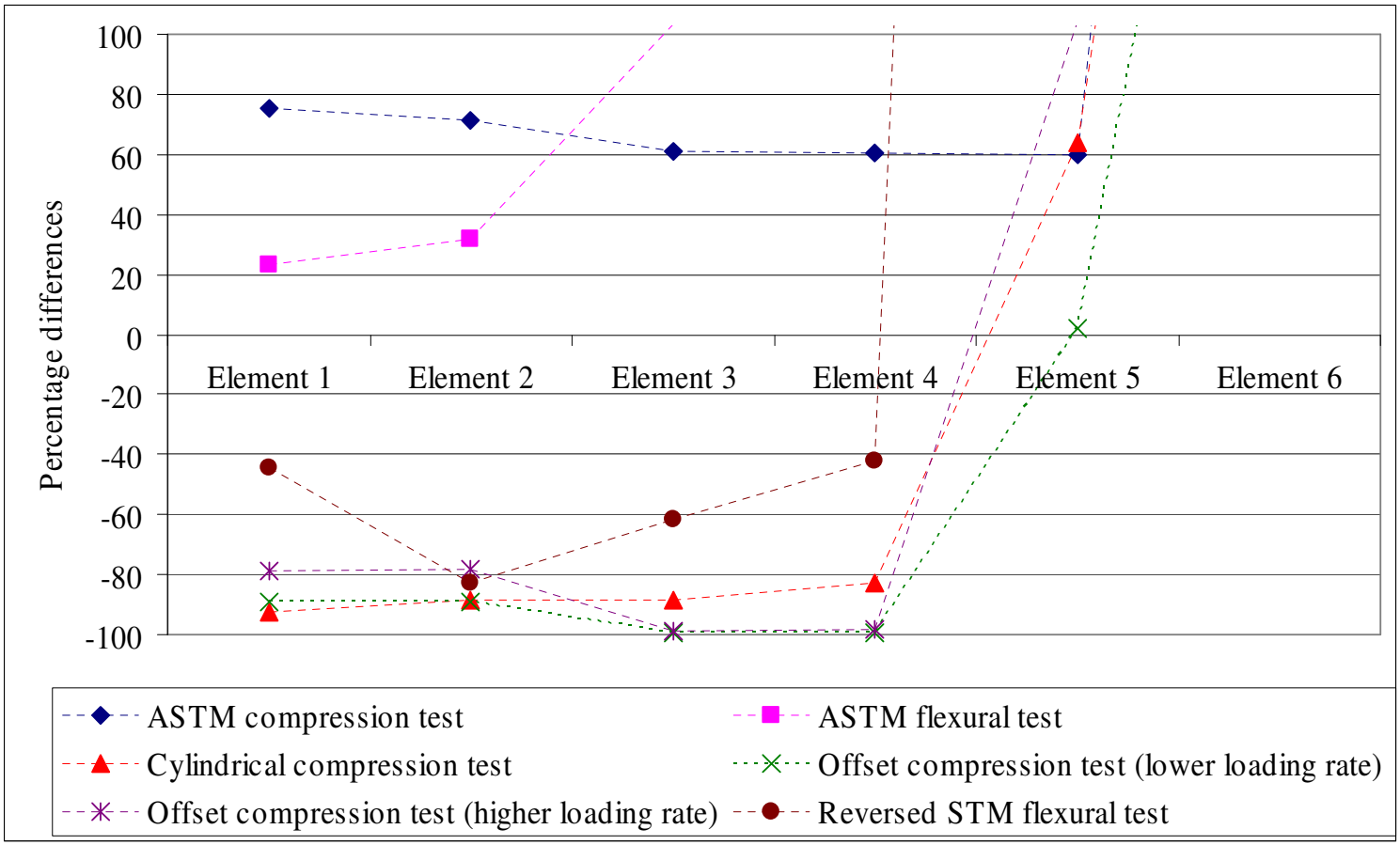

FIGURE 102 Percentage differences between von Mises stresses from the six laboratory tests simulations and the stage 2 of the tire-marker impact simulation in the finite elements 1-6 (RRPM Type C).

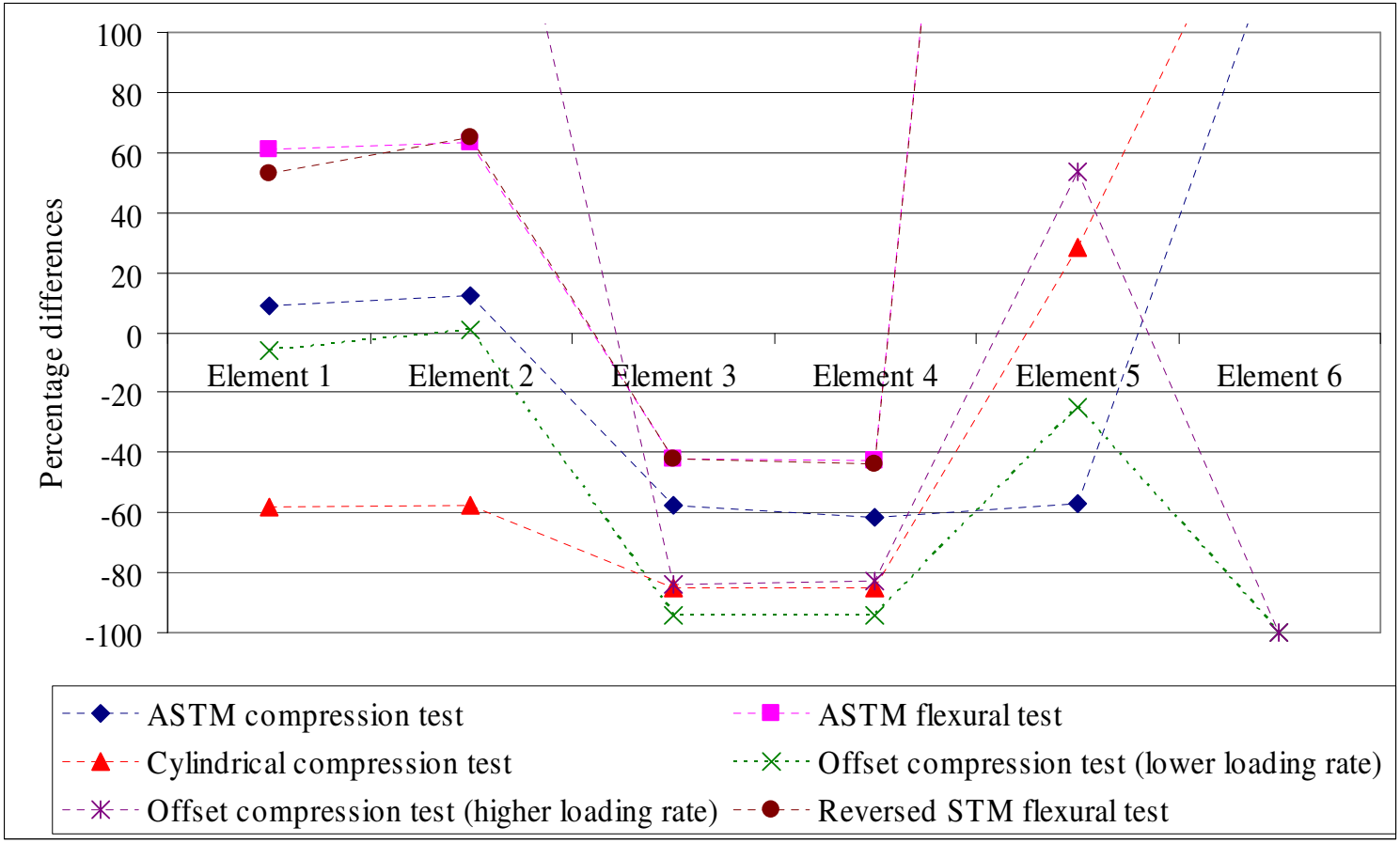

FIGURE 103 Percentage differences between von Mises stresses from the six laboratory tests simulations and the stage 3 of the tire-marker impact simulation in the finite elements 1-6 (RRPM Type A).

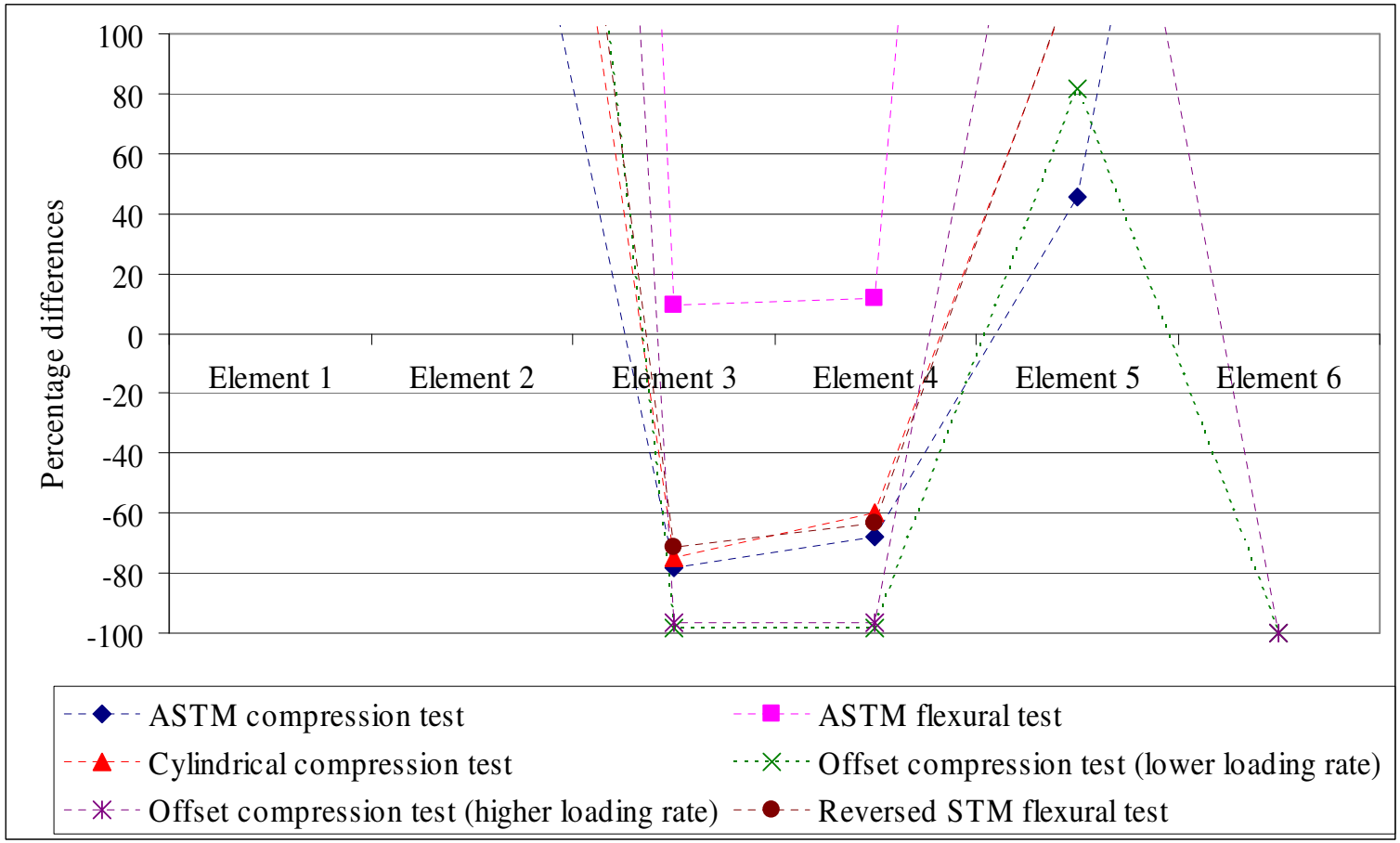

FIGURE 104 Percentage differences between von Mises stresses from the six laboratory tests simulations and the stage 3 of the tire-marker impact simulation in the finite elements 1-6 (RRPM Type B).

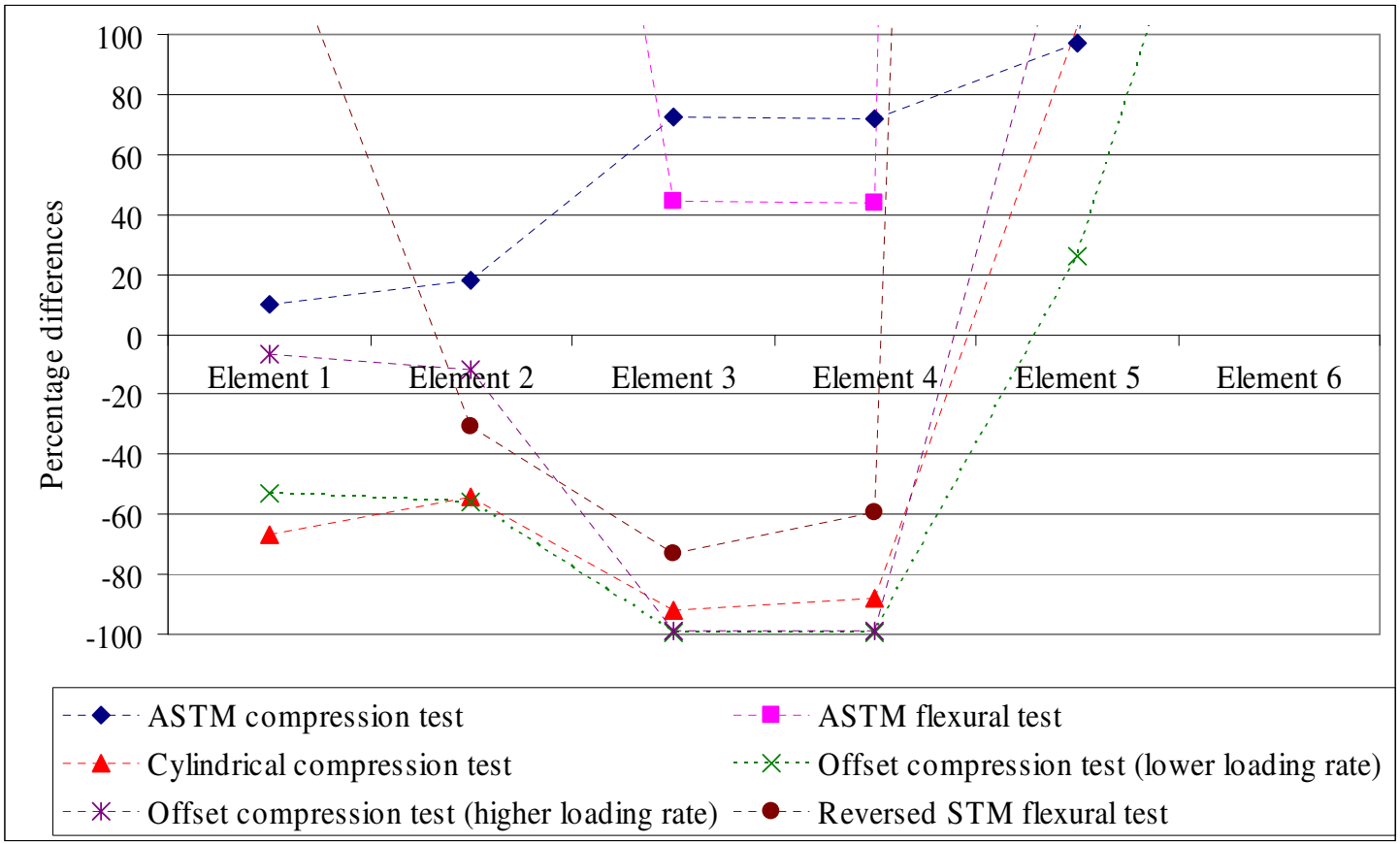

FIGURE 105 Percentage differences between von Mises stresses from the six laboratory tests simulations and the stage 3 of the tire-marker impact simulation in the finite elements 1-6 (RRPM Type C).

VITA

Name:	Ravi Prakash Agrawal
Address:	Department of Civil Engineering, Texas A&M University, MS 3136, College Station, TX 77843-3136, USA
E-mail Address:	ravip.ag@gmail.com

Education:	M. S., Civil Engineering, Texas A&M University, 2006 B. Tech., Civil Engineering, Indian Institute of Technology, Delhi, 2004
Work Experience	Texas Transportation Institute, TAMU, College Station, TX, USA Graduate Research Assistant • Worked on finite element analysis of Retroreflective Raised Pavement Markers (RRPMs) to recommend testing procedures for simulating their field performance • Assisted in developing laboratory and field tests for evaluation of performance of RRPMs
Conferences	Agrawal R. and D. Lord. Effects of Sample Size on the Goodness-of-Fit Statistic and Confidence Intervals of Crash Prediction Models Subjected to Low Sample Mean Values. Presented at the Transportation Research Board (TRB) conference, Washington D.C., January 2006.